Visual pathway morphometry in visual field defects

Hernowo, Aditya Tri

Visual pathway morphometry in visual field defects

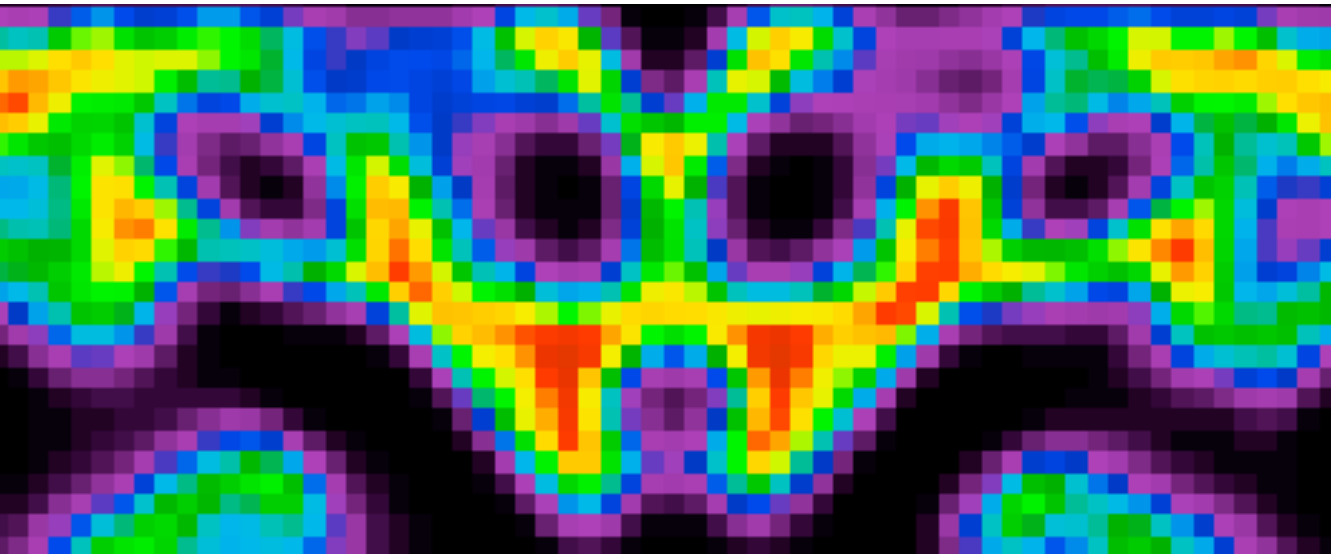

Aditya T. Hernowo

Printing of this thesis has been supported by:

The work in this thesis has been funded by:

Eric Bleumink Fonds
Stichting Nederlands Oogheelkundig Onderzoek (SNOO)
Nelly Reef Fund
Stichting MD Fonds - via UitZicht
Landelijke Stichting voor Blinden en Slechtzienden (LSBS) - via UitZicht
Algemene Nederlandse Vereniging ter Voorkoming van Blindheid (ANVVB) - via UitZicht

Visual pathway morphometry in visual field defects

ISBN	978-90-367-5416-3
Printer	Ipskamp Drukkers BV, Enschede
Publisher	University of Groningen
Document layout	Pages '09 (iWork)
Fonts (Main text)	Cochin, **Cochin bold,** and *Cochin italic*
Fonts (Headings)	Optima and **Optima bold**

The book cover shows a picture of grey matter template creation process, meanwhile the cover page shows a picture of lateral geniculate bodies final template. Both are obtained from brain image processing softwares, SPM8 e3 FSL.

rijksuniversiteit groningen

Visual pathway morphometry in visual field defects

Proefschrift

ter verkrijging van het doctoraat in de
Medische Wetenschappen
aan de Rijksuniversiteit Groningen
op gezag van de
Rector Magnificus, dr. E. Sterken,
in het openbaar te verdedigen op
maandag 19 maart 2012
om 16.15 uur

door

Aditya Tri Hernowo

geboren op 21 maart 1981
te Pontianak, Indonesië

Promotor	: Prof. dr. J.M.M. Hooymans
Copromotores	: Dr. F.W. Cornelissen
	Dr. N.M. Jansonius
Beoordelingscommissie	: Prof. dr. R.J.W. de Keizer
	Prof. dr. J.B.M. Kuks
	Prof. dr. A.B. Morland

“I was born not knowing and have had only a little time to change that here and there.”

- Richard P. Feynman

Untuk Maya...

Contents

Chapter 1

Introduction

Chapter contents

Humans evolved from primate ancestors who relied heavily on their vision for survival. To survive, they learned from visual information and then decided on the most appropriate behaviour for that situation. Visual information has been so essential to human survival that the optic nerve, which connects the eye to the brain, has evolved to become one of the densest nerves in the human body, containing millions of axons[1-5]. These bundles of axons connect to the basal aspect of the brain and from there, other neurons take over the task. These nerve bodies subsequently connect with the terminus of visual pathway, the visual cortex, which is located at the back of the brain.

Despite the crucial importance of these visual pathways, many aspects of their functioning are only now being elucidated. In particular, their relationship with ophthalmic pathology remains poorly understood. This introductory chapter describes the knowledge a priori to the experimental studies which are described in Chapter 2, 3, 4, and 5.

1.1. Aim and outline of this thesis

This thesis describes a number of magnetic resonance imaging studies of the human visual pathway in participants with two prevalent causes of visual field defect due to ophthalmic pathology: macular degeneration and glaucoma. The main research question was whether these ocular pathologies, with their associated visual field defects, affect the integrity of the visual pathways leading to the visual cortex.

The first chapter addresses the basic anatomy and physiology of the eye and brain, vision and the relevant pathologies. The methodological approaches used in the studies are described in the chapters to follow. The next four chapters describe the experimental studies that were performed to answer the main question. Chapter 2 describes the first investigation on the density of the primary visual cortex grey matter in subjects with glaucoma and subjects with age-related macular degeneration. As the first follow-up study, further morphometric exploration of the visual pathway in the two major types of macular degeneration, the age-related and the juvenile type, is described in Chapter 3. For purposes of comparison, similar morphometric explorations in primary open-angle glaucoma are reported in the Chapter 4. In Chapter 5, the integrity of the visual pathway in glaucoma is further assessed by means of an imaging technique specifically geared towards imaging nerve fibres. Finally, Chapter 6 contains a general discussion of the work presented in this thesis.

1.2. Anatomy of the visual pathway

The term visual pathway refers to the structures connecting the eye to the visual brain. These include the neuro-sensory retina of the eye, the optic nerve, chiasm and tract, the lateral geniculate bodies, and the visual cortex.

1.2.1. The eye

The human eye is an intricate combination of an efficient optical system and an intricate bio-electrical signal processing system. The function of the optics is to transmit and refract the light entering the eye so as to fit the structural arrangement of the retina, which senses the light entering the eye and processes the light into electrical signals.

Starting from the foremost part of the eye, the optical system consists of the cornea, aqueous humour, lens and vitreous body. All of those components, except for the lens, are relatively fixed in terms of their refractive power. The lens, which is suspended on a set of ciliary muscles, can change its refractive power by altering its convexity. Ideally, the optical system continuously focuses the light onto the central part if the retina to form a sharp image there. Less focused rays fall onto the peripheral retina. All of these rays of light are processed by the retina.

The processing stream of the retina starts from signal transduction, in this case the transformation of light photons into electrical currents. The photoreceptors occupying the outer segment do this task. These electrical signals are carried from cell to cell by means of interneuronal synapses. The next neuron to receive these signals is the bipolar cell, which then transmits them to the retinal ganglion cell (RGC). The axons of the RGCs form the retinal nerve fibre layer (RNFL) and subsequently converge at the optic nerve head to form a bundle, which is popularly known as the optic nerve. *

* This, however, is a misnomer. The fact that the optic nerve is consisted of the axons from third order neurons makes it a tract rather than a nerve[5]. The proper optic nerve should then be the axons of the bipolar cells. Nonetheless, for the sake of simplicity, we will just call the bundle of axons exiting the eyeball as the optic nerve, as popularly known.

1.2.2. Optic nerve, chiasm, and tract

The optic nerve is a collection of axons originating from the layer of RGCs. The bundle coming from one eye diverges halfway; some of the axons cross the midline to reach the contralateral side of the brain, while the others stay on the ipsilateral side. This midline half-crossing or hemi-decussation occurs in the chiasm. In this way, the chiasm contains both non-crossing and crossing fibres. The fibres coming from temporal side of the retina follow its course ipsilaterally, whereas the fibres from nasal side cross the midline.

After crossing and forming the chiasm, the crossing fibres from the left eye and the non-crossing ones from the right eye form a bundle called the right optic tract. A similar rule applies to the left optic tract. These tracts reach the basal aspect of the diencephalic part of the brain, where they form synapses with a group of neuronal cell bodies called the lateral geniculate bodies (LGB).

1.2.3. Lateral geniculate body and the geniculocalcarine radiation

Signals travelling through the optic tract are relayed by synapses to the neurons of the LGB. In these structures, both the cell bodies and the axons projecting out from them maintain their retinotopy, i.e. they maintain their relative spatial arrangement as it was in the retina. From these two nuclei, thin structures containing the axons that run on the lateral side of the lateral ventricles fan out to reach the calcarine fissures, hence the name geniculocalcarine radiation. The geniculocalcarine radiation is often called the optic radiation; these terms can be used interchangeably .

The fibres carrying the signals originating from the central part of the retina terminate at the posterior end of the calcarine fissures, occupying the poles of the occipital lobe. The fibres carrying the signals from the peripheral retina terminate more anteriorly in the fissures. The ends of fibres in the visual cortex are therefore retinotopically arranged.

1.3. Visual field

The anatomy of human eyes and their surrounding structures of orbit and eyelids normally determine the width of the visual field. From the fixation point, the visual field extents approximately 60° in the superior and nasal field, 75° in the inferior field, and slightly beyond 90° in the temporal field[6].

1.3.1. Measurement of the visual field

The visual field is the field of vision when the eye fixates on a single point. The width and the sensitivity of the field is then measured while maintaining the fixation. Quantitative measurement of visual field is called perimetry. Perimetry is routinely done monocularly, where the fields of the right and left eyes are measured separately.

Two perimetry methods are commonly used in the clinic: kinetic and static perimetry. Kinetic perimetry is performed by moving a light stimulus over the visual field. Since the stimulus can be varied in size and intensity, using one stimulus at a time enables an investigator to map the boundaries of the visual field sensitivity. It is commonly done using Goldmann perimeter. This method allows measurement of up to 90° of the field in every direction

from the fixation point. Static perimetry is performed by presenting light stimuli at several fixed locations over the visual field, one at a time, while varying the intensity. This method usually allows measurement of the central 30° of visual field. Automated static perimetry, conducted with instruments such as the Humphrey Visual Field Analyzer, is currently one of the commonest procedures in eye clinics. Such instruments can detect any defect up to 30° from central vision, and they automatically generate a sensitivity deviation map of the visual field, thus reducing the potential subjective bias in the measurement.

1.3.2. Visual field defect

With some types of ophthalmic pathology, the visual field can be impaired locally or globally. The impairment can be either temporary or permanent, and can be stable or progressive. Various ocular and cerebral conditions may impair the field. Two of the commonest causes of ocular field defect are glaucoma and macular degeneration. These two conditions are distinguished by the typical location of the defect. Glaucoma typically causes a peripheral visual field defect, which progresses centripetally and ultimately leaves the most central portion of the field intact. As the name implies, macular degeneration disrupts the central visual field, leaving the peripheral visual field intact.

1.3.2.1. Visual field defect in glaucoma

Glaucomatous visual field defects may take any of five typical forms: nasal step, wedge, arcuate, constriction and/or depression[7]. These forms depend on the stage of the disease The defect typically starts from the nasal field (nasal step), sometimes connects to the (enlarged) blind spot on the temporal field, together forming a bow-shaped defect called the arcuate defect. In the end stage, some patients have only residual sensitivity on the temporal field (temporal island) and some other patients have small residual central visual field (tunnel vision). Ultimately glaucoma leads to total blindness.

1.3.2.2. Visual field defects in macular degeneration

The structural degeneration in this pathology takes place in the central part of the retina, the macula. Because the macula with its fovea provides central vision, this condition results in a central visual field defect. This can be a relative or an absolute depression in the central 10° of the field of vision. And as the name implies, the peripheral visual field is spared.

1.4. Glaucoma

Glaucoma is an umbrella term for a collection of diseases primarily characterised by progressive visual field defect[8]. In primary open-angle glaucoma (POAG), intraocular pressure is one of many risk factors and is often increased[8-11]. Other risk factors include the presence of family history of glaucoma and myopia[8, 12, 13]. RGC death is a key event heralding the corresponding loss in the RNFL and its continuation, i.e. the optic nerve.

1.4.1. Aetiology

The chromosomal loci associated with POAG are numerous, and have been detected on chromosomes 1, 2, 3, 4, 5, 7, 8, 9, 10, 15, 19, and 20[14]. Distortion of lamina cribrosa, extracellular matrix changes in the optic nerve, disruption of the microcirculation at the optic nerve head and increasing intraocular pressure may all be involved in the development of glaucoma[15]. Numerous genetic dispositions and other mechanisms of RGC loss with POAG[16-21] confirm the multifactorial nature of glaucoma aetiology.

1.4.2. Symptoms and signs

In an early stage of glaucoma, the peripheral visual field may be loss. For example, an individual may go to an ophthalmologist because he or she have difficulty climbing or descending stairs due to the loss of inferior visual field. However, another individual with POAG might seek medical help only when the disease is already beyond the early stage. This could be due to the nature of the progressive visual field loss, which starts from the periphery and progresses centripetally. Because most activities rely on central vision, any defect or deterioration of the peripheral field might go unnoticed until it creeps into the central vision. During the late stage of this condition, peripheral vision may become very limited, while central vision remains relatively unaffected. In the worst case, vision is lost entirely. Ophthalmologic examination typically reveals quantifiable and relatively consistent, yet progressively worsening visual field sensitivity.

1.4.3. Brain studies pertaining to POAG

The brain has not usually been implicated in glaucoma. However, several recent studies have indicated an association between glaucoma and morphometric changes in the brain. A postmortem study indicated that the size of the optic nerve, the LGB, and the thickness of the visual cortex, is reduced in glaucoma[22]. Involvement of the LGB[22-24], the visual cortex[22, 24, 25], and the interconnecting white matter (tracts)[26, 27] has been reported.

1.5. Macular degeneration

In contrast to glaucoma, individuals with macular degeneration commonly seek medical help at an early stage. This is due to the nature of central vision involvement in macular degeneration[28-30]. Central vision is used in virtually every activity of daily living. Blurred or distorted central vision is definitely troublesome, so help is sought immediately.

1.5.1. Aetiology

No conclusive research has yet been published on the exact cause of macular degeneration. However, the pathology is known to begin with basal or choroidal capillary leakage[31], which is due to a dysfunctional blood retinal barrier[32]. This process may or may not advance to continuous leakage and neovascularization[31], which leads to macular oedema. The involvement of nutrient deficiencies in the aetiology of macular degeneration (concerning nutrients such as lipofuscin, lutein or zeaxanthine compounds, vitamin A or other antioxidants) is still a matter of debate[33-36].

1.5.2. Symptoms and signs

The disruption of macular anatomy, especially involving the fovea, causes the image that falls onto the area to lack sharpness or even become distorted[30, 37]. Moreover, deposited materials and fluid accumulation in the foveal area may hinder incoming light, thus generating a positive scotoma: an appearance of something dark that 'floats' and blocks the central vision.

Based on the onset of the disease, macular degeneration can be classified into the senile type (age-related macular degeneration or AMD) and the juvenile type (juvenile-type macular degeneration or JMD). AMD can be further classified into dry/non-exudative and wet/exudative/neovascular AMD. In wet AMD, the decrease in visual acuity is caused by intraretinal and/or subretinal fluid and haemorrhage, which may block the incoming light. Meanwhile in dry AMD, vision loss may be due to geographic atrophy[38, 39], presumably caused by photoreceptors layer disruption due to retinal pigment epithelial (RPE) degeneration.

The impairment of the central vision occurs early in life in juvenile-type macular degeneration (JMD). JMD includes Stargardt's disease (the most common form[39]), Best's disease, juvenile retinoschisis[40] and other diseases, and the retinal pathology varies accordingly[41, 42], such as foveal atrophy with surrounding yellowish flecks in Stargardt's disease and yolk-like macular lesion in Best's disease[39]. The resulting RPE degeneration in the macula may be related to the visual acuity loss.

1.5.3. Brain studies pertaining to macular degeneration

A number of reports have been published on visual cortex function in various types of macular degeneration: age-related and various kinds of juvenile-type macular degenerations. In many of these reports, the primary visual cortex that primarily represents the macular area remains silent during macular visual stimulation[43-46], while the activities in the more peripheral projection zone in the primary visual cortex are preserved. However, the presence of functional reorganisation of the primary visual cortex in macular degeneration is still controversial[28, 43-45, 47-50]. The relationship between the presence of macular degeneration and any structural deviation in the primary visual cortex is also a matter of some controversy, with some investigators suggesting an absence of structural changes in macular degeneration[51], while others suggest the existence of such changes [52].

1.6. Structural brain imaging and the analyses

The advent of neuro-imaging techniques has greatly advanced our understanding of many neurological processes and of the pathologies of many kinds of diseases, including those affecting vision. For many modalities of neuro-imaging, magnetic resonance imaging (MRI) has been used extensively and intensively in both routine clinical and experimental practice. This is due to its relative safety and the high quality of the images that MRI can generate. High resolution brain tissue images can be used to identify and assess brain structures.

Structural MRI may require several types of acquisition, for example T_1- and T_2-weighted acquisition. Although T_1-weighted imaging can produce high resolution anatomical images, this acquisition does not allow us to optimally differentiate projections or fibres connecting different brain areas. For this purpose, diffusion tensor imaging (DTI) was developed.

1.6.1. Underlying concepts of MRI

The human body consists of 70% water by volume. A water molecule, H_2O, contains two protons (hydrogen atoms). The spin of these protons defines the magnetic field of the molecule. By applying a strong magnetic field to part of the body, the brain for example, the protons in water molecules will be aligned almost uniformly. A certain amount of energy (a pulse) can be delivered to change the alignment of a group of protons in the brain. When the pulse is stopped, the protons begin to return to their normal alignment. While returning to normal alignment, they release the energy received from the pulse. This energy is received by the MRI machine, where it is transformed into an image.

1.6.2. Voxel-based morphometry

Anatomical MRI allows us to inspect the human brain in vivo with resolution to the millimetre scale. This allows an observer to perform manual quantitative measurements of many brain structures with a digital calliper. However, this manual measurement raises the issue of inter-observer variation in the result, even when the measurements are taken by competent neuro-radiologists or neuro-anatomists. As with many other assessments, individual or subjective bias of measurement has been a potential problem, especially if such assessments must be very precise. This issue triggered the development of automated measurement technique, sometimes called automated morphometry, which minimises the involvement of human judgement in measuring brain structures in terms of their volume or density.

Thus far, automated morphometry has been used more often in research than in clinical settings. This is because automated morphometry uses many different approaches developed by different groups of researchers. Due to the absence of a standard approach, the clinical use of this technique is still limited. However, the development of automated morphometry is ongoing and we can expect further advances in the future.

One of the approaches for performing such morphometric analyses involves statistical analyses, such as voxel-wise comparison[53-59]. This approach relies quite heavily on the processes of image registration and segmentation. The registration process allows many different brain images to be compared on a voxel-by-voxel basis. Meanwhile, to increase the sensitivity of the statistical tests, the grey and white matter and the cerebrospinal fluid are separated from each other using automated segmentation procedures. This step allows the comparison of one type of brain tissue (e.g. grey matter) between individual brains or groups of brains.

For the present study I used VBM, which is included in the SPM8 software package (Wellcome Department of Imaging Neuroscience, London, UK; http://www.fil.ion.ucl.ac.uk/spm), to compare the volume of subcortical structures between the glaucoma group and control group[60]. VBM statistically assesses local changes in grey and/or white matter volume between groups of anatomical scans.

1.6.3. Diffusion-weighted image-based analysis

Water molecules tend to diffuse with equal probability in all directions. Given a certain amount of time, the diffusion will therefore be spherical. This is called isotropic diffusion. However, in tubular structures, such as vessels in the brain, diffusion is more likely to occur along the longer axis. The overall probability of diffusion will therefore be ellipsoidal, This is called anisotropic diffusion. The anisotropy becomes higher as the diameter becomes narrower and the longer axis is stretched out, as with axons.

1.6.3.1. Image acquisition and pre-processing

DW images are prone to water-fat shift artefacts. This is readily visible in the frontal lobe. To correct for these artefacts, two acquisitions with opposing directions were performed: (1) anterior-posterior (AP); and (2) posterior-anterior (PA). The two resulting images were then independently eddy-corrected to correct for movement artefact due to the eddy current inside the scanner.

The next step was the susceptibility correction, which takes advantage of the two images acquired with opposing direction as explained earlier. This was done using a script provided by Farrell[61]. The susceptibility-corrected image was further processed for tensor estimation or fibre tracking (tractography).

1.6.3.2. Tensor estimation

The tensor estimation step, as implemented in DTIFIT (a tool available within FMRIB Software Library or FSL), yielded three eigenvectors (V_1, V_2, and V_3), and three eigenvalues (λ_1, λ_2, and λ_3) which are scalar. From the three eigenvalues, various invariants can be calculated, including the fractional anisotropy (FA). The FA was computed using the following formula:

$$FA=\sqrt{\frac{3\left[\left(\lambda_1-D_{av}\right)^2+\left(\lambda_2-D_{av}\right)^2+\left(\lambda_3-D_{av}\right)^2\right]}{2\left(\lambda_1^2+\lambda_2^2+\lambda_3^2\right)}}$$

A completely spherical diffusion (isotropic) has an FA value of 1, while a completely anisotropic diffusion will be 0.

1.6.3.3. Tract-based spatial statistics

Tract-based spatial statistics (TBSS) was developed by Smith et al.[62]. This method tackled the problem of how to register FA images from multiple subjects and circumvented the problem of choosing the

appropriate amount of smoothing needed prior to voxel-wise statistics. This was done by (1) non-linearly aligning multiple subject FA images to achieve reasonable alignment; (2) creating a mean FA image; (3) skeletonising the mean FA image by suppressing low FA voxels; (4) projecting the aligned individual FA images onto the skeletonised mean and filling the skeleton with the maximum FA value from relevant voxels in the search area; (5) performing voxel-wise statistics on the skeleton space across subjects without any need of smoothing.

Bibliography

1. Repka MX, Quigley HA. The effect of age on normal human optic nerve fiber number and diameter. Ophthalmology 1989;96(1):26-32.
2. Jonas JB, Schmidt AM, Muller-Bergh JA, Naumann GO. Optic nerve fiber count and diameter of the retrobulbar optic nerve in normal and glaucomatous eyes. Graefes Arch Clin Exp Ophthalmol 1995;233(7):421-4.
3. Mikelberg FS, Drance SM, Schulzer M, et al. The normal human optic nerve. Axon count and axon diameter distribution. Ophthalmology 1989;96(9):1325-8.
4. Mikelberg FS, Yidegiligne HM, Schulzer M. Optic nerve axon count and axon diameter in patients with ocular hypertension and normal visual fields. Ophthalmology 1995;102 (2):342-8.
5. Hartono, Hernowo AT, Sasongko MB. Anatomi dan fisiologi penglihatan. Ilmu Kesehatan Mata 2008.
6. Niederhauser S, Mojon DS. Normal isopter position in the peripheral visual field in goldmann kinetic perimetry. Ophthalmologica 2002;216(6):406-8.
7. Stamper RL. The effect of glaucoma on central visual function. Trans Am Ophthalmol Soc 1984;82:792-826.
8. West SK. Looking forward to 20/20: a focus on the epidemiology of eye diseases. Epidemiol Rev 2000;22(1):64-70.
9. Salinas-Navarro M, Alarcon-Martinez L, Valiente-Soriano FJ, et al. Ocular hypertension impairs optic nerve axonal transport leading to progressive retinal ganglion cell degeneration. Exp Eye Res;90(1):168-83.
10. Urcola JH, Hernandez M, Vecino E. Three experimental glaucoma models in rats: comparison of the effects of intraocular pressure elevation on retinal ganglion cell size and death. Exp Eye Res 2006;83(2):429-37.
11. Bengtsson B, Leske MC, Hyman L, Heijl A. Fluctuation of intraocular pressure and glaucoma progression in the early manifest glaucoma trial. Ophthalmology 2007;114(2): 205-9.
12. Saw SM, Gazzard G, Shih-Yen EC, Chua WH. Myopia and associated pathological complications. Ophthalmic Physiol Opt 2005;25(5):381-91.
13. Marcus MW, de Vries MM, Montolio FG, Jansonius NM. Myopia as a risk factor for open-angle glaucoma: a systematic review and meta-analysis. Ophthalmology;118(10): 1989-94 e2.
14. Allingham RR, Liu Y, Rhee DJ. The genetics of primary open-angle glaucoma: a review. Exp Eye Res 2009;88(4):837-44.
15. Fechtner RD, Weinreb RN. Mechanisms of Optic-Nerve Damage in Primary Open-Angle Glaucoma. Survey of Ophthalmology 1994;39(1):23-42.
16. Li Y, Schlamp CL, Poulsen GL, et al. p53 regulates apoptotic retinal ganglion cell death induced by N-methyl-D-aspartate. Mol Vis 2002;8:341-50.
17. Nickells RW. Apoptosis of retinal ganglion cells in glaucoma: an update of the molecular pathways involved in cell death. Surv Ophthalmol 1999;43 Suppl 1:S151-61.
18. Nickells RW. Retinal ganglion cell death in glaucoma: the how, the why, and the maybe. J Glaucoma 1996;5(5):345-56.
19. Quigley HA, Nickells RW, Kerrigan LA, et al. Retinal ganglion cell death in experimental glaucoma and after axotomy occurs by apoptosis. Invest Ophthalmol Vis Sci 1995;36(5): 774-86.
20. Carelli V, Ross-Cisneros FN, Sadun AA. Mitochondrial dysfunction as a cause of optic neuropathies. Prog Retin Eye Res 2004;23(1):53-89.
21. Carelli V, Ross-Cisneros FN, Sadun AA. Optic nerve degeneration and mitochondrial dysfunction: genetic and acquired optic neuropathies. Neurochem Int 2002;40(6): 573-84.

22. Gupta N, Ang LC, Noel de Tilly L, et al. Human glaucoma and neural degeneration in intracranial optic nerve, lateral geniculate nucleus, and visual cortex. Br J Ophthalmol 2006;90(6):674-8.
23. Gupta N, Greenberg G, de Tilly LN, et al. Atrophy of the lateral geniculate nucleus in human glaucoma detected by magnetic resonance imaging. Br J Ophthalmol 2009;93 (1):56-60.
24. Yucel YH, Zhang Q, Weinreb RN, et al. Effects of retinal ganglion cell loss on magno-, parvo-, koniocellular pathways in the lateral geniculate nucleus and visual cortex in glaucoma. Prog Retin Eye Res 2003;22(4):465-81.
25. Duncan RO, Sample PA, Weinreb RN, et al. Retinotopic organization of primary visual cortex in glaucoma: Comparing fMRI measurements of cortical function with visual field loss. Prog Retin Eye Res 2007;26(1):38-56.
26. Garaci FG, Bolacchi F, Cerulli A, et al. Optic nerve and optic radiation neurodegeneration in patients with glaucoma: in vivo analysis with 3-T diffusion-tensor MR imaging. Radiology 2009;252(2):496-501.
27. Kashiwagi K, Okubo T, Tsukahara S. Association of magnetic resonance imaging of anterior optic pathway with glaucomatous visual field damage and optic disc cupping. J Glaucoma 2004;13(3):189-95.
28. Cheung SH, Legge GE. Functional and cortical adaptations to central vision loss. Vis Neurosci 2005;22(2):187-201.
29. Nazemi PP, Fink W, Lim JI, Sadun AA. Scotomas of age-related macular degeneration detected and characterized by means of a novel three-dimensional computer-automated visual field test. Retina 2005;25(4):446-53.
30. Gohel PS, Mandava N, Olson JL, Durairaj VD. Age-related macular degeneration: an update on treatment. Am J Med 2008;121(4):279-81.
31. Zarbin MA. Current concepts in the pathogenesis of age-related macular degeneration. Arch Ophthalmol 2004;122(4):598-614.
32. Scholl S, Kirchhof J, Augustin AJ. Pathophysiology of macular edema. Ophthalmologica; 224 Suppl 1:8-15.
33. Richer S, Stiles W, Thomas C. Molecular medicine in ophthalmic care. Optometry 2009;80(12):695-701.
34. Rein DB, Wittenborn JS, Zhang X, et al. Forecasting age-related macular degeneration through the year 2050: the potential impact of new treatments. Arch Ophthalmol 2009;127(4):533-40.
35. Zhang B, Osborne NN. Oxidative-induced retinal degeneration is attenuated by epigallocatechin gallate. Brain Res 2006;1124(1):176-87.
36. Thompson DA, Gal A. Vitamin A metabolism in the retinal pigment epithelium: genes, mutations, and diseases. Prog Retin Eye Res 2003;22(5):683-703.
37. Roquet W, Roudot-Thoraval F, Coscas G, Soubrane G. Clinical features of drusenoid pigment epithelial detachment in age related macular degeneration. Br J Ophthalmol 2004;88(5):638-42.
38. Agni AN, Widayanti TW, Hernowo AT. Retina. Ilmu Kesehatan Mata 2008.
39. Regillo C, Chang, T.S., Johnson, M.W., Kaiser, P.K., Scott, I.U., Spaide, R., Griggs, P.B. Age-Related Macular Degeneration. In: Zorab RA, Straus, H., Dondrea, C.L., Arturo, C., DuCharme, N., Tanaka, S., Huebner, S., ed. Basic and Clinical Science Course Section 12: Retina and Vitreous. San Fransisco, CA: American Academy of Ophthalmology, 2007.
40. Krill AE, Deutman AF. The various categories of juvenile macular degeneration. Trans Am Ophthalmol Soc 1972;70:220-45.
41. Aaberg TM. Stargardt's disease and fundus flavimaculatus: evaluation of morphologic progression and intrafamilial co-existence. Trans Am Ophthalmol Soc 1986;84:453-87.
42. Mullins RF, Oh KT, Heffron E, et al. Late development of vitelliform lesions and flecks in a patient with best disease: clinicopathologic correlation. Arch Ophthalmol 2005;123 (11):1588-94.
43. Liu T, Cheung SH, Schuchard RA, et al. Incomplete cortical reorganization in macular degeneration. Invest Ophthalmol Vis Sci;51(12):6826-34.
44. Baker CI, Peli E, Knouf N, Kanwisher NG. Reorganization of visual processing in macular degeneration. J Neurosci 2005;25(3):614-8.
45. Baker CI, Dilks DD, Peli E, Kanwisher N. Reorganization of visual processing in macular degeneration: replication and clues about the role of foveal loss. Vision Res 2008;48(18): 1910-9.
46. Little DM, Thulborn KR, Szlyk JP. An FMRI study of saccadic and smooth-pursuit eye movement control in patients with age-related macular degeneration. Invest Ophthalmol Vis Sci 2008;49(4):1728-35.
47. Baseler HA, Gouws A, Haak KV, et al. Large-scale remapping of visual cortex is absent in adult humans with macular degeneration. Nat Neurosci.

48. Masuda Y, Dumoulin SO, Nakadomari S, Wandell BA. V1 projection zone signals in human macular degeneration depend on task, not stimulus. Cereb Cortex 2008;18(11): 2483-93.
49. Schumacher EH, Jacko JA, Primo SA, et al. Reorganization of visual processing is related to eccentric viewing in patients with macular degeneration. Restor Neurol Neurosci 2008;26(4-5):391-402.
50. Dilks DD, Baker CI, Peli E, Kanwisher N. Reorganization of visual processing in macular degeneration is not specific to the "preferred retinal locus". J Neurosci 2009;29(9): 2768-73.
51. Grosso A, Mosley TH, Klein R, et al. Is early age-related macular degeneration associated with cerebral MRI changes? The Atherosclerosis Risk in Communities study. Am J Ophthalmol 2007;143(1):157-9.
52. Plank T, Frolo J, Brandl-Ruhle S, et al. Gray matter alterations in visual cortex of patients with loss of central vision due to hereditary retinal dystrophies. Neuroimage;56(3): 1556-65.
53. Wright IC, McGuire PK, Poline JB, et al. A voxel-based method for the statistical analysis of gray and white matter density applied to schizophrenia. Neuroimage 1995;2(4): 244-52.
54. Vargha-Khadem F, Watkins KE, Price CJ, et al. Neural basis of an inherited speech and language disorder. Proc Natl Acad Sci U S A 1998;95(21):12695-700.
55. Sowell ER, Thompson PM, Holmes CJ, et al. Localizing age-related changes in brain structure between childhood and adolescence using statistical parametric mapping. Neuroimage 1999;9(6 Pt 1):587-97.
56. Krams M, Quinton R, Ashburner J, et al. Kallmann's syndrome: mirror movements associated with bilateral corticospinal tract hypertrophy. Neurology 1999;52(4):816-22.
57. May A, Ashburner J, Buchel C, et al. Correlation between structural and functional changes in brain in an idiopathic headache syndrome. Nat Med 1999;5(7):836-8.
58. Woermann FG, Free SL, Koepp MJ, et al. Voxel-by-voxel comparison of automatically segmented cerebral gray matter--A rater-independent comparison of structural MRI in patients with epilepsy. Neuroimage 1999;10(4):373-84.
59. Shah PJ, Ebmeier KP, Glabus MF, Goodwin GM. Cortical grey matter reductions associated with treatment-resistant chronic unipolar depression. Controlled magnetic resonance imaging study. Br J Psychiatry 1998;172:527-32.
60. Ashburner J, Friston KJ. Voxel-based morphometry--the methods. Neuroimage 2000;11(6 Pt 1):805-21.
61. Farrell JA, Landman BA, Jones CK, et al. Effects of signal-to-noise ratio on the accuracy and reproducibility of diffusion tensor imaging-derived fractional anisotropy, mean diffusivity, and principal eigenvector measurements at 1.5 T. J Magn Reson Imaging 2007;26(3):756-67.
62. Smith SM, Jenkinson M, Johansen-Berg H, et al. Tract-based spatial statistics: voxelwise analysis of multi-subject diffusion data. Neuroimage 2006;31(4):1487-505.

Chapter 2

Changes in cortical grey matter density associated with long-standing retinal visual field defects

Based on:
Boucard CC, Hernowo AT*, Maguire RP, Jansonius NM, Roerdink JBTM, Hooymans JMM, Cornelissen FW. Changes in cortical grey matter density associated with long-standing retinal visual field defects. Brain 2009;132(Pt 7):1898-906.

* The first and second author contributed equally to this work.

ABSTRACT

Retinal lesions caused by eye diseases such as glaucoma and age-related macular degeneration can, over time, eliminate stimulation of parts of visual cortex. This could lead to degeneration of inactive cortical neuronal tissue, but this has not been established in humans. Here, we used magnetic resonance imaging to assess the effects of prolonged sensory deprivation in human visual cortex. High-resolution anatomical magnetic resonance images were obtained in subjects with foveal (age-related macular degeneration) and peripheral (glaucoma) retinal lesions as well as age-matched controls. Comparison of grey matter between patient and control groups revealed density reductions in the approximate retinal lesion projection zones in visual cortex. This indicates that long-term cortical deprivation due to retinal lesions acquired later in life is associated with retinotopic specific neuronal degeneration of visual cortex. Such degeneration could interfere with therapeutic strategies such as the future application of artificial retinal implants to overcome lesion-induced visual impairment.

Chapter contents

2.1. Introduction

Age-related macular degeneration (AMD) and glaucoma, eye diseases associated with the occurrence of visual field defects, are the two leading causes of visual impairment in the developed world[1]. AMD is caused by accumulated waste products in the tissues underneath the macula that interfere with retinal metabolism and lead to retinal atrophy[2, 3]. The disease causes field defects that are located in or near the central visual field. In glaucoma, progressive retinal ganglion cell loss and optic nerve damage occurs, in most cases induced by an elevated intra-ocular pressure[4, 5]. Visual field deterioration typically starts peripherally and progresses towards the fovea. Due to the retinotopic organisation of the visual cortex[6, 7], when field defects occur in both eyes and overlap, the corresponding part of visual cortex is no longer stimulated. An absence of stimulation may result in changes in the cortical structure[8, 9]. This makes it relevant to ask whether field defects that have their origin at the level of the retina can lead to deterioration in the structure of the occipital cortex.

Indeed, there is evidence that developmental visual disorders such as amblyopia[10] and albinism[11] affect the structure of human occipital cortex. However, surprisingly little is known about the consequence of visual deprivation later in life. A recent case study showed degenerative changes in the visual cortex of a glaucoma patient based on post-mortem examination[12]. Previously, using magnetic resonance imaging, Kitajima and colleagues had reported wider calcarine sulci in a small group of patients with a variety of retinal pathology indicating a possible link between visual field defects and cortical degeneration[13]. In another study, compared to healthy participants, subjects with normal-tension glaucoma, but not those with glaucoma, showed more pathological findings (ischemia) in sulci, fissures, subarachnoid spaces, and ventricles[14]. However, the status of the grey matter was not examined. Finally, in glaucoma patients, a reduced size of the lateral geniculate nuclei was reported[15].

In the present paper, we determined whether structural changes in human visual cortex occur once disease of the eye has resulted in an established homonymous visual field defect. This question is also relevant given conflicting reports on the presence of functional occipital reorganisation following retinal lesions[16-19]. In the present study, visual field measurements were used to chart changes in visual sensitivity associated with the retinal visual field defects from AMD and glaucoma. Magnetic resonance imaging and subsequent voxel-based morphometric analysis methods were used to selectively assess the presence of any associated changes in grey matter density in the two groups.

2.2. Materials and methods

2.2.1. Subjects

Subjects with visual field defects were recruited amongst the patient population of the Department of Ophthalmology of the University Medical Center Groningen (Groningen, The Netherlands) and through advertisements in magazines of patient associations. The group consisted of nine patients suffering from AMD (two females and seven males; mean age 73 years-old, range 51 – 82 years-old), and eight patients with primary open-angle glaucoma (one female and seven males; mean age 72-years-old, range 61 – 85 years old).

Age-related macular degeneration was defined as the presence of a decreased visual acuity in a patient with abnormalities in the macular area without any other explanation. Abnormalities might be either drusen, hyper-/depigmentation, geographic atrophy or signs of previous exudative changes. A glaucoma patient was defined as a patient with a reproducible visual field defect on conventional perimetry. The defects had to be compatible with glaucoma and without other explanation. Optic disc excavation had to be in line with glaucoma as well. In addition, in both AMD and glaucoma groups, patients had to have an homonymous scotoma of at least 10 degrees diameter in at least one quadrant, for a minimum of 3 years. Patients with any other (neuro-)ophthalmic disease that might affect the visual field were excluded.

Homonymous visual fields defects in both groups were located centrally or paracentrally. In glaucoma, the visual field defect generally starts paracentrally, progresses peripherally and finally expands towards central parts in the last stage of the disease. This difference in location and severity of visual field losses is reflected in the visual acuity (logMAR; logarithmic minimum angle of resolution) and in the mean deviation (MD) scores of both groups. LogMAR is a logarithmic transformation of the more common clinically used decimal notation. A logMAR value of 0 corresponds to a visual acuity of 1.0 in decimal notation. More positive numbers indicate that the minimum angle of resolution is larger, and thus correspond to a lower visual acuity. The mean deviation is the weighted average decrease in visual field sensitivity relative to the norm for a particular age group. Negative values indicate a reduced sensitivity. Table 1 lists these characteristics.

For the control group, 12 healthy age-matched subjects (three females and nine males; mean age 66 years, range 60-82) were recruited. They were recruited from amongst the partners of the visual field impaired participants or via advertisement in a local newspaper. Control subjects were required to have good (or corrected to good) visual acuity (logMAR≤0), not to have any visual field defect and to be free of any ophthalmic, neurologic, or general health problem.

This study conformed to the tenets of the Declaration of Helsinki and was approved by the medical review board of the University Medical Center Groningen (Groningen, The Netherlands). All participants gave their informed written consent prior to participation.

Subject	Group	Age	Visual acuity (logMAR)		Visual field mean deviation (dB)	
			OD	OS	OD	OS
1	AMD	74	1.8	1.3	n/a	-7.57
2	AMD	67	0.5	0.1	-5.5	-4.50
3	AMD	62	1.3	0.7	-11.48	-2.69
4	AMD	82	1.1	1.0	-6.28	-4.96
5	AMD	78	1.0	1.8	-3.51	-7.04
6	AMD	81	1.1	0.7	-6.06	-3.64
7	AMD	76	0.5	0.8	-5.79	-2.64
8	AMD	51	1.0	1.0	-12.01	-14.08
9	AMD	82	0.5	0.4	-3.43	-2.20
	Mean	**72.6**				
10	POAG	66	0.1	0.1	-25.08	-22.96
11	POAG	69	0.1	0.1	-27.20	-13.82
12	POAG	85	0.0	1.0	-8.80	-24.59
13	POAG	80	0.2	0.1	-5.23	-16.15
14	POAG	64	l.p.	0.7	l.p.	-14.45
15	POAG	61	0.05	0.05	-11.62	-3.67
16	POAG	74	0.0	0.1	-23.28	-18.27
17	POAG	79	0.1	0.15	-6.36	-13.41
	Mean	**72.3**				

Table 1. Subject characteristics. Characteristics of the two patient groups (AMD and glaucoma) were visual acuity for one or both eyes (expressed in logMAR), visual sensitivity (expressed as MD in dB), and age. logMAR – logarithm of minimum angle of resolution; MD – mean deviation; dB – decibel; AMD – age-related macular degeneration; POAG – primary open-angle glaucoma; l.p. - light perception; n/a – not available.

2.2.2. Visual field measurements

Visual fields were recorded using the Humphrey Field Analyzer (Carl Zeiss Meditec, Dublin, California, USA) running the 30-2 program SITA (Swedish Interactive Threshold Algorithm)-Fast, a standard method for the examination of the 30 degree central visual field. In this type of measurement, the subject is facing a white illuminated sphere, on which points of light with varying intensities are briefly flashed. The subject has to fixate a set of centrally positioned fixation points during the measurement. Stimuli are presented one by one on a grid in the central 30 degrees of the visual field. Subjects respond when they perceive the flash. The sensitivity at each location in the visual field is determined by changing the intensity of the flash on subsequent presentations. Each eye is measured independently, one eye is covered while the other is tested.

To assess the relationship between the reduction in visual field sensitivity and changes in cortical grey matter density, for each group, mean sensitivity deviation maps were calculated. This was done in two steps. First, for each subject, a combined visual field map was created by taking at each

position the smallest sensitivity deviation from the left and right eye's monocular measurements. Second, the combined maps from all subjects in a group were averaged to yield an average binocular sensitivity deviation map for each group.

2.2.3. Magnetic resonance imaging

High-resolution magnetic resonance imaging was performed on a 3.0 Tesla Philips Intera (Eindhoven, The Netherlands). A three-dimensional structural image was acquired on each subject using a T_1-weighted magnetisation sequence T1W/3D/TFE-2, 8 degrees flip angle, repetition time 8.70 ms, matrix size 256 x 256, field of view 230 x 160 x 180, yielding 160 slices, voxel size 1x1x1 mm.

2.2.4. Voxel-based morphometric analysis

We performed voxel-based morphometry analysis[20], which is part of the SPM5 (Statistical Parametric Mapping) software (Wellcome Department Imaging Neuroscience, London, UK; http://www.fil.ion.ucl.ac.uk/spm). Voxel-based morphometry statistically assesses local changes in grey matter density between groups of anatomical scans. The brain images were registered to the International Consortium for Brain Mapping space template. Using the standard segmentation protocol in SPM5, each voxel was classified into one of the 3 different tissues: grey matter, white matter and cerebrospinal fluid. Non-brain voxels were excluded from the statistical analysis by applying a brain mask. Finally, the images resulting from the segmentation were smoothed with a gaussian kernel of 10-mm full-width at half-maximum.

For the statistical analysis, two contrasts were defined, the first comparing grey matter density in the AMD group and the control group, the second comparing grey matter density in the glaucoma group and the control group. Even though the participant groups were age-matched, there were some slight differences in the age distribution. The subjects' age was therefore added as a covariate to the analysis as an additional measure to control for any potential remaining effect of age.

2.2.5. Volume of interest based analysis

In addition to the voxel-based morphometric analysis, an anatomical volume-of-interest (VOI) analysis was performed. For this analysis, in each individual participant, 21 mm diameter sphere VOIs were defined at the location that corresponded to the approximate expected anatomical position of the foveal and peripheral visual field representations. In each hemisphere, posterior (at the occipital pole; foveal projection zone) and anterior (approximately 10 mm posterior to the junction of parieto-occipital and calcarine sulci) VOIs were defined in both the superior and inferior banks of the calcarine sulcus. Mean grey matter density values were extracted from each subject's grey matter for each VOI and averaged over groups. For each VOI, relative grey matter densities were calculated for the AMD and glaucoma group by dividing mean grey matter values by those of the control group. Analysis of variance was used to examine the interaction between the factors group (AMD and glaucoma) and cortical location (posterior and anterior).

2.3. Results

2.3.1. Binocular visual fields

Figure 1 shows the binocular sensitivity deviation maps for six representative subjects, three from each group. Based on the individual maps, for each group a mean binocular sensitivity deviation map was calculated. These mean maps are shown in Figure 2D and 3D.

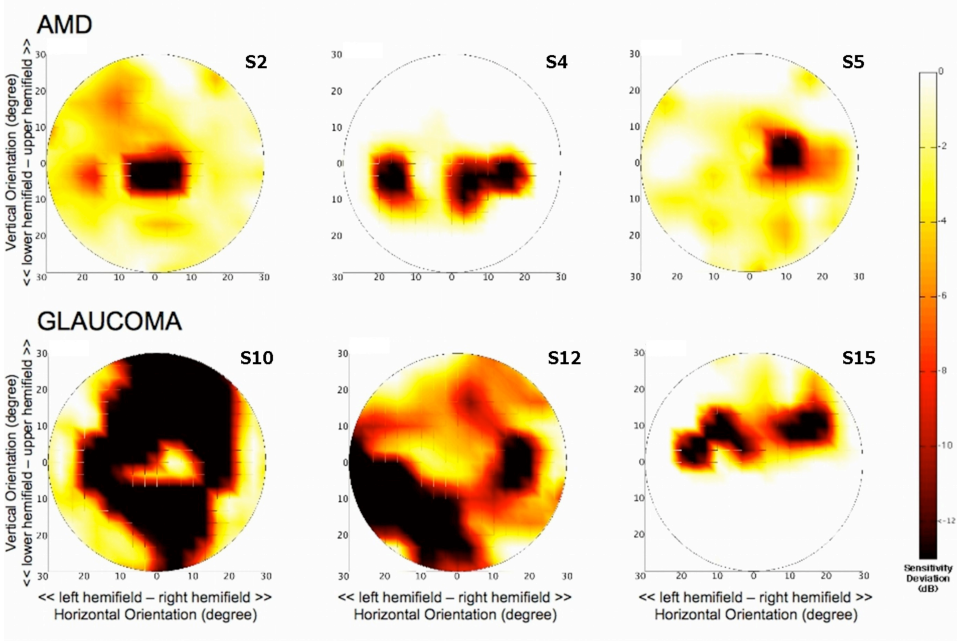

Figure 1. Individual binocular sensitivity deviation maps. Upper row shows maps for three representative subjects from the age-related macular degeneration (AMD) group, the lower row shows maps for three subjects with glaucoma. Subject numbers correspond to those in Table 1.

2.3.2. Visual cortex grey matter density

Figure 2D shows the mean visual field sensitivity deviation map for the AMD group. A reduction in sensitivity is evident centrally on and near the location of the fovea (< -6 dB). Figure 2A-C show the comparison of grey matter density in the AMD group compared to controls superimposed on the mean anatomical image of all subjects. In subjects with AMD, grey matter density is reduced compared to the control group. This main reduction in density is located near the occipital pole (primarily in the left hemisphere), particularly around the posterior part of the calcarine fissure ($p<0.001$). Figure 3D indicates that in the glaucoma group, mean visual field sensitivity is markedly reduced in the periphery of the visual field, in both the upper and lower hemifields (< -8 dB). Importantly, in contrast to the AMD group, the sensitivity is relatively spared in the macular region. Figure 3A-C show the comparison of grey matter density between the glaucoma and control groups. The results indicate the presence of a bilateral reduction of grey matter density on the medial aspect of the occipital lobe, at the anterior half of the calcarine fissures ($p<0.001$).

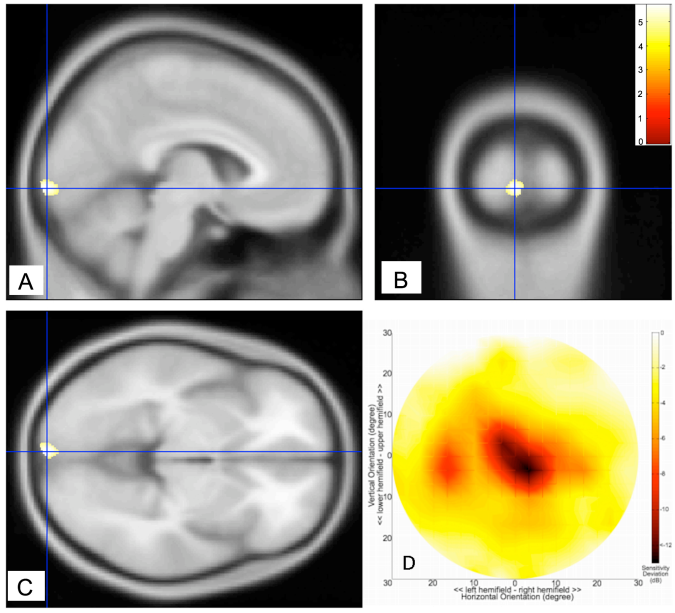

Figure 2. Analysis of subjects with age-related macular degeneration. A-C: sections of the brain showing regions of grey matter density reduction. Colours indicate statistical significance (t-values), with red indicating more significant changes, and yellow/green indicating less significant changes (all changes are at least p<0.001, uncorrected). D: mean visual field sensitivity deviation (in dB). The largest change in sensitivity is located centrally in the visual field. dB – decibel.

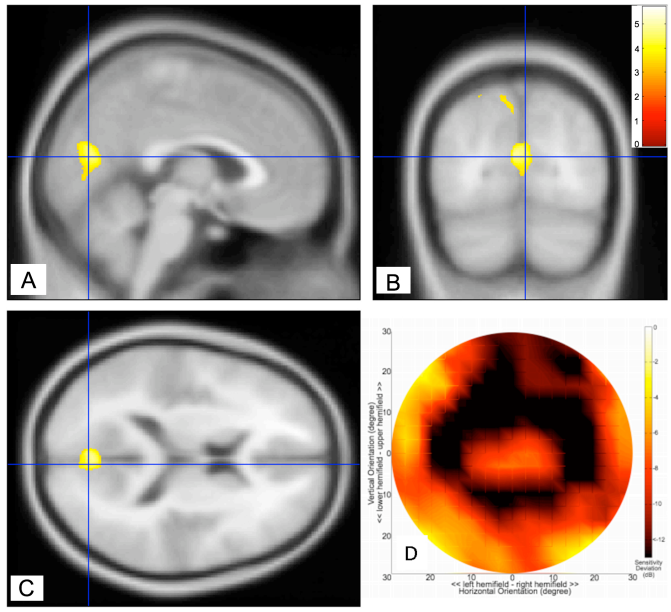

Figure 3. Analysis of subjects with glaucoma. A-C: sections of the brain showing the regions of grey matter density reduction. Colours indicate statistical significance (t-values), with red indicating more significant changes, and yellow/green indicating less significant changes (all changes are at least p<0.001, uncorrected). D: mean visual field sensitivity deviation (in dB). The largest changes in sensitivity are located peripherally in the visual field, leaving the macular region relatively unaffected. dB – decibel.

Figure 4 shows the results of an additional volume-of-interest based analysis. For this analysis, on each participant's brain, small sphere VOIs were defined that correspond to the approximate anatomical projection zones of the fovea and peripheral visual field. For each participant group, average relative grey matter density in the anterior and posterior VOIs is plotted. This analysis confirms the results of the voxel-based morphometric analysis. In the AMD group, the relative grey matter density is more reduced in the posterior than in the anterior region. The glaucoma group shows exactly the opposite result. Relative grey matter density is more reduced in the anterior than in the posterior region. This interaction was statistically significant ($p<0.01$).

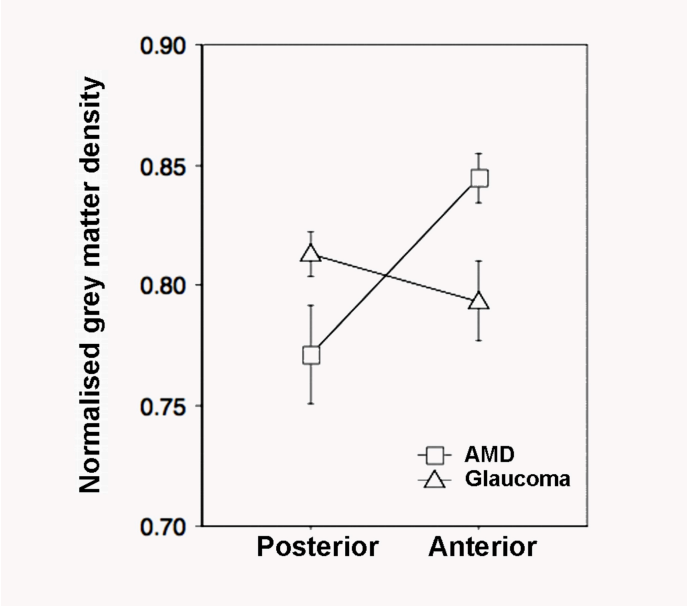

Figure 4. Results from a volume-of-interest based analysis. Relative change in grey matter density for the age-related macular degeneration and glaucoma groups compared to the control group in anatomically defined volumes of interest in posterior (approximate foveal projection zone) and anterior (approximate peripheral visual field projection zone) visual cortex. Relative changes were calculated by dividing for each participant group the averaged grey matter density in each volume-of-interest by that of the control group.

Figure 5 summarises the main results of this study, and shows the pattern of decrements in grey matter density in the glaucoma and AMD groups, as well as their respective (thresholded) sensitivity deviation maps. Retinotopically, the pattern of grey matter reduction that we find in our study correlates well with the pattern of changes in visual field sensitivity in both types of pathology. In AMD, the reduction in visual field sensitivity is most pronounced in the foveal region (Figure 5A). Corresponding with this, the focus of grey matter reduction in this group is located near the posterior pole of the occipital cortex (Figure 5A).

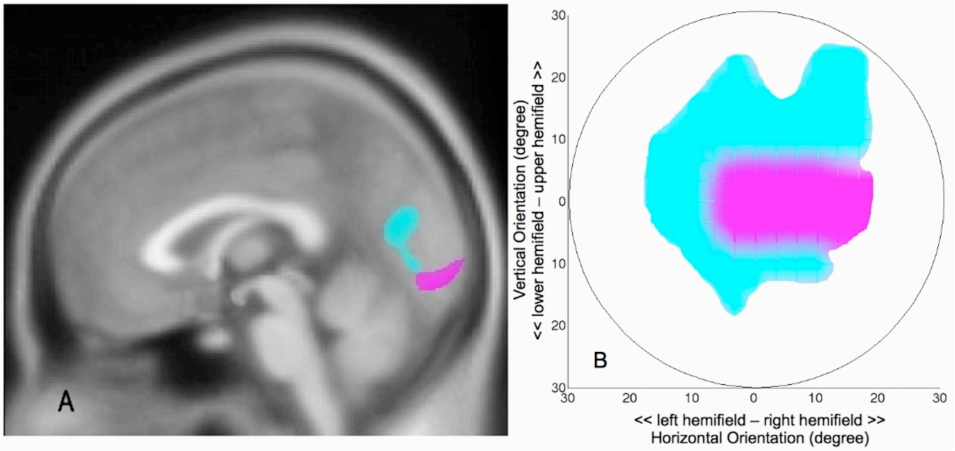

Figure 5. Summary of visual field sensitivity and grey matter reduction in age-related macular degeneration (AMD) and glaucoma. A: cortical grey matter density reduction in glaucoma is found in the anterior half of the medial occipital cortex (cyan). Cortical grey matter density reduction in AMD (magenta) is found in the posterior part of the occipital cortex. B: thresholded mean visual field sensitivity deviation maps indicating central defects in AMD (magenta) and more peripheral defects in glaucoma (cyan). For this thresholded map, for the glaucoma group, sensitivity deviations below –12 dB are shown in cyan. For the AMD group, sensitivity deviations below –8 dB are shown in magenta.

In glaucoma, the main reductions in visual field sensitivity are located more peripherally (Figure 5B). Consistent with this, the focus of the grey matter reduction in this group is located more anterior in occipital cortex (Figure 5A).

2.4. Discussion

The main finding of this study is that visual field defects caused by long-standing retinal pathology due to glaucoma and age-related macular degeneration (AMD) are associated with reductions in grey matter density in occipital cortex. Moreover, in both the AMD and glaucoma participant groups, the location of the grey matter density reduction corresponded with the approximate visual field defect projections in visual cortex. The more central scotoma of the AMD subjects correlated with a reduction located more posteriorly in occipital cortex, in correspondence with the location of the foveal representation in visual cortex. The difference was more pronounced in the left hemisphere. In agreement, the sensitivity deviation map shows a macular defect that was more pronounced in the right visual field. The more peripherally located scotoma in the glaucoma subjects correlated with a reduction of grey matter density located more anterior in occipital cortex. This is in correspondence with the location of the cortical representation of the peripheral visual field. Therefore, our results suggest that retinal visual field defects acquired later in life can lead to retinotopically specific grey matter density reduction in visual cortex.

An earlier report on this study[21] reported no significant difference in grey matter density between the AMD and control groups. The analysis carried out in this preliminary report used SPM99 rather than SPM5 as in the present study. The difference in results can be attributed to improvements in the segmentation process where SPM5 reaches a more detailed segmentation than SPM99. The segmentation process in SPM5 takes advantage of a spatial normalisation that does not rely on the simple relationship between the intensities of two images. The segmentation is

achieved by warping tissue probability maps in order to overlay them on to the image to segment. The obtained spatially normalised tissue class images of each subjects are averaged and used as prior probabilities for each voxel to belong to a particular tissue class[22]. Since this procedure is more refined and accurate, we report here the results obtained with SPM5. Nevertheless, we believe that discrepancies in results originating from differences in analyses should be considered serious issues and hence be reported.

Our present results indicate a good correspondence between the locations of the mean scotoma and the cortical regions showing a reduction in grey matter density. When examining the results at a more detailed level, however, a number of factors may contribute to uncertainty (and thus deviations) in the correspondence. First, we rely on normalisation of the brains of the subjects. Normalisation, in particular in occipital cortex, is delicate due to anatomical variability. Second, there will be differences in how the functional visual field maps onto the anatomy. Third, we show the grey matter density reductions on the mean anatomical image of all participants. Each participant's contribution to the average anatomy is equal. Yet, the contribution to the group's focus of the density reduction is not necessarily equal for each participant. Fourth, the extent of the cortical regions showing a reduction varies with the statistical threshold used. Finally, it is not *a priori* clear when (in terms of sensitivity deviation and diameter) a retinal scotoma will result in a reduction of grey matter density. We have here, for both the participant selection and analysis of the visual field, made the assumption that this is only in case of relatively large, homonymous scotoma. For this reason, we computed the binocular maps for individual participants using the minimum deviation in sensitivity and averaged these. Yet, grey matter density reduction may occur for monocular defects as well. A more extensive analysis including patients with different (also monocular) field defects would be required to indicate precisely how depth and extent of the retinal lesion is related to changes in grey matter density and functional anatomy of the visual cortex.

This study involved older participants, so the possibility that the reported changes are simply due to ageing effects should be considered. Salat and colleagues showed that cortical thinning due to ageing may involve the primary visual cortex among other cortical areas, although the correlation with age was only weak[23]. Raz and colleagues confirmed that regional volume change due to ageing in the visual cortex is very weak[24]. To control for possible ageing effects, we made sure that the groups were on average age-matched. Our volume-of-interest based analysis indicates a slight overall reduction in grey matter density in both patient groups compared to the control group, in addition to the specific scotoma related reductions. In the voxel-based comparisons of cortical grey matter density we included age as a covariate to remove any age-related residual influences. Hence, we are confident that the present results are not merely due to age. The generalised reduction in grey matter density observed in the VOI based analysis could be due to variability in the field defects. The defects in both patient groups, although primarily centrally located for AMD and more peripherally for glaucoma patients, do show some spreading between individual subjects (see Figure 1). Grey matter density reduction related to field defects that vary between the individual members of a patient group could show up as a generalised effect. Nevertheless, for each patient group the location of the focus of the grey matter density reduction clearly corresponds to the expected lesion projection zone of mean visual field defect (Figure 2, 3 and 5).

We believe this to be the first report that establishes a firm relationship between acquired retinal visual field loss and grey matter degeneration in human visual cortex. An earlier magnetic resonance imaging study, had suggested calcarine atrophy to be related to retinal degeneration[13]. However, the participants in this study had not only widely varying retinal pathology, but also a relatively coarse measure of degeneration was used (width of the calcarine sulcus). Since no segmentation of grey and white matter was performed the findings need not be due to grey matter degeneration. A post-mortem study reported to have found a reduction of the cortical ribbon thickness in the visual cortex in glaucoma. However, this study reported on anatomical and histological examination of a single subject only[12].

In glaucoma, cortical degeneration can be interpreted as a result of the loss of retinal ganglion cells. The atrophy from damaged parts of the retina likely propagates by means of transneuronal degeneration through the optic nerve towards the cortex thereby provoking its subsequent degeneration. Experimentally, this sequence of events has been shown to occur in cats and monkeys where the retina was experimentally injured by an induced elevated intra-ocular pressure[25].

In AMD, the relationship between retinal pathology and cortical degeneration might be slightly more indirect, in that photoreceptor damage may first lead to retinal ganglion cell loss. It has been shown that the retinal ganglion cell count is significantly lower in wet AMD than in otherwise healthy eyes[26]. Eyes with geographic atrophy due to AMD also have lower count of retinal ganglion cells[27]. In agreement with the idea that cortical atrophy is linked to a reduction in retinal ganglion cell count and optic nerve damage, a voxel-based morphometry study reported abnormally reduced grey matter volume at the occipital poles of a group of human albinos[11]. There is no direct evidence demonstrating that retinal ganglion cell loss occurred in our AMD group. However, a reduction in visual field sensitivity is linked to retinal ganglion cell loss and not to other components of the neuro-retina[28, 29]. Moreover, foveal sensitivity is greatly reduced in AMD. Together, this suggests the possibility that retinal ganglion cell loss does occur in AMD-associated visual field defects. This loss could be responsible for the cortical degeneration we have observed.

A number of studies have examined whether functional reorganisation accompanies retinal lesions. Thus far, reports have presented conflicting results with some groups reporting an absence of reorganisation[18, 19] and others reporting its presence[16]. This difference in findings has recently been attributed to differences in stimuli and tasks used in the various studies[17]. More cognitively engaging tasks appear to result in feedback signals from later visual areas that also drive neuronal activity in the lesion projection zones. Such feedback signals appear absent in visually healthy subjects. While one could argue that this indicates a form of functional reorganisation, it leaves open the question whether the lesion projection zone of primary visual cortex is still able to process retinal signals. This question is particular relevant given the rapid developments in retinal prostheses. Our study indicates a reduction in grey matter in the approximate lesion projection zones of primary visual cortex. Given that feedback signals still appear to be processed, we speculate that the grey matter reduction reported on here could be selective to the input layers of primary visual cortex.

In summary, this study shows that long-standing visual field defects due to retinal pathology are associated with retinotopic specific grey matter reduction in early visual cortex. These findings contribute to the understanding of brain plasticity at later age. Besides, from a clinical point of view, a better understanding of the

relation between retinal visual field defects and structural changes in visual cortex may help understand disease symptoms as well as their progression. For instance, cortical degeneration may limit the efficacy of rehabilitation and training programs[30], retinal prostheses[31], and may require new therapeutic strategies[32, 33] to prevent blindness. Prevention of cortical degeneration associated with eye diseases may also need to become a new therapeutic goal.

Acknowledgements

The first and second authors contributed equally to this study. A.T.H is supported by the "RuG Fellowship Program" and C.C.B. is supported by an Ubbo Emmius grant, both from the University of Groningen, The Netherlands. This work was supported by Uitzicht and an equipment grant from the Prof. Mulder foundation. The authors want to thank the BCN Neuroimaging center for the use of their scanner, Hans Hoogduin and Anita Kuiper for assistance in magnetic resonance scan accquisition, Michiel Kunst for assistance in setting up the voxel-based morphometry analysis, Shriprakash Sinha for assistance with the region of interest analysis, Remco Renken for fruitful suggestions regarding data analysis, and Martin Pavlovsky for contributing to the discussion.

Bibliography

1. Resnikoff S, Pascolini D, Etya'ale D, et al. Global data on visual impairment in the year 2002. Bull World Health Organ 2004;82(11):844-51.
2. Holz FG, Pauleikhoff D, Klein R, Bird AC. Pathogenesis of lesions in late age-related macular disease. Am J Ophthalmol 2004;137(3):504-10.
3. Zarbin MA. Current concepts in the pathogenesis of age-related macular degeneration. Arch Ophthalmol 2004;122(4):598-614.
4. Nickells RW. Retinal ganglion cell death in glaucoma: the how, the why, and the maybe. J Glaucoma 1996;5(5):345-56.
5. Fechtner RD, Weinreb RN. Mechanisms of Optic-Nerve Damage in Primary Open-Angle Glaucoma. Survey of Ophthalmology 1994;39(1):23-42.
6. Dougherty RF, Koch VM, Brewer AA, et al. Visual field representations and locations of visual areas V1/2/3 in human visual cortex. J Vis 2003;3(10):586-98.
7. Horton JC, Hoyt WF. The representation of the visual field in human striate cortex. A revision of the classic Holmes map. Arch Ophthalmol 1991;109(6):816-24.
8. Johansson BB. Brain plasticity in health and disease. Keio J Med 2004;53(4):231-46.
9. Merzenich MM, Nelson RJ, Stryker MP, et al. Somatosensory cortical map changes following digit amputation in adult monkeys. J Comp Neurol 1984;224(4):591-605.
10. Mendola JD, Conner IP, Roy A, et al. Voxel-based analysis of MRI detects abnormal visual cortex in children and adults with amblyopia. Hum Brain Mapp 2005;25(2): 222-36.
11. von dem Hagen EA, Houston GC, Hoffmann MB, et al. Retinal abnormalities in human albinism translate into a reduction of grey matter in the occipital cortex. Eur J Neurosci 2005;22(10):2475-80.
12. Gupta N, Ang LC, Noel de Tilly L, et al. Human glaucoma and neural degeneration in intracranial optic nerve, lateral geniculate nucleus, and visual cortex. Br J Ophthalmol 2006;90(6):674-8.
13. Kitajima M, Korogi Y, Hirai T, et al. MR changes in the calcarine area resulting from retinal degeneration. AJNR Am J Neuroradiol 1997;18(7):1291-5.
14. Acaroglu G, Tali T, Batman A, et al. Comparative study of brain magnetic resonance imagings in normal tension glaucoma, primary open-angle glaucoma, and normal subjects. Neuro-Ophthalmology 2001;26(2):103-7.
15. Gupta N, Greenberg G, de Tilly LN, et al. Atrophy of the lateral geniculate nucleus in human glaucoma detected by magnetic resonance imaging. Br J Ophthalmol 2009;93 (1):56-60.
16. Baker CI, Peli E, Knouf N, Kanwisher NG. Reorganization of visual processing in macular degeneration. J Neurosci 2005;25(3):614-8.

17. Masuda Y, Dumoulin SO, Nakadomari S, Wandell BA. V1 projection zone signals in human macular degeneration depend on task, not stimulus. Cereb Cortex 2008;18(11): 2483-93.
18. Smirnakis SM, Brewer AA, Schmid MC, et al. Lack of long-term cortical reorganization after macaque retinal lesions. Nature 2005;435(7040):300-7.
19. Sunness JS, Liu T, Yantis S. Retinotopic mapping of the visual cortex using functional magnetic resonance imaging in a patient with central scotomas from atrophic macular degeneration. Ophthalmology 2004;111(8):1595-8.
20. Ashburner J, Friston KJ. Voxel-based morphometry--the methods. Neuroimage 2000;11(6 Pt 1):805-21.
21. Boucard CC. Neuro-imaging of visual field defects. 2006. ISBN: 90-367-2621-2
22. Ashburner J, Friston KJ. Unified segmentation. Neuroimage 2005;26(3):839-51.
23. Salat DH, Buckner RL, Snyder AZ, et al. Thinning of the cerebral cortex in aging. Cereb Cortex 2004;14(7):721-30.
24. Raz N, Lindenberger U, Rodrigue KM, et al. Regional brain changes in aging healthy adults: general trends, individual differences and modifiers. Cereb Cortex 2005;15(11): 1676-89.
25. Yucel YH, Zhang Q, Weinreb RN, et al. Effects of retinal ganglion cell loss on magno-, parvo-, koniocellular pathways in the lateral geniculate nucleus and visual cortex in glaucoma. Prog Retin Eye Res 2003;22(4):465-81.
26. Medeiros NE, Curcio CA. Preservation of ganglion cell layer neurons in age-related macular degeneration. Invest Ophthalmol Vis Sci 2001;42(3):795-803.
27. Kim SY, Sadda S, Humayun MS, et al. Morphometric analysis of the macula in eyes with geographic atrophy due to age-related macular degeneration. Retina 2002;22(4):464-70.
28. Garway-Heath DF, Caprioli J, Fitzke FW, Hitchings RA. Scaling the hill of vision: the physiological relationship between light sensitivity and ganglion cell numbers. Invest Ophthalmol Vis Sci 2000;41(7):1774-82.
29. Swanson WH, Felius J, Pan F. Perimetric defects and ganglion cell damage: interpreting linear relations using a two-stage neural model. Invest Ophthalmol Vis Sci 2004;45(2): 466-72.
30. Safran AB, Landis T. Plasticity in the adult visual cortex: implications for the diagnosis of visual field defects and visual rehabilitation. Curr Opin Ophthalmol 1996;7(6):53-64.
31. Hossain P, Seetho IW, Browning AC, Amoaku WM. Artificial means for restoring vision. BMJ 2005;330(7481):30-3.
32. Gupta N, Yucel YH. Should we treat the brain in glaucoma? Can J Ophthalmol 2007;42 (3):409-13.
33. Taub E, Uswatte G, Elbert T. New treatments in neurorehabilitation founded on basic research. Nat Rev Neurosci 2002;3(3):228-36.

Chapter 3

Morphometric analyses of the visual pathway in macular degeneration

Based on:
Hernowo AT, Prins D, Baseler HA, Plank T, Greenlee MW, Morland AB, Hooymans JMM, Cornelissen FW. Morphometric analyses of the visual pathway in macular degeneration. *To be submitted.*

ABSTRACT

Macular degeneration causes central visual field loss and there have been reports on its effect on the functionality of the primary visual cortex. In this multicentre study, we used voxel-based morphometry on high resolution anatomical images to investigate the visual pathway structure of subjects with age-related and juvenile type macular degeneration (AMD and JMD, respectively). Compared to healthy controls, subjects with any type of macular degeneration showed lower volume of the visual pathway. However, the involvement of the pathway is more extensive in JMD group, starting from the pregeniculate structures up to the primary visual cortex. These findings showed that the presence macular degeneration is associated negatively with the structure of the visual pathway.

Chapter contents

3.1. Introduction

World Health Organization indicated that in 2002 there were almost *37* millions (0.57%) blind people and another 124 millions (2%) had to live with low vision in the world, with age-related macular degeneration (AMD) and childhood blindness being the causes of the blindness in 8.7% and 3.9% of cases, respectively[1]. In Europe, retinal pathologies have been in the top five causes of visual loss in both childhood and adulthood[2], and from those, AMD has again been the most common culprit in the adult population[3].

Similar macular pathologies to AMD may start early in childhood or teenage, yet there is no singular disease entity. They are mostly inherited and since they start early in life, their period of illness are longer than of AMD. Commonly referred as juvenile-type macular degeneration (JMD), they include Stargardt's disease, Best's vitelliform retinal dystrophy (Best's disease), cone-rod dystrophy, central areolar choroidal dystrophy, and others. Visual field loss in both type of macular degeneration is primarily due to the loss of photoreceptors. While in JMD the pathology varies, the accumulation of sub-macular deposit called drusen in AMD compromise retinal metabolism and leading to the degeneration of the macula with or without neovascularization[4-7].

Structural brain changes due to non-use (no afferent or efferent) have also been reported in many conditions[8, 9]. Macular degeneration produces central visual field defect (central scotoma), which binocular overlaps lead to non-stimulation of the visual cortex[10, 11], which may further changes the visual cortex structure[12]. Various retinal and optic nerve conditions are indeed found to be associated with cortical changes as thinning or grey matter loss[12-14], and as well as with the more proximal visual pathway structures as volumetric reduction[15]. These findings might indicate that the visual pathway structures are vulnerable to retinal and optic nerve pathologies, such as macular degeneration and glaucoma. This in turn raised a question whether macular degeneration might also affect the structural integrity of the the visual pathways. If it does affect the pathway, the clinical practice pattern in macular degeneration management might need to adapt itself in the best interest of the patients. This question is also relevant given conflicting reports on the presence of functional occipital reorganisation following retinal lesions[10, 16-21]. Here, we reported our investigation on the visual pathway structure morphometry in macular degeneration patients and healthy control individuals.

3.2.1. Subjects

Participants of this study were recruited from three university medical centres: York (United Kingdom), Regensburg (Germany), and Groningen (the Netherlands). This study conformed to the tenets of the Declaration of Helsinki and was approved by the respective medical review board of each centres in the study. The inclusion criteria required that subject must be free from neurological or psychiatric disorders, and having central visual field defect attributed to macular degeneration. All participants gave their written informed consent before participation. The participants with macular degeneration were classified into two groups: the ones with the juvenile type of macular degeneration (JMD) and the ones with the age-related type (AMD). In the beginning, there were 114 subjects participating in this study: 25 with AMD, 34 with JMD, whereas the remaining 55 were the healthy controls. However, one subject with AMD decided to quit the study, leaving in total 113 included in the analyses.

The control subjects mean age was 49.6 years (range 13 to 83 years), and 46% of them were males. From those controls, 22 subjects were age-matched (mean age 68, range 61-83 years) to AMD group. The other 33 subjects (mean age 37.4, range 13 - 60 years) were age matched to the JMD. The characteristics of the affected participants were described in the Table 1.

Characteristics	Values	
	AMD	JMD
Number of subjects	24	34
Age, mean (range), years	75.2 (52 - 91)	40.2 (12 - 66)
Female, sex, %	42	38
Visual acuity in logMAR, mean (range)		
OD	0.96 (1.60 - 0.50)	1.12 (3.00 - 0.30)
OS	0.88 (1.80 - 0.10)	1.16 (3.00 - 0.66)
Scotoma diameter, mean (range), degree	14 (4 - 25)	20 (3 - 65)

Table 1. Baseline patient characteristics. Characteristics of the two patient groups (AMD and JMD) were age, sex proportion (in percentage), visual acuity for one or both eyes (expressed in logMAR), and scotoma diameter (expressed in degree). AMD – age-related macular degeneration; JMD – juvenile type macular degeneration; logMAR – logarithm of minimum angle of resolution; OD - right eye (oculus dexter); OS - left eye (oculus sinister).

3.2.2. Magnetic resonance data analyses

Since the datasets were from three different study centres, the acquisition parameters were different. However, all of the acquisitions were of 1 mm × 1 mm × 1 mm resolution. Magnetic resonance (MR) imaging were done in three different scanners. *Groningen* datasets were acquired on a 3.0 Tesla Philips Intera (Eindhoven, The Netherlands), at the MRI Centrum, University Medical Center Groningen. A three-dimensional structural image was acquired on each subject using a sequence T1W/3D/TFE-2, 8° flip angle, repetition time 8.70 ms, matrix size 256 × 256, field of view 230 × 160 × 180, yielding 160 slices. *York* dataset were acquired using 8-channel, phase- array head coils on either a Siemens Trio 3 Tesla at the Combined Universities Brain Imaging Center (Royal Holloway University of London), or on a GE 3-Tesla Signa HD Excite scanner at the York Neuroimaging Center (University of York). Multi-average, whole-head T1-weighted anatomical volumes were acquired for each participant. Sequences used were 3D-MDEFT on the Siemens Trio or 3D-FSPGR on the GE Signa. *Regensburg* dataset were acquired on a 3.0 Tesla Allegra Scanner (Siemens, Erlangen, Germany). One hundred and sixty slices covering the whole brain, FOV=256×256 mm2 were obtained from each subject, using the ADNI sequence (TR = 2250 ms, TE = 2.6 ms, flip angle 9°) taken at Laboratory for Neuro Imaging, UCLA, Los Angeles, US.

We defined six regions-of-interest (ROIs) along the visual pathway: pregeniculate structures (pgcl), lateral geniculate bodies (lgb), geniculocalcarine radiation (gcr), occipital pole (ocp), the intracalcarine (icc) and supracalcarine regions (scc). For the first three ROIs, the brain images were cropped so that the desired ROI is captured with minimum extra-ROIs structure. For the second three ROIs, the occipital lobes of the brains were cropped and used. The image processing involved the following steps: rigid-body registration, segmentation, registration, and modulation of the segments. Image processing for the AMD group and its age-matched controls were done separately from the JMD group and its age-matched controls. Finally volumetric comparison of different tissue segments between the patients and control groups within the visual pathway were performed. The process from the segmentation to the voxelwise statistical analyses is known as voxel-based morphometry or VBM, which is implemented in SPM8 software package (Wellcome Department of Imaging Neuroscience, London, UK; http://www.fil.ion.ucl.ac.uk/spm)[22]. VBM statistically assesses local changes in grey and/or white matter volumes between groups of anatomical scans. The steps in the data analysis procedure are described in more detail below.

3.2.2.1. Bias correction and noise reduction

The images were converted from their raw formats into analysable (NIFTI) format. We performed bias correction (implemented in SPM8 segmentation tool) and noise reduction using SUSAN (Smallest Univalue Segment Assimilating Nucleus)[23] prior to the next steps. SUSAN is available for free as a part of FSL (FMRIB Software Library).

3.2.2.2. Rigid body registration

We performed rigid body registration on the brains to a common template using SPM8's tool for co-registration. In this step, the brains are reoriented into the common template space using six linear transformation parameters: 3 translations and 3 rotations. All transformations are performed within 3-dimensional coordinate, with x, y, and z as its axes. This rendered the images to have uniform dimensions and to be in approximate orientation to each other.

3.2.2.3. Segmentation, registration, and modulation

We used SPM8's DARTEL (Diffeomorphic Anatomical Registration through Exponentiated Lie Algebra) suite of tools[24, 25]. DARTEL tools enabled us to create modulated gray and white matter images that were registered to a common reference image specifically representing our sample. The study-specific approach we used here enabled a more accurate inter-subject registration of brain images with improved localization and sensitivity of the VBM.

The process began with SPM8's segmentation which segmented the co-registered T_1-weighted images, except for lateral geniculate bodies extraction. For the latter structure, we used FAST (FMRIB's Automated Segmentation Tool) and feed the output into the DARTEL pipeline. After all the brains were segmented, a reference –or template– image was generated. The first step in generating this reference image was averaging the images of all brains. Following this, the individual brains were deformed and registered as closely as possible to this reference image. Next, using the registered brain images, a new average reference image was created to which the individual brain images were again registered. After 6 of these averaging and registration cycles, the final reference image was generated. The final reference image was then used as the template to which the native segmentations of the individual brains in the study were registered and modulated.

3.2.2.4. Statistical analyses

There were three groups in the model: controls, AMD, and JMD. Group comparisons were performed while taking into account the age as covariates. We performed two type of analyses: (1) region-of-interest or ROI-based analysis; and (2) voxel-wise analyses. In ROI-based analysis, we used masks to extract the ROI volumes and investigate the distribution of the extracted values prior to choosing the appropriate statistical analysis. The ROI volumes were extracted from modulated normalised brain segments. While in voxel-wise analyses, we compared the brains voxel by voxel along the visual pathway.

As we had mentioned earlier, the six ROIs we compared are *pgcl, lgb, gcr, ocp, icc,* and *scc*. The masks used to extract the volume of the pregeniculate structures and the lateral geniculate bodies were manually made by the investigator, for the boundaries of those structures are feasible to define visually. The mask for the geniculocalcarine radiation were derived from Jülich histological atlas[26, 27], whereas the mask for the occipital pole, intracalcarine and supracalcarine regions were derived from Harvard Center for Morphometric Analysis[28-31].

The second type of analysis was voxel-wise in nature (VBM). The method made it possible for the investigators to spatially detect any deviation in the pathway. We performed factorial design analyses, with age as a covariate. Comparisons were done separately for the AMD group and its age-matched controls, and the JMD and its age-matched controls. Threshold-free cluster enhancement (TFCE) method were applied to minimize the need of large scale smoothing or of predefining the significant cluster size.

3.3. Results

3.3.1. ROI-based findings

We first illustrate the distribution of the morphometric measurements in all ROIs for every group as boxplots (see Figure 1).

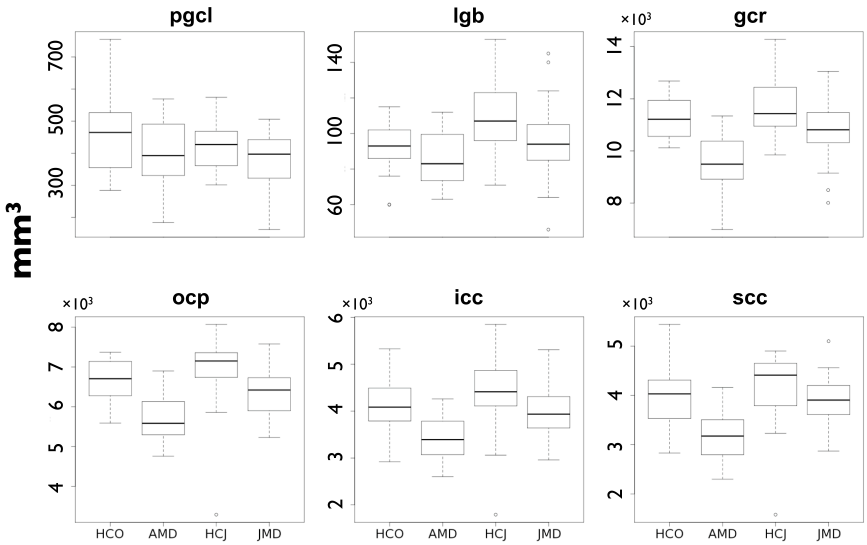

Figure 1. Morphometric comparisons of ROI located along the visual pathway, between the AMD, JMD, and their respective age-matched controls. Boxplots show the median, the 25th and 75th percentiles of all six ROIs. Data were extracted from modulated normalized segments of T1-weighted brain images. ROI - regions of interest; AMD - age-related macular degeneration; HCO - healthy controls (age-matched to AMD); JMD - juvenile type macular degeneration; HCJ - healthy controls (age-matched to JMD); pgcl - pregeniculate structures; lgb - lateral geniculate bodies; gcr - geniculocalcarine radiation; ocp - occipital poles; icc - intracalcarine; scc - supracalcarine.

In all ROIs, the controls have larger median volumes than the patient groups (AMD or JMD). Table 2 describes the mean morphometric values and the patient groups differences relative to their age-matched controls.

	ROI $\mu \pm \sigma_\mu$					
	pgcl (mm^3)	**lgb (mm^3)**	**gcr (cm^3)**	**ocp (cm^3)**	**icc (cm^3)**	**scc (cm^3)**
AMD	401.58 ± 21.94	86.67 ± 3.17	9.51 ± 0.23	5.72 ± 0.12	3.46 ± 0.10	3.20 ± 0.10
HCO	459.41 ± 24.75	91.77 ± 3.02	11.29 ± 0.17	6.64 ± 0.12	4.11 ± 0.14	3.98 ± 0.16
JMD	382.62 ± 13.44	95.94 ± 3.48	10.78 ± 0.18	6.35 ± 0.11	3.99 ± 0.08	3.90 ± 0.08
HCJ	419.06 ± 12.64	109.76 ± 3.49	11.68 ± 0.19	6.95 ± 0.15	4.38 ± 0.13	4.19 ± 0.11
	Relative difference to the controls (%)					
AMD	-12.6	-5.6	-15.8	-13.9	-15.8	-19.6
JMD	-8.7	-12.6	-7.7	-8.6	-8.9	-6.9

Table 1. ROI morphometry. Morphometric values in term of area or volume were extracted from along visual pathway. ROI - regions of interest; μ - mean; σ_μ - standard errors of mean; AMD - age-related macular degeneration; HCO - healthy controls (age-matched to AMD); JMD - juvenile type macular degeneration; HCJ - healthy controls (age-matched to JMD); pgcl - pregeniculate structures; lgb - lateral geniculate bodies; gcr - geniculocalcarine radiation; ocp - occipital poles; icc - intracalcarine; scc - supracalcarine.

We also investigated the distribution of ROI volumes with regards to the distribution of age (Figure 2). In *gcr* and cortical ROIs, age seems to correlate negatively with the morphometric values. We therefore took the age as a covariate in our subsequent voxel-wise analyses.

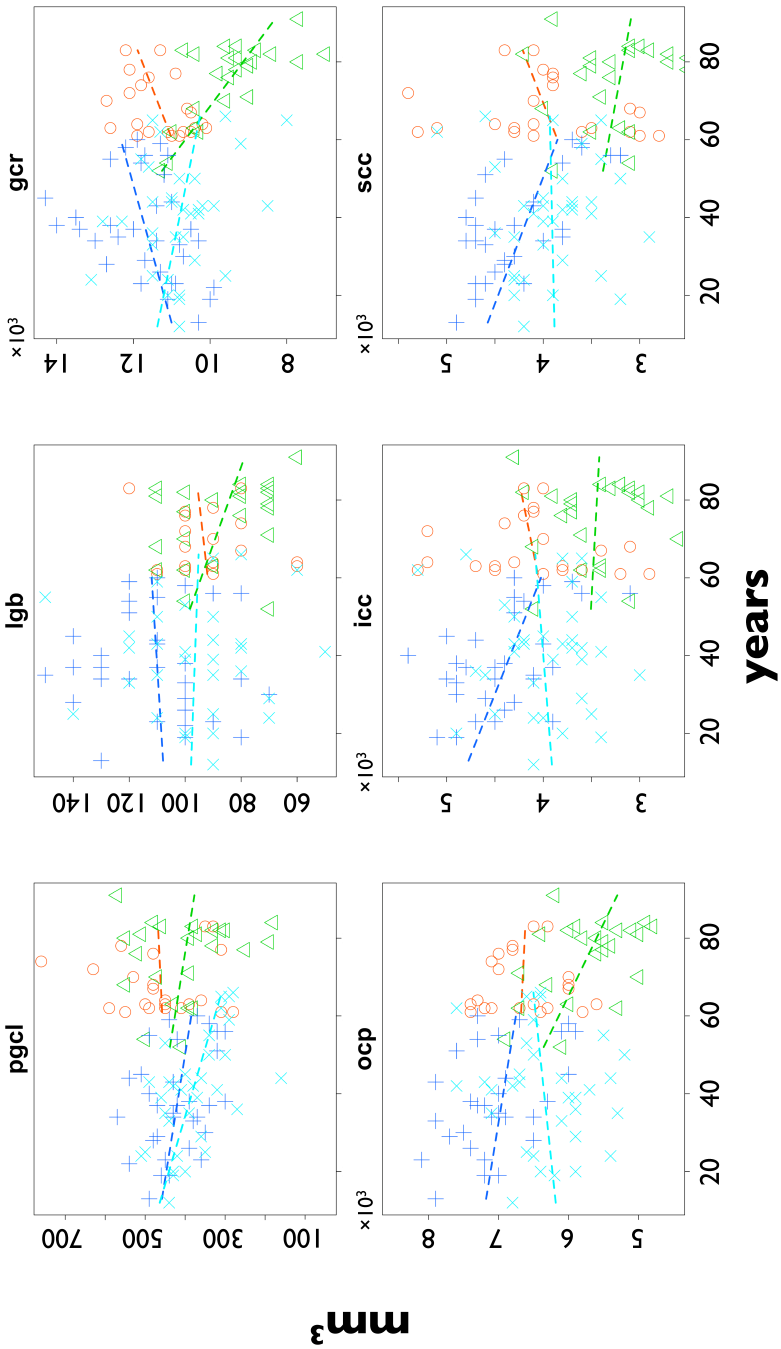

Figure 2. Scatter plots of the volume of ROIs along the visual pathway as against age. Data points were categorized into AMD, JMD, and their respective age matched controls. Morphometry were performed on modulated normalized segments of T1-weighted brain images. ROI - regions of interest; AMD - age-related macular degeneration; HCO - healthy controls (age-matched to AMD); JMD - juvenile type macular degeneration; HCJ - healthy controls (age-matched to JMD); pgcl - pregeniculate structures; lgb - lateral geniculate bodies; gcr - geniculocalcarine radiation; ocp - occipital poles; icc - intracalcarine; scc - supracalcarine.

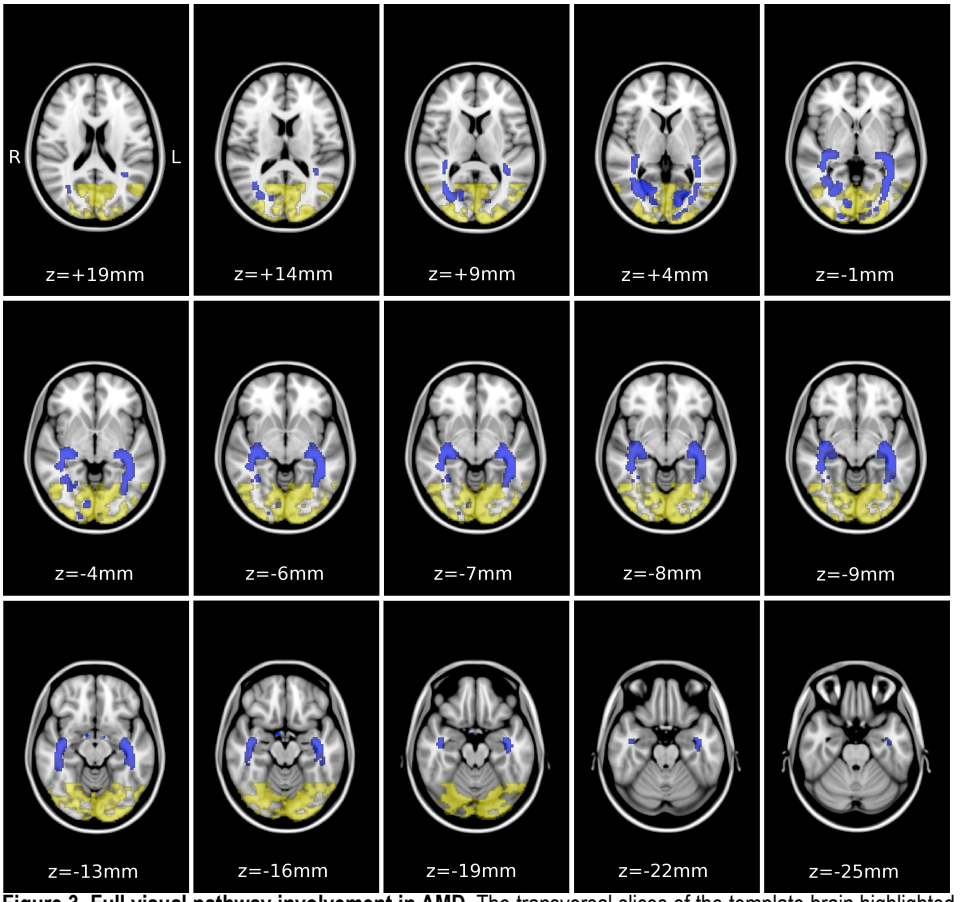

Figure 3. Full visual pathway involvement in AMD. The transversal slices of the template brain highlighted the areas where AMD group shows significantly lower cortical volume their age-matched controls ($p<0.05$, uncorrected). Involvement of the grey matter can be seen in the visual cortex (yellow), whereas white matter involvement can be seen in the optic tract and in region corresponding to the geniculocalcarine radiation (blue). The Talairach position of the slices are given as "z". AMD - age-related macular degeneration.

3.3.2. Voxel-wise findings

Voxel-wise statistics were done in the brain regions of the visual pathway. Figure 3 shows comparison between AMD patients and their age-matched controls, without correction for multiple voxels comparison. Figure 4 shows comparison between JMD patients and their age-matched controls, without correction for multiple voxels comparison.

In both types of macular degeneration, almost the whole retrobulbar afferent visual pathway structures are volumetrically lower than the healthy controls ($p<0.05$, uncorrected). The lateral geniculate bodies in AMD group however, did not show any statistically significant difference to its age-matched control. We then performed similar comparison, this time with small volume family-wise error correction. The result can be seen in Figure 5.

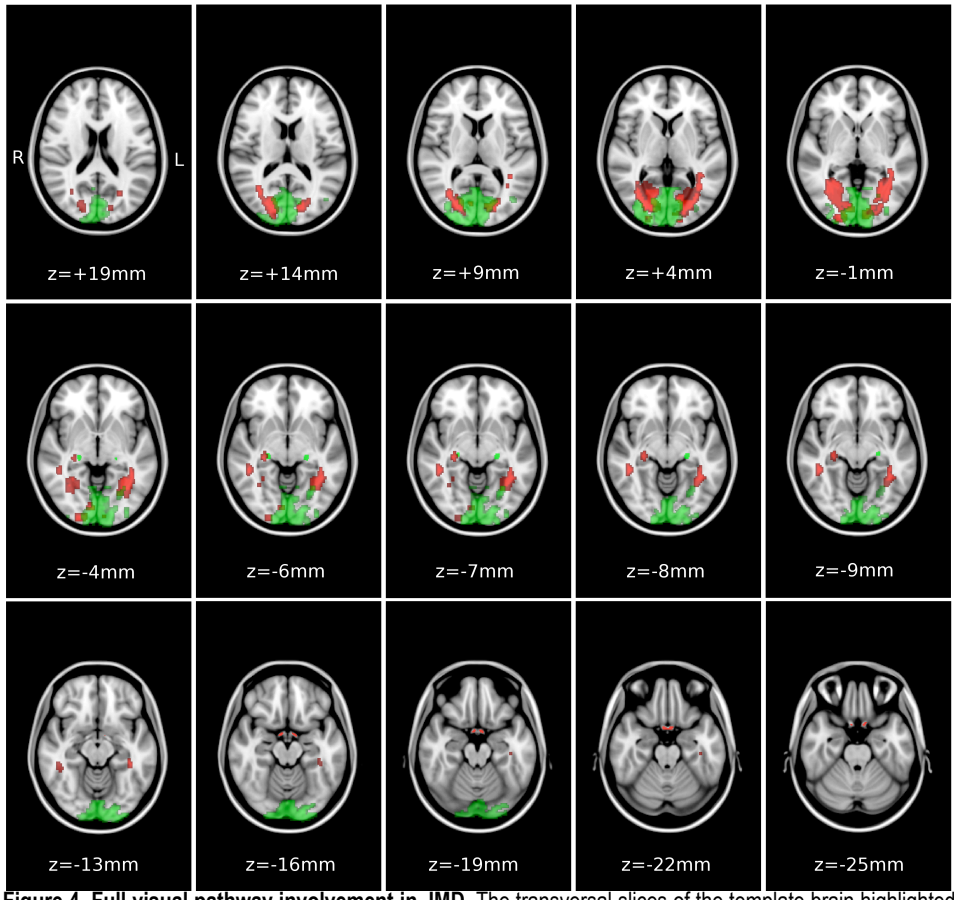

Figure 4. Full visual pathway involvement in JMD. The transversal slices of the template brain highlighted the areas where JMD group shows significantly lower cortical volume their age-matched controls ($p<0.05$, uncorrected). Involvement of the grey matter can be seen in the visual cortex and at the lateral geniculate bodies (green), whereas white matter involvement can be seen in the pregeniculate structures and in region corresponding to the geniculocalcarine radiation (red). The Talairach position of the slices are given as "z". JMD - juvenile-type macular degeneration.

As can be seen in Figure 5, the full length of the visual pathway in JMD showed significantly lower volume than its age-matched controls ($p<0.05$, FWE-corrected). Whereas in AMD, the remaining significant lower volume of the pathway is only visible in the visual cortex and in the geniculocalcarine radiation ($p<0.05$, FWE-corrected).

Figure 5. The extent of visual pathway involvement in AMD and JMD. Smaller volume of the visual cortex and the geniculocalcarine radiation in AMD vs HCO, but not the lateral geniculate bodies nor the pregeniculate structures, remain significant following small volume family-wise error correction for multiple voxels comparison. On the other hand, the full length of the pathway showed smaller volume in JMD vs HCJ, retaining their significance even after the similar correction. Statistical threshold: $p<0.05$, small volume FWE-corrected. AMD - age-related macular degeneration; HCO - healthy controls (age-matched to AMD); JMD - juvenile type macular degeneration; HCJ - healthy controls (age-matched to JMD).

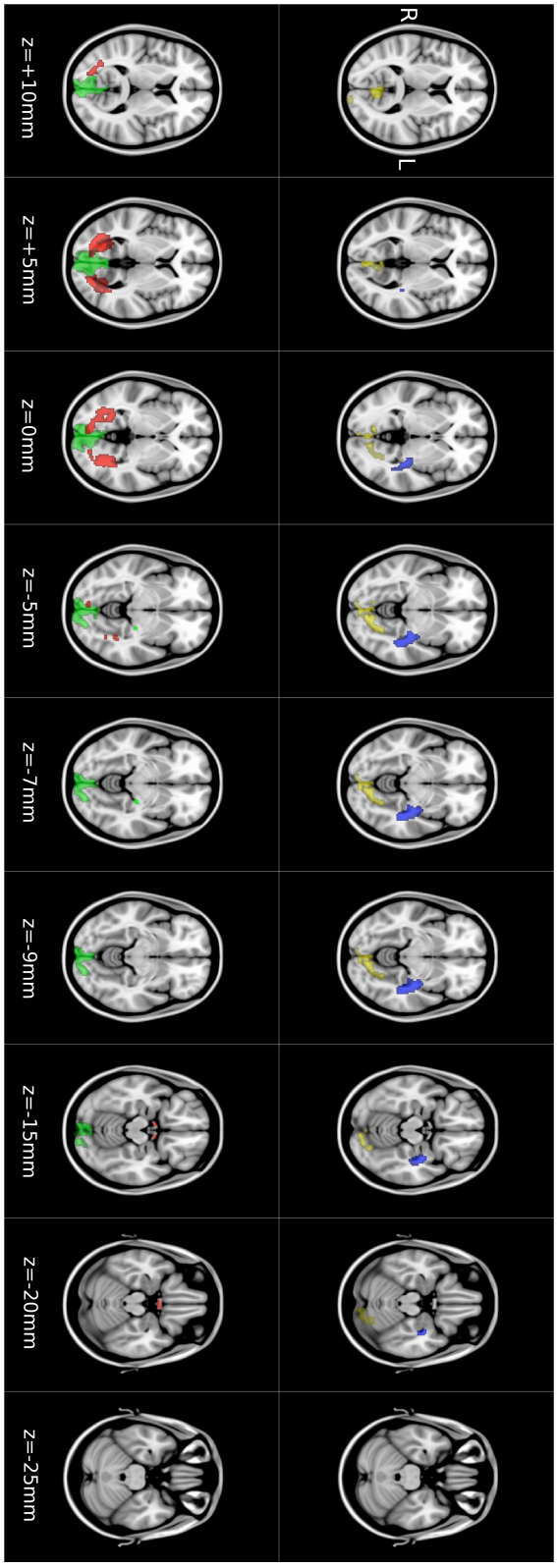

3.4. Discussion

Macular degeneration has been known as one of the primary cause of blindness and its ocular or retinal pathology has been studied extensively. The cerebral involvement, however, has been studied more only in the recent decade[10, 12, 16, 19, 32-34]. Our previous finding on the loss of grey matter density in AMD[12], and visual pathway volumetric loss in glaucoma[15] had raised further question on the (pre-cortical) volumetric condition of the visual pathway in macular degeneration. Here, we found that in macular degeneration, especially in the juvenile type, there was indeed volumetric loss of visual pathway structures.

While in primary open-angle glaucoma (POAG) it becomes intuitive to think that the retrobulbar visual pathway may be involved in its pathology, it may not necessarily be the case for macular degeneration. In the latter, the primary loss of retinal layer occurs due to the damage of photoreceptors, which are first order neurones. Therefore, any degeneration does not necessarily be translated across the retinal layers to the bipolar (second order neuron) and retinal ganglion cell (RGC, third order neuron) layers and their projecting axons, as suggested by Margalit et al. [35], let alone the geniculate and post-geniculate structures. However, the loss of RGC may also be attributed to the loss of photoreceptors, as revealed by Medeiros and Curcio[36] in wet AMD and Kim et al.[37] in AMD in later stage of dry AMD (geographic atrophy). These showed that RGC is not free from the adverse effect of photoreceptors disruption.

When we plotted the means of all ROIs as depicted in Figure 1, the degree of volumetric defect as compared to the age-matched controls along the visual pathway is almost similar in AMD and JMD. However, Table 1 showed that the relative volume differences to the controls were greater in AMD group. The findings shown in Table 1 suggest that the volumetric loss is greater in AMD than in JMD. Since by definition AMD is age-related, we plotted the ROIs' mean volumes against the age to see if there is any sort of correlation with the age. Indeed, negative correlation seemed to be present at the geniculocalcarine, occipital pole, intracalcarine, and supracalcarine regions. To account for this possible age effect, in the subsequent voxel-wise analyses, age was accounted for. When voxel-wise statistics were used, volumetric differences between JMD and the age-matched control group survived even more conservative statistical confidence thresholding. The discrepancy between ROI-based and voxel-wise findings may be explained by several following reasoning. First, any individual value extracted from any ROI is a mean value over a sizeable ROI, which contained several to thousands of voxels. This practically made ROI-based analyses somehow more coarse in nature, as opposed to the voxel-based one. Second, taking age into account in the analyses became essential, as one of the disease was explicitly age-related while the other was not. Therefore, ROI-based approach might underestimate the age effect. Even when the visual cortex is one of the least age-affected compared to the rest of cerebral cortex, we believe it was a good practice to account for age-effect in the analyses of the human visual pathway. Juvenile-type macular degeneration starts earlier in life and thus the disease period is relatively longer, hence there will probably be more chance that JMD affects the retrobulbar visual pathway than the AMD does in term of temporal aspect. Some studies had shown how brain is functionally affected by JMD[11]. But then again, structural involvement as we have reported earlier in this paper, as far as we know, have not been reported earlier.

Our study design was cross-sectional, therefore we can not determine which happened first, the volumetric reduction in the brain, or the degeneration in the macula. Nonetheless, considering the fact that macular degenerations have been mainly managed clinically as ocular pathologies, the structural changes, mainly in the LGB and the visual cortex, should alert clinicians on the possibility of brain-related mechanism involved in the disease. Neuroprotective approach to preserve the photoreceptors and retinal pigment epithelium by the administration of ciliary neurotrophic factors[38] or anti-inflammatory[39] drugs may be worthwhile to consider. A better comprehension of the pathology of various macular degeneration types and diagnostic approach are of utmost importance to allow the quantification of the treatment outcome. We believe that neuroimaging and retinal imaging[40], as well as their quantification methods[12, 22, 41, 42], would be a clinically viable option to evaluate the progress of the disease and the treatment outcome.

In summary, we reported our visual pathway morphometric study on macular degeneration. In both types of macular degeneration (age-related and juvenile) the volume of the visual pathway was reduced. However, the extent of involvement was different for the two types of disease, the JMD being the one with more widespread involvement of the visual pathway. These warrant the necessity of further investigation on the chronology of the visual pathway changes in macular degeneration.

Bibliography

1. Resnikoff S, Pascolini D, Etya'ale D, et al. Global data on visual impairment in the year 2002. Bull World Health Organ 2004;82(11):844-51.
2. Kocur I, Resnikoff S. Visual impairment and blindness in Europe and their prevention. Br J Ophthalmol 2002;86(7):716-22.
3. Augood CA, Vingerling JR, de Jong PT, et al. Prevalence of age-related maculopathy in older Europeans: the European Eye Study (EUREYE). Arch Ophthalmol 2006;124(4): 529-35.
4. Holz FG, Pauleikhoff D, Klein R, Bird AC. Pathogenesis of lesions in late age-related macular disease. Am J Ophthalmol 2004;137(3):504-10.
5. Zarbin MA. Current concepts in the pathogenesis of age-related macular degeneration. Arch Ophthalmol 2004;122(4):598-614.
6. Arden GB. Age-related macular degeneration. J Br Menopause Soc 2006;12(2):64-70.
7. Gehrs KM, Anderson DH, Johnson LV, Hageman GS. Age-related macular degeneration--emerging pathogenetic and therapeutic concepts. Ann Med 2006;38(7):450-71.
8. Johansson BB. Brain plasticity in health and disease. Keio J Med 2004;53(4):231-46.
9. Merzenich MM, Nelson RJ, Stryker MP, et al. Somatosensory cortical map changes following digit amputation in adult monkeys. J Comp Neurol 1984;224(4):591-605.
10. Masuda Y, Dumoulin SO, Nakadomari S, Wandell BA. V1 projection zone signals in human macular degeneration depend on task, not stimulus. Cereb Cortex 2008;18(11): 2483-93.
11. Baseler HA, Gouws A, Haak KV, et al. Large-scale remapping of visual cortex is absent in adult humans with macular degeneration. Nat Neurosci.
12. Boucard CC, Hernowo AT, Maguire RP, et al. Changes in cortical grey matter density associated with long-standing retinal visual field defects. Brain 2009;132(Pt 7): 1898-906.
13. Kitajima M, Korogi Y, Hirai T, et al. MR changes in the calcarine area resulting from retinal degeneration. AJNR Am J Neuroradiol 1997;18(7):1291-5.
14. Alcauter S, Barrios FA, Diaz R, Fernandez-Ruiz J. Gray and white matter alterations in spinocerebellar ataxia type 7: an in vivo DTI and VBM study. Neuroimage;55(1):1-7.
15. Hernowo AT, Boucard CC, Jansonius NM, et al. Automated Morphometry of The Visual Pathway in Primary Open-Angle Glaucoma. Invest Ophthalmol Vis Sci.
16. Baker CI, Peli E, Knouf N, Kanwisher NG. Reorganization of visual processing in macular degeneration. J Neurosci 2005;25(3):614-8.
17. Smirnakis SM, Brewer AA, Schmid MC, et al. Lack of long-term cortical reorganization after macaque retinal lesions. Nature 2005;435(7040):300-7.

18. Sunness JS, Liu T, Yantis S. Retinotopic mapping of the visual cortex using functional magnetic resonance imaging in a patient with central scotomas from atrophic macular degeneration. Ophthalmology 2004;111(8):1595-8.
19. Baker CI, Dilks DD, Peli E, Kanwisher N. Reorganization of visual processing in macular degeneration: replication and clues about the role of foveal loss. Vision Res 2008;48(18): 1910-9.
20. Dilks DD, Baker CI, Peli E, Kanwisher N. Reorganization of visual processing in macular degeneration is not specific to the "preferred retinal locus". J Neurosci 2009;29(9): 2768-73.
21. Schumacher EH, Jacko JA, Primo SA, et al. Reorganization of visual processing is related to eccentric viewing in patients with macular degeneration. Restor Neurol Neurosci 2008;26(4-5):391-402.
22. Ashburner J, Friston KJ. Voxel-based morphometry--the methods. Neuroimage 2000;11(6 Pt 1):805-21.
23. Smith SM, Brady JM. SUSAN - a new approach to low level image processing. Int Journal of Computer Vision 1997;23(1):45-78.
24. Klein A, Andersson J, Ardekani BA, et al. Evaluation of 14 nonlinear deformation algorithms applied to human brain MRI registration. Neuroimage 2009;46(3):786-802.
25. Ashburner J. A fast diffeomorphic image registration algorithm. Neuroimage 2007;38(1): 95-113.
26. Burgel U, Schormann T, Schleicher A, Zilles K. Mapping of histologically identified long fiber tracts in human cerebral hemispheres to the MRI volume of a reference brain: position and spatial variability of the optic radiation. Neuroimage 1999;10(5):489-99.
27. Burgel U, Amunts K, Hoemke L, et al. White matter fiber tracts of the human brain: three-dimensional mapping at microscopic resolution, topography and intersubject variability. Neuroimage 2006;29(4):1092-105.
28. Makris N, Goldstein JM, Kennedy D, et al. Decreased volume of left and total anterior insular lobule in schizophrenia. Schizophrenia Research 2006;83(2-3):155-71.
29. Frazier JA, Chiu S, Breeze JL, et al. Structural brain magnetic resonance imaging of limbic and thalamic volumes in pediatric bipolar disorder. Am J Psychiatry 2005;162(7): 1256-65.
30. Desikan RS, Segonne F, Fischl B, et al. An automated labeling system for subdividing the human cerebral cortex on MRI scans into gyral based regions of interest. Neuroimage 2006;31(3):968-80.
31. Goldstein JM, Seidman LJ, Makris N, et al. Hypothalamic abnormalities in schizophrenia: sex effects and genetic vulnerability. Biol Psychiatry 2007;61(8):935-45.
32. Clarke S. Modular organization of human extrastriate visual cortex: evidence from cytochrome oxidase pattern in normal and macular degeneration cases. Eur J Neurosci 1994;6(5):725-36.
33. Liu T, Cheung SH, Schuchard RA, et al. Incomplete cortical reorganization in macular degeneration. Invest Ophthalmol Vis Sci;51(12):6826-34.
34. Nguyen TH, Stievenart JL, Saucet JC, et al. [Cortical response to age-related macular degeneration (Part II). Functional MRI study]. J Fr Ophtalmol 2004;27(9 Pt 2):3S72-86.
35. Margalit E, Sadda SR. Retinal and optic nerve diseases. Artif Organs 2003;27(11): 963-74.
36. Medeiros NE, Curcio CA. Preservation of ganglion cell layer neurons in age-related macular degeneration. Invest Ophthalmol Vis Sci 2001;42(3):795-803.
37. Kim SY, Sadda S, Humayun MS, et al. Morphometric analysis of the macula in eyes with geographic atrophy due to age-related macular degeneration. Retina 2002;22(4):464-70.
38. Biarnes M, Mones J, Alonso J, Arias L. Update on geographic atrophy in age-related macular degeneration. Optom Vis Sci;88(7):881-9.
39. Forrester JV, Xu H, Kuffova L, et al. Dendritic cell physiology and function in the eye. Immunol Rev;234(1):282-304.
40. Keane PA, Sadda SR. Imaging chorioretinal vascular disease. Eye (Lond);24(3):422-7.
41. Gobel AP, Fleckenstein M, Schmitz-Valckenberg S, et al. Imaging Geographic Atrophy in Age-Related Macular Degeneration. Ophthalmologica.
42. Menke MN, Dabov S, Knecht P, Sturm V. Reproducibility of retinal thickness measurements in patients with age-related macular degeneration using 3D Fourier-domain optical coherence tomography (OCT) (Topcon 3D-OCT 1000). Acta Ophthalmol;89(4):346-51.

Chapter 4

Automated morphometry of the visual pathway in primary open-angle glaucoma

Based on:
Hernowo AT, Boucard CC, Jansonius NM, Hooymans JMM, Cornelissen FW.
Automated Morphometry of The Visual Pathway in Primary Open-Angle Glaucoma.
Investigative Ophthalmology and Visual Science 2011; Vol. 52, No. 5: 2758-2766

ABSTRACT

This study aimed to establish whether primary open-angle glaucoma (POAG) is associated with a change in volume of the visual pathway structures between the eyes and the visual cortex. To do so, we used magnetic resonance imaging (MRI) in combination with automated segmentation and voxel-based morphometry (VBM). Eight patients with POAG and twelve age-matched controls participated in the study. Only POAG patients with bilateral glaucomatous visual field loss were admitted to the study. The scotoma in both eyes had to include the paracentral region and had to be at least partially overlapping. All participants underwent high-resolution, T1-weighted 3T MRI scanning. Subsequently, VBM was used to determine the volume of the optic nerves, the optic chiasm, the optic tracts, the lateral geniculate nuclei (LGN), and the optic radiations. Analysis of covariance was used to compare these volumes in the POAG and control groups. The main outcome parameter of the measurement was the volume of visual pathway structures. Compared to the controls, subjects with glaucoma showed reduced volume ($p<0.005$) of all structures along the visual pathway, including the optic nerves, the optic chiasm, the optic tracts, the LGN, and the optic radiations. POAG adversely affects structures along the full visual pathway, from the optic nerve to the optic radiation. Moreover, MRI in combination with automated morphometry can be used to aid the detection and assessment of glaucomatous damage in the brain.

Chapter contents

4.1. Introduction

In the developed world, glaucoma is one of the most notorious causes of visual field defects[1]. Typically, over the course of the disease the visual field becomes narrower, but foveal vision remains relatively intact. The pathogenesis of the disease is not well understood, which hampers early diagnosis and advances in treatment.

Degeneration of retinal ganglion cells (RGC) is currently thought to play a key role in the pathogenesis of glaucoma[2-22]. The resulting damage to the RGC axonal projections[2, 22-25] is reflected by thinning of the retinal nerve fiber layer (RNFL)[26]. Analysis of RNFL thickness has thus become a primary tool for investigating volumetric changes in the most anterior part of the visual pathway[27-37]. Moreover, growing evidence suggests translation of the RGC degeneration to more distal parts of the visual pathway[25, 38-41]. In mice, the loss of RGC is followed by a reduction in thickness and area of the optic tract[38]. In non-human primates, an experimentally induced increase in intraocular pressure led to RGC loss and to the degeneration of the lateral geniculate nuclei (LGN) cell layers[25]. In humans, magnetic resonance (MR) imaging studies have shown that patients with glaucoma, compared to healthy individuals, have smaller optic nerves, a smaller optic chiasm[40], and smaller LGN[41]. A diffusion tensor imaging (DTI) study found marked, disease stage correlated changes in the optic nerves and weak changes in the optic radiations when comparing glaucoma patients and healthy controls[42]**.** Finally, the visual cortex was shown to decline in volume in glaucoma, as revealed in one post-mortem study by Gupta et al.[43] and in a recent in vivo MR study from our group[44]. The degeneration in these central portions of the visual pathway in humans might also be a sign of trans-synaptic neuronal degeneration, which is provoked by the death of the RGCs.

Thus far, MR-based measurements of the size of the human pre-cortical portion of the visual pathway have all been performed manually[39-41, 45]. Besides being time consuming, this manual assessment can result in subjective measurement bias. To overcome these disadvantages, in a recent study, our group used an automated morphometric technique that can objectively compare anatomical changes at all locations in the brain simultaneously. Using this new approach, we found MR evidence for grey matter density loss in the primary visual cortex in individuals with a

long-standing visual field defect due to primary open-angle glaucoma (POAG)[44]. This, together with the DTI findings mentioned earlier[42], implies that the optic radiation that carries visual information from the LGN to the visual cortex may also be affected in POAG. To our knowledge, morphological changes have not yet been reported for these structures.

If morphological changes in the visual pathway can be reliably measured, this could assist a clinician in deciding on the diagnosis, prognosis, and further management of individual patients. In the present study we investigated volumetric changes along the entire afferent visual pathway in individuals with POAG by using automated morphometric methods. Specifically, we addressed the following research questions. (1) Compared to healthy controls, do subjects with glaucoma exhibit changes in the volume of the visual pathway? (2) If there is such a change, does the change in volume correlate with changes in visual field sensitivity?

4.2. Methods

4.2.1. Subjects

This study conformed to the tenets of the Declaration of Helsinki and was approved by the medical review board of the University Medical Center Groningen (Groningen, the Netherlands). All participants gave their informed written consent prior to participation.

Patients with POAG were recruited from participants in the Groningen Longitudinal Glaucoma Study[46]. Eight patients participated (one female and seven males; mean age 72 years old, range 62-85 years old). The participant inclusion criteria were the following: 1) a glaucomatous visual field defect of at least 10 degrees in diameter in at least one quadrant, affecting both eyes; 2) these visual field defects had to include the paracentral regions in both eyes; 3) these defects had to have been present for at least three years. The severity of the visual field loss was determined by the mean deviation (MD) scores; Humphrey Field Analyzer (Carl Zeiss Meditec AG, Jena, Germany). Table 1 lists the characteristics of the patients. Patients with any other ophthalmic or neuro-ophthalmic disease that might affect the visual field were excluded. Table 1 lists these characteristics.

For the control group, 12 healthy age-matched subjects (three females and nine males; mean age 67 years, range 61-83) were recruited. They were recruited from among the partners and unrelated acquaintances of the visual field impaired participants or via advertisements in a local newspaper. Control subjects were required to have good best-corrected visual acuity (logMAR≤0), not to have any visual field defect (according to the Groningen Longitudinal Glaucoma Study)[46] and to be free of any ophthalmic, neurologic, or general health problems. Detection of an abnormal visual field
is explained in the Perimetry section below.

This study involved participants reported in another study[44]; the participants of our present study are the same as those listed in the POAG group in that study; the healthy controls in that study were also the same. The present study used the same MRI scans as those used in the prior study[44], but addressed volumetric changes along the visual pathway, rather than being limited to grey matter changes in the visual cortex.

4.2.2. Data acquisition

4.2.2.1. Perimetry

The visual field was tested with the Humphrey Field Analyzer (HFA; Carl Zeiss Meditec AG, Jena, Germany). A standardized method for examining the central visual field up to 30 degrees eccentricity, the 30-2 Swedish Interactive Threshold Algorithm (SITA)-Fast, was employed. A visual field defect was considered to be present if one of the the glaucoma hemifield test is outside of the normal limit, or if the pattern standard deviation's p is less than 0.05, or if if there were at least three adjacent non-edge points (with $p<0.05$) in the pattern deviation probability plot, with at least one point having a p-value less than 0.01[47]. This defect had to be present on at least two consecutive, reliable tests in the same region of the visual field (not including the first visual field measurement ever made). A test result was considered unreliable if false positive catch trials exceeded 10%, or if both false negative catch trials and fixation losses exceeded 10% and 20%, respectively. Moreover, deficits had to be compatible with glaucoma and have no other explanation.

4.2.2.2. T1-weighted image acquisition

All participants were scanned on the 3.0 Tesla MRI scanner (Philips Intera, Eindhoven, the Netherlands) located at the BCN Neuro-imaging Center of the University Medical Center Groningen. For each participant, a high-resolution, T1-weighted, anatomical scan was made using magnetization sequence T1W/3D/TFE-2, 8 degrees flip angle, repetition time 8.70 ms, matrix size 256 x 256, field of view 230 x 160 x 180, yielding 160 slices, and a voxel dimension of 1 x 1 x 1 mm.

4.2.3. MR data analysis

The data analysis procedure involved the following steps: image preprocessing, generation of study specific tissue probability maps (TPM), segmentation, registration, modulation of the segments, and finally a statistical comparison of differences in the volumes of different tissue segments between the POAG and control groups within the visual pathway. The process from the segmentation to the voxelwise statistical analyses is known as voxel-based morphometry or VBM. We used the voxel-based morphometry (VBM) that is part of the SPM8 software package (Wellcome Department of Imaging Neuroscience, London, UK; http://www.fil.ion.ucl.ac.uk/spm) to compare the volume of subcortical structures between the glaucoma and control groups[48]. VBM statistically assesses local changes in grey and/or white matter volumes between groups of anatomical scans. The steps in the data analysis procedure are described in more detail below.

4.2.3.1. Image pre-processing

Several pre-processing steps were performed on the scanned images before the actual measurement and statistical analyses. Image reorientation to the average image of all subjects' brains was applied, to

ensure registration of the images.

4.2.3.2. Generating study-specific tissue probability maps

One problem was that the standard TPMs available in the SPM8 software did not facilitate the detection of diencephalic nuclei, including the LGN. As a solution, we generated our own TPMs. TPM generation began by extracting the brains using the Brain Extraction Tool (BET)[49], available within the FMRIB Software Library (FSL; http://www.fmrib.ox.ac.uk/fsl). Next, for the segmentation, we used the FMRIB Automated Segmentation Tool (FAST)[50]. However, instead of letting FAST segment the extracted brains into the standard three tissue classes (grey, white and cerebral spinal fluid (CSF)), we made it segment the brains into six tissue classes. Next, we created average tissue class images based on the data from all subjects from the POAG and the control groups. After this, these average images were smoothed using a Gaussian kernel with a full-width half-maximum (FWHM) of 8 mm. In the SPM8 segmentation, the sixth tissue class image was used as the TPM containing the prior for the optic nerves, chiasm, tracts and radiations. The fifth tissue class image was used as the TPM with the prior for the thalamus and other diencephalic nuclei. The 1st to 4th tissue classes were collated and used as the TPM with the prior for other brain tissues.

4.2.3.3. Segmentation, registration, and modulation

We used SPM8's DARTEL (Diffeomorphic Anatomical Registration through Exponentiated Lie Algebra) suite of tools[51, 52]. In short, the DARTEL tools enabled us to create modulated grey and white matter images that were registered to a common reference image specifically representing our sample, instead of registering them to a more general template, such as the MNI (Montreal Neurological Institute) template that comes with SPM8. The study-specific method we used here enabled a more accurate inter-subject registration of brain images with improved localization and sensitivity of the VBM.

The process began with SPM8's segmentation using the TPMs we had created (as we explained in the paragraph above). After all the brains were segmented, a reference –or template– image was generated. The first step in generating this reference image was averaging the images of all brains. Following this, the individual brains were deformed and registered as closely as possible to this reference image. Next, using the registered brain images, a new average reference image was created to which the individual brain images were again registered. After 6 of these averaging and registration cycles, the final reference image was generated. The final reference image was then used as the template to which the native segmentations of the individual brains in the study were registered and modulated.

4.2.3.4. Smoothing

To increase the signal-to-noise ratio prior to statistical testing, we

smoothed the segmented images using a Gaussian kernel (FWHM = 4 mm).

4.2.3.5. Statistical testing

Covariance analysis was used to examine between-group differences in the segments, with age as a covariate. Statistical testing was restricted to the visual pathway. The visual pathway was demarcated using a mask that included the optic nerves up to the white matter regions where the optic radiations can be expected to be situated. The visual pathway mask was created manually, based on the average brain image from all participants. Regarding statistical testing, no correction for multiple comparison was used, because we only compared the groups within a well-defined region (the visual pathway). Hence, our hypothesis was an anatomically-closed one and no further correction for overall brain volumes was necessary.

In addition to the VBM analysis, we also performed a region-of-interest (ROI)-based statistical analysis. For this analysis, we defined nine ROIs: the right optic nerve (RON), the left optic nerve (LON), the optic chiasm (OC), the right optic tract (ROT), the left optic tract (LOT), the right lateral geniculate nucleus (RLGN), the left lateral geniculate nucleus (LLGN), the right optic radiation (ROR), and the left optic radiation (LOR). The spatial variation in the position and size of the optic radiations is less uniform; this is why we defined a relatively large region of interest to capture the ROR and LORs in individual brains. Figure 1 shows these latter two regions of interest. In the ROI-based analyses, statistical comparison was done using ANCOVA, with age as a covariate.

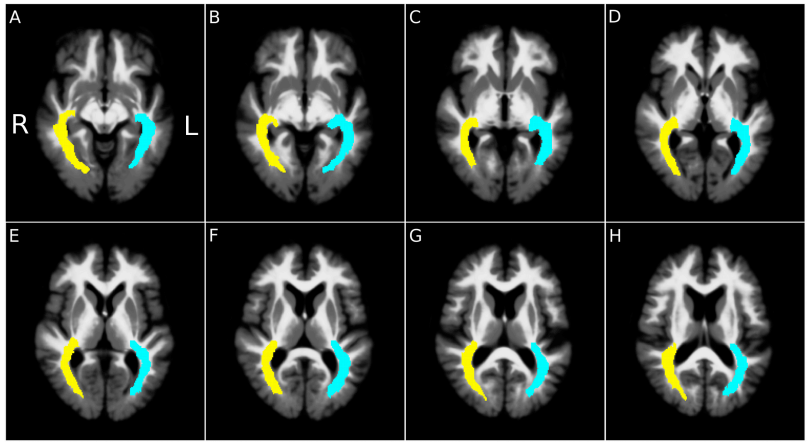

Figure 1. Regions of interest defining the possible locations of the optic radiations. The optic radiation ROIs are shown on the reference brain image created for this study. The yellow ROI represents the right optic radiation, whereas cyan represents the left optic radiation. ROI = region of interest.

4.3.1. Groups comparison

Patients' characteristics are listed in Table 1. Statistical testing (Mann-Whitney U-test) revealed no significant difference in age between the glaucoma and control groups (p=0.13).

Characteristics	Values
Age, median (range), years	72.5 (62 - 85)
Male sex, %	87.5
Family history of glaucoma, %	85.7
Visual acuity in logMAR, median (range)	0.1 (0.0 - 0.7)
IOP	
Highest ever recorded, median (range), mmHg	30 (17 - 55) mmHg
Treated, median (range), mmHg	14 (12 - 16) mmHg
Visual field MD	
Right eye, median (range), in dB	-11.62 (-5.23 to -27.20)
Left eye, median (range), in dB	-15.30 (-3.67 to -24.59)
Scanning laser polarimetry (GDx), the number	
Right eye, median (range)	63 (51 - 97)
Left eye, median (range)	61 (38 - 95)
Scanning laser polarimetry (GDx) ellipse average thickness	
Right eye, median (range), μm	59 (45 - 69)
Left eye, median (range), μm	62 (46 - 72)

Table 1. Baseline patient characteristics. Characteristics of the patients were age, sex and positive family history proportion (in percentage), visual acuity for one or both eyes (expressed in logMAR), intraocular pressure (in mmHg), visual field sensitivity (expressed as MD in dB), nerve fiber indicator, and nerve fiber layer thickness (in μm). logMAR – logarithm of minimum angle of resolution; IOP - intraocular pressure; MD – mean deviation; dB – decibel; μm – micrometer.

We then used automated voxel-based morphometry to examine differences along the visual pathway between the glaucoma and control groups. Figure 2 depicts the region in the brain where the white matter volume is reduced in the glaucoma group as compared to the control group (thresholded at $p<0.005$, uncorrected). Significant reductions in volume are present bilaterally in the optic nerves, the optic chiasm, and in both optic tracts.

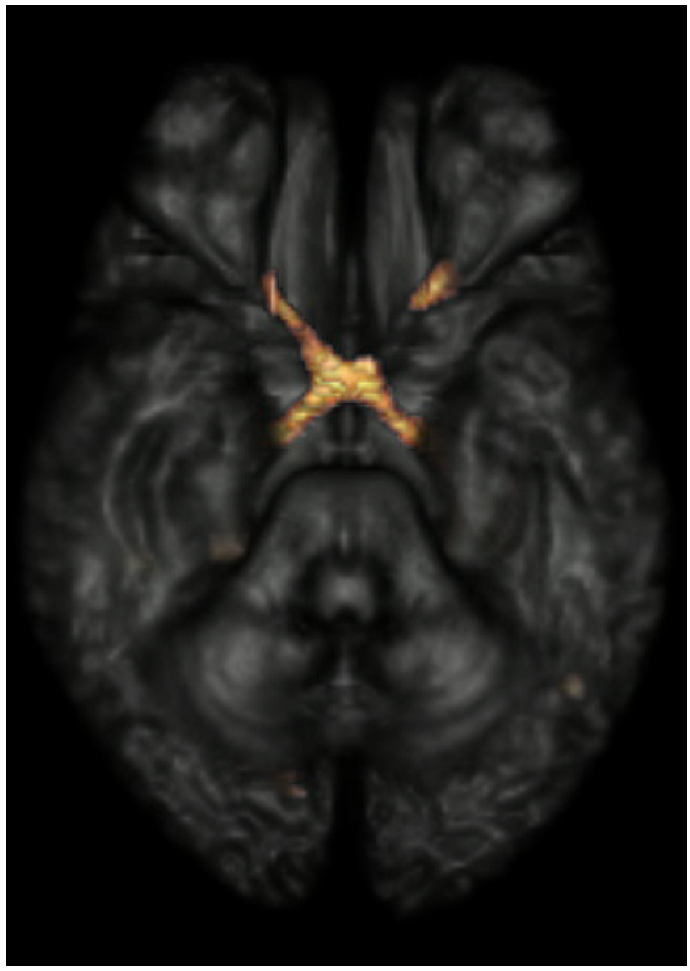

Figure 2. Reductions in volume along the pre-geniculate visual pathway in glaucoma, as determined by using voxel-based morphometry. Highlighted structures (including the optic nerves, chiasm, and tracts) indicate regions with statistically significant volumetric reductions in subjects with glaucoma, compared to age-matched controls (thresholded at $p<0.005$, uncorrected). Lateral geniculate nuclei and optic radiations are not shown in this rendering.

The volumetric reductions extend beyond the optic tracts, but this cannot be observed in Figure 2. For this reason, Figure 3 shows a series of axial slices that allow examination of reductions beyond the optic tract.

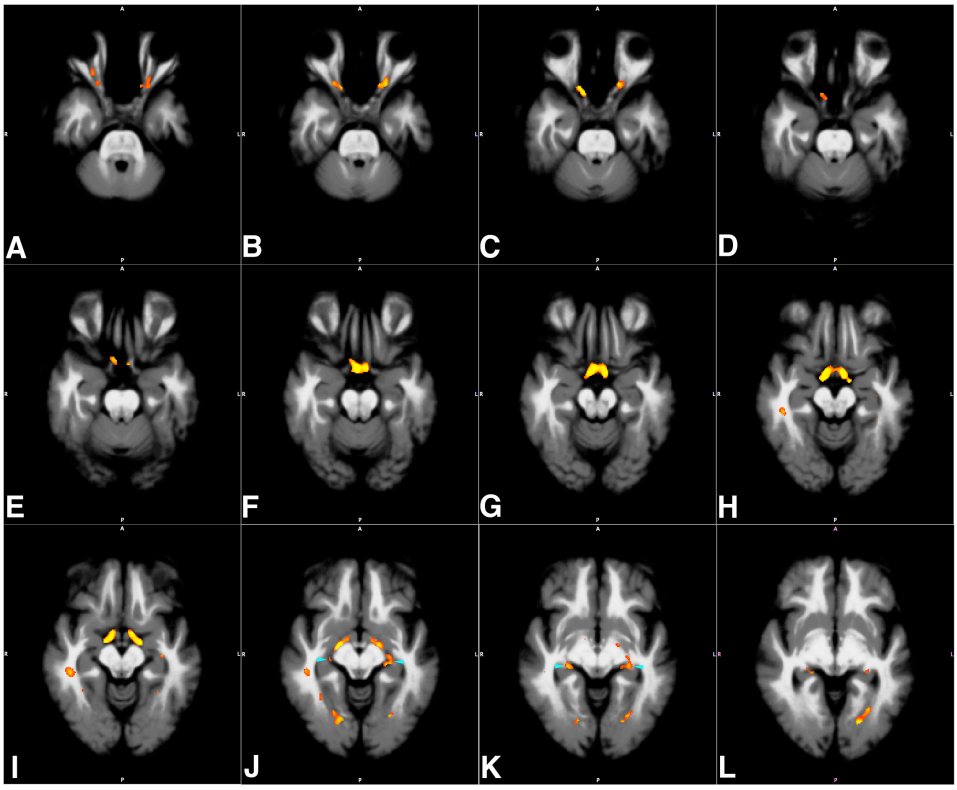

Figure 3. Axial slices indicating reductions in volume along the visual pathway in glaucoma, as found using voxel-based morphometry. Compared to the age-matched controls, subjects in the glaucoma group have a reduced volume of the pre-cortical visual pathway structures (Figure 3A-L). Statistically significant volumetric reductions in the lateral geniculate nuclei are indicated by cyan arrowheads in Figure 3J and 3K. Statistically significant changes in the optic radiations are depicted in Figures 3I - L. Statistical maps are thresholded at a level of p<0.005 (uncorrected).

Compared to the age-matched controls, participants in theglaucoma group had a reduced volume of the pre-cortical visual pathway structures, as shown in Figure 3. Marked changes to the optic chiasm are visible in Figures 3F-H. Volumetric reductions in the lateral geniculate nuclei can be observed in Figures 3J and 3K, whereas changes in the optic radiations can be observed in Figures 3I-L. We repeated the VBM analysis using TPMs based on an independent set of brains. The results of this analysis were highly comparable to those reported above (see Supplementary Materials, http://www.iovs.org/lookup/suppl/ doi:10.1167/iovs.10-5682/-/DCSupplemental).

Figure 4 shows boxplots for the ROI-based volumetric measurements for the individual subjects in control and glaucoma groups. Table 2 lists the individual subject's volumes for each ROI, as well as the relative volume loss in each ROI. The final row of Table 2 lists the values related to the statistical comparison.

Table 2 and Figure 4 indicate that the ROI-based comparisons of the glaucoma and control groups showed significant volumetric differences in nearly all ROIs. With exception of the left optic radiation, the glaucoma group had an overall lower volume along the full visual pathway.

	Volume (mm^3)								
	RON	LON	OC	ROT	LOT	RLGN	LLGN	ROR	LOR
CONTROL									
Subject 01	74	123	44	368	499	135	134	8627	8127
Subject 02	80	99	35	371	526	137	127	10213	10510
Subject 03	79	135	32	374	481	132	142	11643	12580
Subject 04	92	148	50	448	599	174	162	12028	11910
Subject 05	93	128	16	371	584	173	160	11961	11944
Subject 06	67	151	40	421	541	149	141	12677	12935
Subject 07	125	138	58	477	630	156	160	11740	11906
Subject 08	103	121	40	427	551	133	121	10582	11006
Subject 09	102	149	52	428	564	159	154	10269	10864
Subject 10	112	149	58	434	568	171	206	11191	10108
Subject 11	107	144	34	489	660	144	121	11949	12316
Subject 12	102	165	54	402	536	156	136	11825	12225
Mean ± SD	94.6 ± 17.1	137.6 ± 17.6	42.8 ± 12.5	417.4 ± 41.5	561.5 ± 51.5	151.7 ± 15.7	147.0 ± 23.9	11225.3 ± 1116.8	11369.1 ± 1337.9
POAG									
Subject 13	27	143	1	260	388	122	126	9159	10098
Subject 14	43	105	12	299	403	137	131	8675	7983
Subject 15	52	81	11	323	458	108	112	8504	8661
Subject 16	33	116	4	278	366	110	108	7333	7204
Subject 17	52	76	11	333	420	87	103	6211	6903
Subject 18	53	112	6	317	436	141	123	9555	10215
Subject 19	74	122	29	383	517	148	126	11591	12138
Subject 20	34	117	3	360	545	151	132	12304	12958
Mean ± SD	45.8 ± 15.0	109.1 ± 21.9	9.5 ± 8.9	319.3 ± 40.7	441.6 ± 62.3	125.7 ± 22.7	120.1 ± 11.2	9166.6 ± 2023.2	9519.9 ± 2229.5
% volume loss (relative to the control group)	52%	21%	78%	23%	21%	17%	18%	18%	16%
ANCOVA (age)	F=32.11; p<0.0001	F=6.34; p=0.023	F=30.76; p<0.0001	F=21.60; p=0.0003	F=18.79; p=0.0005	F=5.18; p=0.037	F=5.19; p=0.037	F=5.31; p=0.035	F=2.58; p=0.13

Table 2. Comparison of volumetric measurements in ROIs along the precortical visual pathway in glaucoma patients and controls. ROI - region of interest; RON - right optic nerve; LON - left optic nerve; OC - optic chiasm; ROT - right optic tract; LOT - left optic tract; RLGN - right lateral geniculate nucleus; LLGN - left lateral geniculate nucleus; ROR - right optic radiation; LOR - left optic radiation; SD - standard deviation.

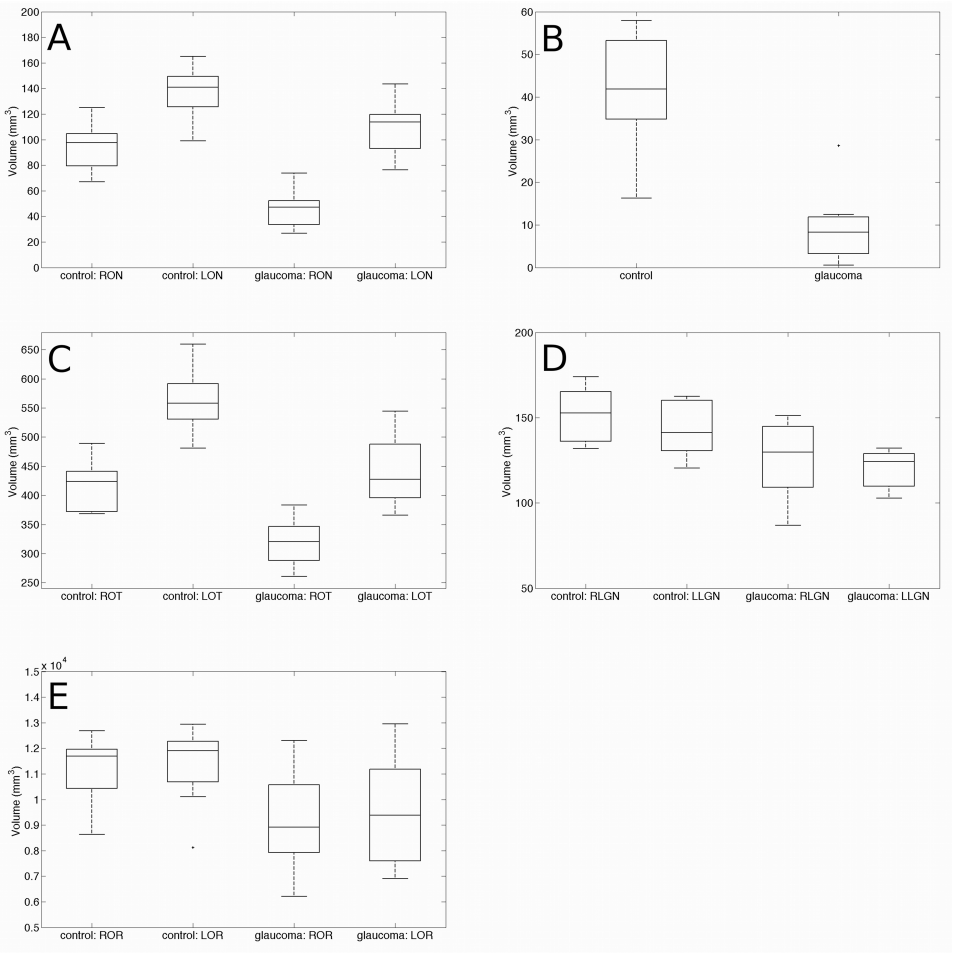

Figure 4. Comparison of volumetric measurements in ROIs along the precortical visual pathway in glaucoma patients and controls. Boxplots show the average and 25th and 75th percentiles for nine ROIs: RON, LON, OC, ROT, LOT, RLGN, LLGN, ROR, and LOR (abbreviations are the same as those for Table 2). Data was extracted from the unsmoothed modulated segments of the T1-weighted brain images.

4.3.2. Correlation analyses

We determined the correlations between the binocular average of the mean deviation of visual field sensitivity (MD) and the volume of the ROIs described above. Table 3 shows that none of the correlations between the ROI volume and the MD of the glaucoma group reached statistical significance. The scatter plots in Figure 5 show relative volume change for individual patients as a function of the binocular average of the MD.

	Region of Interest								
	RON	LON	OC	ROT	LOT	RLGN	LLGN	ROR	LOR
Mean deviation OD	R=0.24; p=0.57	n/a	-	-	-	-	-	-	-
Mean deviation OS	n/a	R=0.58; p=0.13	-	-	-	-	-	-	-
Binocular average of mean deviation	-	-	R=0.55; p=0.16	R=0.15; p=0.73	R= -0.13; p=0.76	R=0.28; p=0.49	R=0.12; p=0.77	R=0.02; p=0.97	R= -0.09; p=0.83

Table 3. Correlations between visual field sensitivity and volume of visual pathway structure in the glaucoma group. Abbreviations: MD - mean deviation (of visual field sensitivity); OD - oculus dexter (right eye); OS - oculus sinister (left eye); ROI - region of interest; RON - right optic nerve; LON - left optic nerve; OC - optic chiasm; ROT -right optic tract; LOT - left optic tract; RLGN - right lateral geniculate nucleus; LLGN - left lateral geniculate nucleus; ROR - right optic radiation; LOR - left optic radiation.

4.4. Discussion

Our results show that in comparison to healthy controls, subjects with glaucoma exhibited significant reductions in the volume of the visual pathway including the optic nerves, chiasm, tracts, LGN, and optic radiations. In subjects with long-standing POAG, volumetric reductions were therefore present in the visual pathway. Starting from the optic nerve, we found that the intraorbital and intracranial optic nerve volumes were markedly reduced in glaucoma.

These findings corroborate earlier reports on structural damage to these sections of the visual pathway[38-40, 42]. The volumetric reduction need not be symmetrical, as can be seen in Figure 1. The reduction was most prominent in the distal half of the right optic nerve and in the middle third of the left nerve. Nonetheless, when we lowered the statistical threshold (to $p<0.05$), we observed the presence of POAG-associated volumetric reductions along the entire length of the optic nerve. This indicates that the shrinkage may occur anywhere along the entire length of the optic nerve.

The volume of the optic chiasm and tracts was reduced in glaucoma as well (Figure 1). Shrinkage was present in the optic chiasm and along the full length of the optic tracts, corroborating results from earlier studies[40, 53]. Since the latter two structures are a direct continuation of the optic nerves, these findings are perhaps less surprising. A more interesting neuro-ophthalmological finding is that also the lateral geniculate nuclei (LGN) showed volumetric reductions in subjects with POAG. This corroborates an earlier report by Gupta et al.[41], who used manual measurements in their study. Our results also indicate that the optic radiations are adversely affected. This is more surprising, as the axonal projections in the optic radiations are not a direct continuation of the retinal ganglion cell layer (RGC) axons, but are projections from LGN relay neurons that transmit the visual information to the visual cortex. The volumetric reduction of the optic radiations complements the grey matter density reduction in visual cortex[44].

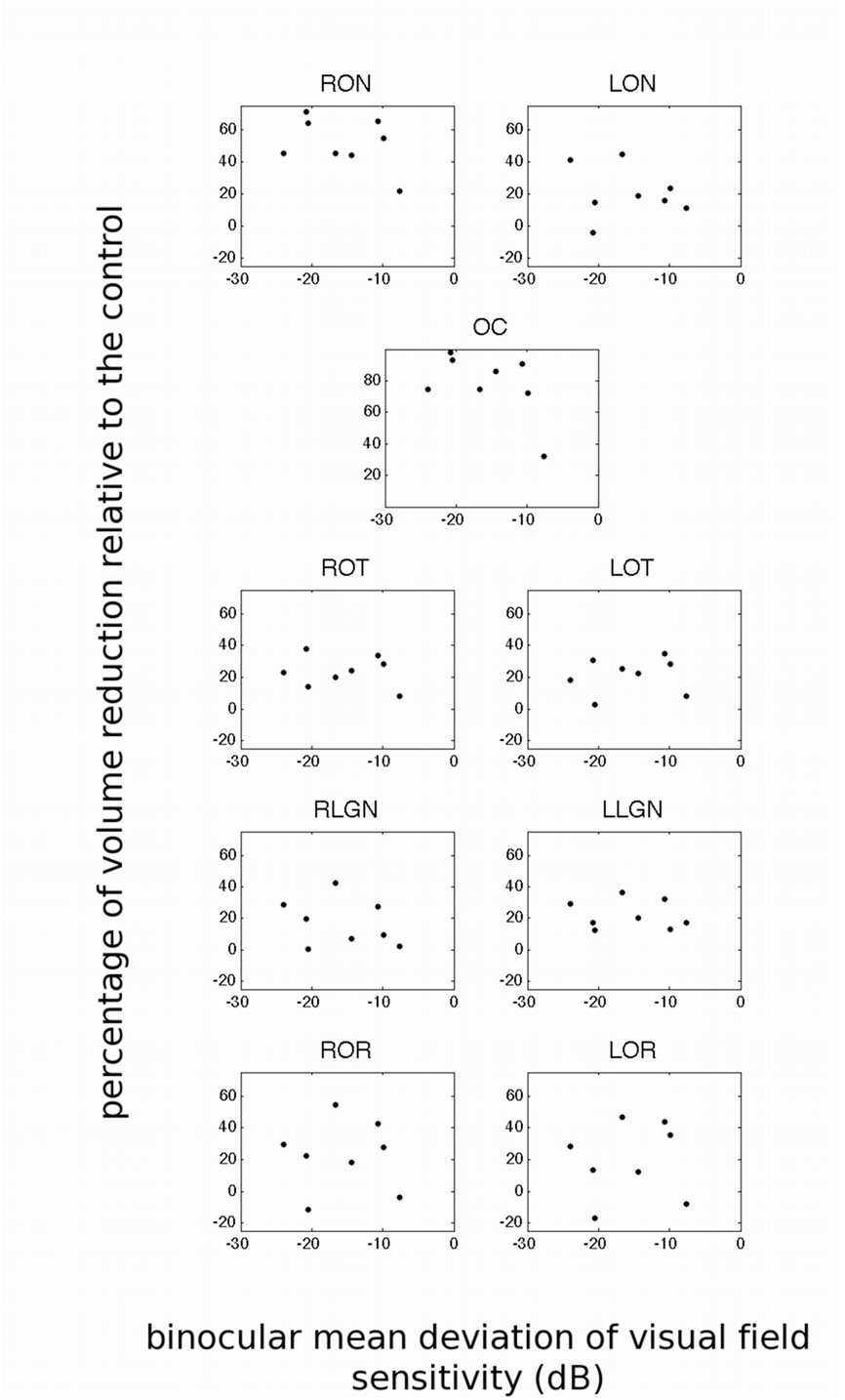

Figure 5. Scatterplots of volume reduction in visual pathway structures as a function of binocular visual field sensitivity deviation. The volume reduction for individual patients is expressed as a percentage compared to the average volume in control participants. Data was extracted from the unsmoothed modulated segments of the T1-weighted brain images. (abbreviations are the same as those for Table 2), dB - decibel.

The volumetric reduction of the optic radiations is also related to the finding – based on diffusion tensor imaging (DTI) – that these structures showed increased mean diffusivity and decreased fractional anisotropy in glaucoma patients[42]. This DTI finding implied that the integrity of the optic radiation in glaucoma is compromised. Our T1-weighted imaging and VBM results indicated that there is also a reduction in the volume of this brain structure in glaucoma. For future assessment of structural changes in patients, DTI and T1-weighted imaging appear to be techniques that provide distinct and complementary information. How these DTI and VBM results exactly relate to each other, as well as to disease severity, would require comparisons in the same group of patients.

The proportion of volume loss in the visual pathway ranges from 78% in the optic chiasm to 16% in the optic radiation. A trend in the data suggests that the glaucoma-associated volume reduction decreases the further away a structure is from the eye. This would fit with the notion that that the pre-geniculate volumetric reduction is transmitted trans-synaptically to the LGN and beyond. Another explanation for the volume reduction could be a change in metabolic activity due to the lack of RGC input as previously shown in primate glaucoma[54] and visual cortex in human glaucoma[55]. However, it is beyond the capacity of the VBM methodology to determine the exact mechanism underlying the volumetric reductions.

For the control participants, our estimate of the average volume of the LGN (149 mm^3) lies in between previous estimates based on a post-mortem, MRI-registered histological investigation (182 mm^3)[56] and another post-mortem histological study (118 mm^3)[57]. The latter estimate is smaller than ours, but this may be due to shrinkage as a result of formalin fixation. Our method measures volume of (parts of) segmented images, so that the specific choice of segmentation parameters may influence absolute size estimates. However, this equally affects the measurements in patients and controls.

In their combined MRI and histological study, Burgel et al.[56] estimated the average size of the optic radiations in healthy individuals to be 6798 mm^3. In this case, we got a larger average optic radiation volume (11297 mm^3). This larger estimate can be explained by us deliberately defining a relatively large region of interest to guarantee that we would capture the ROR and LORs of all the individual brains. In the future, DTI-guided segmentation of high-resolution anatomical images of the brain may allow extraction of the optic radiation in an automated manner and provide even more accurate *in vivo* volumetric measurements.

Our analyses showed no significant correlation between the visual field sensitivity (MD) and the volume of the visual pathway structures (see Table 3 and Figure 5). There may be several methodological reasons for this. ROI-based analyses, as we used here, are a relatively coarse measure in comparison to the resolution offered by VBM. Future studies may explore the structure-function relationship in a finer, voxel-wise manner. These could also consider using more comprehensive visual field measurements (for example, the full SITA method) to enable a more precise determination of the relationship between the severity of the reduction in visual field sensitivity and the volume of the visual pathway. It may be possible to further improve on the methods we used here by fine-tuning the registration parameters so as to focus more on the visual pathway rather than the whole brain, before performing the statistical analyses. With such technical refinements to the present technique and the inclusion of more participants in various severity stages of glaucoma, it might become feasible to determine how far along the pathway damage is occurring and perhaps

even the time sequence of damage. Such could be done through either longitudinal studies or by finding patients for whom damage only extends to certain points along the pathway.

Our study also showed that the combination of MRI and automated morphometry can detect changes in the volume of the visual pathway. Our study is the first to detect such changes simultaneously using fully automated VBM. Standard VBM is not very suitable for detecting changes in the subcortical sections of the visual pathway. Moreover, to the best of our knowledge, surface-based methods only allow investigation of cortical structures as well. To enable detection of subcortical volumetric changes, we slightly modified the standard segmentation protocol of SPM by increasing the number of tissue classes. This allowed better segmentation, especially of the optic radiations and the LGN. This enabled us to greatly improve our assessment of volumetric changes in these structures using VBM.

The TPMs that we used incorporated all the subjects from both groups in the study and in principle do not bias the results in any direction. To verify the validity of this assumption, we repeated our VBM analysis using TPMs based on an independent set of brains. The results of this analysis are highly comparable to the one reported in the main paper (see Supplementary Materials, http://www.iovs.org/lookup/suppl/ doi: 10.1167/iovs.10-5682/-/DCSupplemental). Using TPMs based on the brains of the study participants has the advantage that it results in more accurate registration and improved VBM sensitivity.

Previous reports on structural changes in glaucoma have used different dimensions such as height, area, or thickness of the structures of interest as their outcome parameters[39, 40, 45, 58]. Often, these measures were determined manually. VBM, on the other hand, performs an automated statistical comparison of volume on a voxel-by-voxel basis, thus allowing an unbiased and comprehensive comparison. Moreover, it has the ability to detect subtle differences that manual measurements may not be able to detect.

In the present study, we used VBM primarily for its power in performing group comparisons. However, we believe the method and its components could have a more widespread use. In a group comparison study, all brain images and their derivative grey and white matter segments necessarily have to be normalized to allow any comparisons. However, one can always opt not to do so in order to simply obtain the derivative grey and white matter segments, thereby preserving an individual's brain shape. For example, a clinician could then use the white matter segment – which is virtually free from the other non-white matter brain tissue – to precisely measure the dimensions of the optic chiasm or the optic tracts. In this case, only the accurate segmentation abilities of the VBM method are used to improve the sensitivity of manual measurements.

In our view, a fully automated VBM approach could also be applied at the individual patient level, although this would require further research and development. Based on a large number of images of normal, healthy brains, a normative database of templates for subjects of various ages could be created. Following automated normalization and segmentation, the brain images of an individual patient, could be compared – on a voxel-wise basis – to the appropriate normal template in the database. Deviant structures in the patient's brain could be highlighted. Such measurements and visualizations could assist a clinician in deciding on the diagnosis, prognosis, and further management of an individual patient. Potentially, multivariate pattern classification techniques could be applied to improve

the sensitivity of such automated assistive measurements. In the long run, volume reduction and other MR based assessments could become additional indicators to assess glaucoma progress[42].

In the future, these new methods could also help to decide whether a vision rehabilitation program for a patient is worthwhile, since a degenerated pathway may limit the efficacy of rehabilitation and training programs[59] and retinal prostheses[60]. Furthermore, due to the potentially deteriorative effect of glaucoma, physicians may also need to consider the prevention of degeneration as a new goal. In addition to such clinical implications, our results indicate that the automated and objective procedure of VBM can be applied in future research on the visual pathway. Finally, the present approach need not be restricted to the realms of neuro-ophthalmology. Automatic detection of changes in subcortical structures may also be useful in neurological or psychiatric disorders.

In summary, compared to healthy individuals, glaucoma patients show the presence of volumetric reductions which may extend all the way from the optic nerve to the optic radiations. Glaucoma, besides affecting the eye and optic nerves, may thus also impact the central visual system. Despite the marked changes observed in pre-geniculate structures of the visual pathway, more data is needed, however, to ascertain the extend of the optic radiations involvement.

Acknowledgments

The authors thank Hans de Haas and Sander Paas for their assistance in data extraction, the BCN Neuroimaging Center for the use of their MRI scanner, Anita Kuiper for her assistance in magnetic resonance image acquisition, and Marije van Beilen for useful comments and suggestions on an earlier version of the manuscript.

Bibliography

1. Resnikoff S, Pascolini D, Etya'ale D, et al. Global data on visual impairment in the year 2002. Bull World Health Organ 2004;82(11):844-51.
2. Dandona L, Hendrickson A, Quigley HA. Selective effects of experimental glaucoma on axonal transport by retinal ganglion cells to the dorsal lateral geniculate nucleus. Invest Ophthalmol Vis Sci 1991;32(5):1593-9.
3. Desatnik H, Quigley HA, Glovinsky Y. Study of central retinal ganglion cell loss in experimental glaucoma in monkey eyes. J Glaucoma 1996;5(1):46-53.
4. Fu QL, Li X, Shi J, et al. Synaptic degeneration of retinal ganglion cells in a rat ocular hypertension glaucoma model. Cell Mol Neurobiol 2009;29(4):575-81.
5. Garcia-Valenzuela E, Shareef S, Walsh J, Sharma SC. Programmed cell death of retinal ganglion cells during experimental glaucoma. Exp Eye Res 1995;61(1):33-44.
6. Glovinsky Y, Quigley HA, Dunkelberger GR. Retinal ganglion cell loss is size dependent in experimental glaucoma. Invest Ophthalmol Vis Sci 1991;32(3):484-91.
7. Guo L, Moss SE, Alexander RA, et al. Retinal ganglion cell apoptosis in glaucoma is related to intraocular pressure and IOP-induced effects on extracellular matrix. Invest Ophthalmol Vis Sci 2005;46(1):175-82.
8. Holcombe DJ, Lengefeld N, Gole GA, Barnett NL. Selective inner retinal dysfunction precedes ganglion cell loss in a mouse glaucoma model. Br J Ophthalmol 2008;92(5):683-8.
9. Ikeda Y, Ohguro H, Maruyama I. Two cases of primary open angle glaucoma with serum autoantibody against retinal ganglion cells. Jpn J Ophthalmol 2000;44(6):648-52.
10. Morgan JE. Retinal ganglion cell shrinkage in glaucoma. J Glaucoma 2002;11(4):365-70.
11. Nickells RW. Apoptosis of retinal ganglion cells in glaucoma: an update of the molecular pathways involved in cell death. Surv Ophthalmol 1999;43 Suppl 1:S151-61.
12. Nickells RW. Retinal ganglion cell death in glaucoma: the how, the why, and the maybe. J Glaucoma 1996;5(5):345-56.

13. Pavlidis M, Stupp T, Naskar R, et al. Retinal ganglion cells resistant to advanced glaucoma: a postmortem study of human retinas with the carbocyanine dye DiI. Invest Ophthalmol Vis Sci 2003;44(12):5196-205.
14. Quigley HA, Dunkelberger GR, Green WR. Retinal ganglion cell atrophy correlated with automated perimetry in human eyes with glaucoma. Am J Ophthalmol 1989;107(5): 453-64.
15. Reichstein D, Ren L, Filippopoulos T, et al. Apoptotic retinal ganglion cell death in the DBA/2 mouse model of glaucoma. Exp Eye Res 2007;84(1):13-21.
16. Takatsuji K, Tohyama M, Sato Y, Nakamura A. Selective loss of retinal ganglion cells in albino avian glaucoma. Invest Ophthalmol Vis Sci 1988;29(6):901-9.
17. Morgan JE, Uchida H, Caprioli J. Retinal ganglion cell death in experimental glaucoma. Br J Ophthalmol 2000;84(3):303-10.
18. Urcola JH, Hernandez M, Vecino E. Three experimental glaucoma models in rats: comparison of the effects of intraocular pressure elevation on retinal ganglion cell size and death. Exp Eye Res 2006;83(2):429-37.
19. Wax MB, Tezel G. Immunoregulation of retinal ganglion cell fate in glaucoma. Exp Eye Res 2009;88(4):825-30.
20. Quigley HA, Nickells RW, Kerrigan LA, et al. Retinal ganglion cell death in experimental glaucoma and after axotomy occurs by apoptosis. Invest Ophthalmol Vis Sci 1995;36(5): 774-86.
21. Saleh M, Nagaraju M, Porciatti V. Longitudinal evaluation of retinal ganglion cell function and IOP in the DBA/2J mouse model of glaucoma. Invest Ophthalmol Vis Sci 2007;48(10):4564-72.
22. Soto I, Oglesby E, Buckingham BP, et al. Retinal ganglion cells downregulate gene expression and lose their axons within the optic nerve head in a mouse glaucoma model. J Neurosci 2008;28(2):548-61.
23. Howell GR, Libby RT, Jakobs TC, et al. Axons of retinal ganglion cells are insulted in the optic nerve early in DBA/2J glaucoma. J Cell Biol 2007;179(7):1523-37.
24. Ventura LM, Sorokac N, De Los Santos R, et al. The relationship between retinal ganglion cell function and retinal nerve fiber thickness in early glaucoma. Invest Ophthalmol Vis Sci 2006;47(9):3904-11.
25. Yucel YH, Zhang Q, Weinreb RN, et al. Effects of retinal ganglion cell loss on magno-, parvo-, koniocellular pathways in the lateral geniculate nucleus and visual cortex in glaucoma. Prog Retin Eye Res 2003;22(4):465-81.
26. Medeiros FA, Alencar LM, Zangwill LM, et al. Detection of progressive retinal nerve fiber layer loss in glaucoma using scanning laser polarimetry with variable corneal compensation. Invest Ophthalmol Vis Sci 2009;50(4):1675-81.
27. Chang YC, Tsai RK. Correlation between quadrant specific automatic visual field defect and retinal nerve fiber layer thickness as measured by scanning laser polarimetry in patients with primary open angle glaucoma. Kaohsiung J Med Sci 2008;24(5):233-9.
28. Baraibar B, Sanchez-Cano A, Pablo LE, Honrubia FM. Preperimetric glaucoma assessment with scanning laser polarimetry (GDx VCC): analysis of retinal nerve fiber layer by sectors. J Glaucoma 2007;16(8):659-64.
29. Tsai JC, Chang HW, Teng MC, et al. Scanning laser polarimetry for measurement of retinal nerve fiber layer in absolute, advanced and early glaucoma. Chang Gung Med J 2006;29(2):162-8.
30. Reus NJ, Lemij HG. Scanning laser polarimetry of the retinal nerve fiber layer in perimetrically unaffected eyes of glaucoma patients. Ophthalmology 2004;111(12): 2199-203.
31. Mocan MC, Bozkurt B, Irkec M, et al. The evaluation of retinal nerve fiber layer in pigment dispersion syndrome and pigmentary glaucoma using scanning laser polarimetry. Eur J Ophthalmol 2003;13(4):377-82.
32. Weinreb RN. Evaluating the retinal nerve fiber layer in glaucoma with scanning laser polarimetry. Arch Ophthalmol 1999;117(10):1403-6.
33. Shirakashi M, Abe H, Sawaguchi S, Funaki S. Measurement of thickness of retinal nerve fiber layer by scanning laser polarimetry and high-pass resolution perimetry in patients with primary open-angle or normal-tension glaucoma. Acta Ophthalmol Scand 1997;75 (6):641-4.
34. Shirakashi M, Funaki S, Funaki H, et al. Measurement of retinal nerve fibre layer by scanning laser polarimetry and high pass resolution perimetry in normal tension glaucoma with relatively high or low intraocular pressure. Br J Ophthalmol 1999;83(3): 353-7.
35. Hollo G, Suveges I, Nagymihaly A, Vargha P. Scanning laser polarimetry of the retinal nerve fibre layer in primary open angle and capsular glaucoma. Br J Ophthalmol 1997;81(10):857-61.

36. Heeg GP, Jansonius NM. The groningen longitudinal glaucoma study III. The predictive value of frequency-doubling perimetry and GDx nerve fibre analyser test results for the development of glaucomatous visual field loss. Eye 2009;23(8):1647-52.
37. Jansonius NM, Heeg GP. The Groningen Longitudinal Glaucoma Study. II. A prospective comparison of frequency doubling perimetry, the GDx nerve fibre analyser and standard automated perimetry in glaucoma suspect patients. Acta Ophthalmol 2009;87(4): 429-32.
38. Ito Y, Shimazawa M, Inokuchi Y, et al. Degenerative alterations in the visual pathway after NMDA-induced retinal damage in mice. Brain Res 2008;1212:89-101.
39. Breitenseher M, Uhl F, Prayer Wimberger D, et al. Morphological dissociation between visual pathways and cortex: MRI of visually-deprived patients with congenital peripheral blindness. Neuroradiology 1998;40(7):424-7.
40. Kashiwagi K, Okubo T, Tsukahara S. Association of magnetic resonance imaging of anterior optic pathway with glaucomatous visual field damage and optic disc cupping. J Glaucoma 2004;13(3):189-95.
41. Gupta N, Greenberg G, de Tilly LN, et al. Atrophy of the lateral geniculate nucleus in human glaucoma detected by magnetic resonance imaging. Br J Ophthalmol 2009;93 (1):56-60.
42. Garaci FG, Bolacchi F, Cerulli A, et al. Optic nerve and optic radiation neurodegeneration in patients with glaucoma: in vivo analysis with 3-T diffusion-tensor MR imaging. Radiology 2009;252(2):496-501.
43. Gupta N, Ang LC, Noel de Tilly L, et al. Human glaucoma and neural degeneration in intracranial optic nerve, lateral geniculate nucleus, and visual cortex. Br J Ophthalmol 2006;90(6):674-8.
44. Boucard CC, Hernowo AT, Maguire RP, et al. Changes in cortical grey matter density associated with long-standing retinal visual field defects. Brain 2009;132(Pt 7): 1898-906.
45. Parravano JG, Toledo A, Kucharczyk W. Dimensions of the optic nerves, chiasm, and tracts: MR quantitative comparison between patients with optic atrophy and normals. J Comput Assist Tomogr 1993;17(5):688-90.
46. Heeg GP, Blanksma LJ, Hardus PL, Jansonius NM. The Groningen Longitudinal Glaucoma Study. I. Baseline sensitivity and specificity of the frequency doubling perimeter and the GDx nerve fibre analyser. Acta Ophthalmol Scand 2005;83(1):46-52.
47. Katz J, Sommer A, Gaasterland DE, Anderson DR. Comparison of analytic algorithms for detecting glaucomatous visual field loss. Arch Ophthalmol 1991;109(12):1684-9.
48. Ashburner J, Friston KJ. Voxel-based morphometry--the methods. Neuroimage 2000;11(6 Pt 1):805-21.
49. Smith SM. Fast robust automated brain extraction. Hum Brain Mapp 2002;17(3):143-55.
50. Zhang Y, Brady M, Smith S. Segmentation of brain MR images through a hidden Markov random field model and the expectation-maximization algorithm. IEEE Trans Med Imaging 2001;20(1):45-57.
51. Klein A, Andersson J, Ardekani BA, et al. Evaluation of 14 nonlinear deformation algorithms applied to human brain MRI registration. Neuroimage 2009;46(3):786-802.
52. Ashburner J. A fast diffeomorphic image registration algorithm. Neuroimage 2007;38(1): 95-113.
53. Iba-Zizen MT, Istoc A, Cabanis EA. [The results of MRI exploration of glaucoma patients: what are the benefits?]. J Fr Ophtalmol 2008;31(6 Pt 2):2S24-8.
54. Imamura K, Onoe H, Shimazawa M, et al. Molecular imaging reveals unique degenerative changes in experimental glaucoma. Neuroreport 2009;20(2):139-44.
55. Duncan RO, Sample PA, Weinreb RN, et al. Retinotopic organization of primary visual cortex in glaucoma: Comparing fMRI measurements of cortical function with visual field loss. Prog Retin Eye Res 2007;26(1):38-56.
56. Burgel U, Schormann T, Schleicher A, Zilles K. Mapping of histologically identified long fiber tracts in human cerebral hemispheres to the MRI volume of a reference brain: position and spatial variability of the optic radiation. Neuroimage 1999;10(5):489-99.
57. Andrews TJ, Halpern SD, Purves D. Correlated size variations in human visual cortex, lateral geniculate nucleus, and optic tract. J Neurosci 1997;17(8):2859-68.
58. Wagner AL, Murtagh FR, Hazlett KS, Arrington JA. Measurement of the normal optic chiasm on coronal MR images. AJNR Am J Neuroradiol 1997;18(4):723-6.
59. Safran AB, Landis T. Plasticity in the adult visual cortex: implications for the diagnosis of visual field defects and visual rehabilitation. Curr Opin Ophthalmol 1996;7(6):53-64.
60. Hossain P, Seetho IW, Browning AC, Amoaku WM. Artificial means for restoring vision. BMJ 2005;330(7481):30-3.

Chapter 5

Visual pathway structure and the severity of visual field defect in glaucoma

Based on:
Hernowo AT, Jansonius NM, Hooymans JMM, Cornelissen FW. Visual pathway structure and the severity of visual field defect in glaucoma. *To be submitted.*

ABSTRACT

This study aims to find if there is any structure-function correlation between the visual pathway structures volume and the visual field sensitivity in primary open-angle glaucoma (POAG). Seventeen subjects with varying stage of POAG voluntarily participated in the study. Only POAG patients with a minimum of three years of established diagnosis were included. The visual fields were taken with automated static perimetry to obtain the mean deviation (MD) of the visual field sensitivity. Magnetic resonance (MR) brain diffusion tensor imaging (DTI) and anatomical T1-weighted (T1W) imaging of all subjects were acquired on a 3T MR scanner. T1W images were processed to allow for volume measurement. Diffusion-weighted (DW) image processing were done to obtain fractional anisotropy (FA) maps. Both T1W- and DW-derived images were eventually subjected to voxel-wise analyses to compare the brains in voxel-to-voxel manner. Structure to structure comparison was approached with regions-of-interest (ROI) based analyses. Voxel-wise analyses revealed that the MD was correlated with pregeniculate ($p<0.05$, FWE-corrected) and LGB volumes ($p<0.05$, uncorrected). ROI-based analyses showed only the pregeniculate volume was moderately correlated with MD ($R=0.65$; $p<0.05$, Bonferroni-corrected). Voxel-wise analyses showed that FA was correlated with MD ($p<0.05$, uncorrected) in geniculocalcarine region. ROI-based analyses failed to show any correlation between FA and MD. In summary, visual field sensitivity is primarily correlated with the volume of the pregeniculate visual pathway.

Chapter contents

5.1. Introduction

Glaucoma has been a major interest of study in ophthalmology due to its prevalence and the potentially devastating effect to the sufferers[1, 2]. Because of the visual impairment it causes, the sufferer may experience decrease in the quality of life with extensive implications, e.g. psychologically, socially, and economically. Efforts to manage the condition have been resulting in countless studies on the pathology and treatment of glaucoma.

In recent years, studies on the effects of glaucoma on the brain have yielded many reports indicating the involvement of the visual pathway in glaucoma[3-11]. Brain imaging showed that primary visual cortex [4, 9, 12], lateral geniculate bodies (LGB)[3, 5, 10, 12-15] and pregeniculate structures[3, 10, 16] are affected by the disease. The structural studies reported employed diverse methods, ranging from manual measurement[5] to automated morphometry[3, 4] of the structures of interest. They were performed mainly on histologic slice as a postmortem examination, and also on the high resolution anatomical acquisition (T1- and T2-weighted imaging). Advance in magnetic resonance imaging have brought forward diffusion-weighted acquisition, and this opens possibilities to investigate more properties of the visual pathway structure[6, 16]. Earlier methods of, for example voxel-based morphometry (VBM), already enabled researchers to investigate the visual pathway volume with less subjective bias. Using diffusion-weighted imaging, researchers are now able to infer the integrity of the visual pathway white matter structures in addition to the volumetric measurement derived from T1-weighted scans.

Our previous study has shown lower volumetric measurement of the human visual pathway in subjects with primary open-angle glaucoma or POAG, from the optic nerve to the visual cortex, as compared to healthy subjects[3, 4]. The studies were mainly based on VBM of high resolution T1-weighted imaging of human brain. They were aimed at studying the visual pathway structures in the presence of homonymous visual field defects. With regard to patient management, a clinically relevant question

would be whether there is any relationship between glaucoma severity and the visual pathway structures. Based on anatomical (T1-weighted) and diffusion-weighted imaging analyses, we hope to answer this question.

5.2. Methods

5.2.1. Subjects

This study conformed to the tenets of the Declaration of Helsinki and was approved by the medical review board of the University Medical Center Groningen (Groningen, the Netherlands). All participants gave their written informed consent prior to participation.

Patients with POAG were recruited from participants in the Groningen Longitudinal Glaucoma Study[17]. Seventeen patients participated (eight females and nine males; mean age 63 years old, range 42-71 years old). The participant inclusion criteria were the following: 1) a glaucomatous visual field defect of at least 10° in diameter in at least one quadrant, affecting both eyes homonymously; 2) these visual field defects had to include the paracentral regions in both eyes; 3) these defects had to have been present for at least three years. The severity of the visual field loss was determined by the mean deviation (MD) scores as assessed with a Humphrey Field Analyzer (Carl Zeiss Meditec AG, Jena, Germany). Table 1 lists the characteristics of the patients. Patients with any other ophthalmic or neuro-ophthalmic disease that might affect the visual field or visual acuity were excluded.

5.2.2. Data acquisition

5.2.2.1. Perimetry

The visual field was tested with the Humphrey Field Analyzer (HFA; Carl Zeiss Meditec AG, Jena, Germany). A standardized method for examining the central visual field up to 30° eccentricity, the 30-2 Swedish Interactive Threshold Algorithm (SITA)-Fast, was employed. A visual field defect was considered to be present if at least one of these criteria was present: glaucoma hemifield test outside of the normal limit, or the pattern standard deviation's p less than 0.05, or at least three adjacent non-edge points (with $p<0.05$) in the pattern deviation probability plot on the same side of the horizontal meridian, with at least one point having a p-value less than 0.01[18]. Defects had to be present on at least two consecutive, reliable tests in the same region of the visual field (not including the first visual field measurement ever made). A test result was considered unreliable if false positive catch trials exceeded 10%, or if both false negative catch trials and fixation losses exceeded 10% and 20%, respectively. Moreover, defects had to be compatible with glaucoma and were not allowed to have any other explanation. The outcome measure used in this study was the MD.

Characteristics	Values
Age, mean (range), years	61 (42 - 71)
Male sex, %	64
Family history of glaucoma, %	29
IOP	
Highest ever recorded, mean (range), mmHg	32.6 (20 to 50)
Treated, mean (range), mmHg	15.0 (10 to 20)
Visual field MD	
Right eye, mean (range), in dB	-11.3 (-29.9 to 0.0)
Left eye, mean (range), in dB	-9.1 (-30.5 to -0.8)
Scanning laser polarimetry (GDx) NFI	
Right eye, median (range)	63.9 (44 to 83)
Left eye, median (range)	49.2 (18 to 79)
Scanning laser polarimetry (GDx) ellipse average thickness	
Right eye, mean (range), µm	60.0 (51 - 84)
Left eye, mean (range), µm	66.8 (51 - 102)

Table 1. Baseline patient characteristics. Characteristics of the patients were age, sex and positive family history proportion (in percentage), intraocular pressure (in mmHg), visual field sensitivity (expressed as MD in dB), nerve fiber indicator, and nerve fiber layer thickness (in µm). logMAR – logarithm of minimum angle of resolution; IOP - intraocular pressure; MD – mean deviation; dB – decibel; NFI - nerve fiber indicator; µm – micrometer.

5.2.2.2. Neuroimaging

All participants were scanned on the 3.0 Tesla MRI scanner (Philips Intera, Eindhoven, the Netherlands) located at the BCN Neuro-imaging Centre of the University Medical Centre Groningen. For each participant, a high-resolution, T1-weighted, anatomical scan was made using magnetisation sequence T1W/3D/FFE, repetition time 25 ms, resolution 256 × 256, field of view 256 × 160 × 204, yielding 160 slices, and a voxel dimension of 1 × 1 × 1 mm.

We also acquired two 60-direction gradient diffusion-weighted (DW) images for every subject. The first DW scan was made using DwiSE technique, resolution 128 x 128, APP fat shift 11.722 pixels, degree of angulation 0.57 1.405 -15.9, repetition time 5485 ms, field of view 240 × 102 × 240, echo time 79 ms, diffusion b value 800, EPI factor 45, and voxel dimension 1.875 × 1.875 × 2.000 mm. The second DW scan has similar parameters as the first, except for APA fat shift 12.035 pixels and repetition time 5516 ms.

5.2.2.3. T1-weighted image processing and analyses

We defined six regions-of-interest (ROIs) along the visual pathway: pregeniculate structures (*pgcl*), lateral geniculate bodies (*lgb*), geniculocalcarine radiation (*gcr*), occipital pole (*ocp*), the intracalcarine (*icc*) and supracalcarine regions (*scc*). For the first two ROIs, the brain

images were cropped so that the desired ROI is captured while minimising outside-of-ROI structures. For *gcr*, the registration is performed globally (using the whole white matter of the brains) for the structure is not easily visually separable from the surrounding white matter. Only in the following statistical testing, we applied a mask derived from Jülich probabilistic atlas[19, 20] to extract the geniculocalcarine radiation. For the last three ROIs, the occipital lobes of the brains were cropped and used. The image processing involved the following steps: rigid-body registration, segmentation, registration, and modulation of the segments. The process from the segmentation to the voxelwise statistical analyses is known as voxel-based morphometry (VBM). We used SPM8 software package (Wellcome Department of Imaging Neuroscience, London, UK; http://www.fil.ion.ucl.ac.uk/spm) to implement the VBM[21]. The steps in the data analysis procedure are described in more detail in the following sections.

5.2.2.3.1. Image pre-processing

A number of pre-processing steps were performed on the scanned images prior to actual measurement and statistical analyses. Image reorientation to the average image of all subjects' brains was applied to ensure registration of the images.

5.2.2.3.2. Segmentation, registration, and modulation

Commonly used registration methods allowed sufficiently good registration of the brain. Since we are interested in certain structures only, i.e. the visual pathway, we only registered the structures constituting the pathway. This way we improve the registration of the structures of interest. To do this, after registering the brain as a whole, depending on the structures of interest, we registered the brains locally. For the pregeniculate structures (the optic nerve, chiasm, and tract), we masked the brains of the subjects so to isolate the pregeniculate structures and their surrounding only. Next, we aligned the pregeniculate structures to one another. The same is true for the LGB and the primary visual cortex. These were done prior to performing the following steps described below.

We then used SPM8's DARTEL (Diffeomorphic Anatomical Registration through Exponentiated Lie Algebra) suite of tools [22, 23]. In short, the DARTEL tools enabled us to create modulated grey and white matter images that were registered to a common reference image specifically representing our sample, instead of registering them to a more general template, such as the MNI (Montreal Neurological Institute) template that comes with SPM8. The study-specific method we used here enabled a more accurate inter-subject registration of visual pathway structures with improved localization and sensitivity of the VBM.

The process began with SPM8's segmentation using the TPMs we had created (as we explained in the paragraph above). After the entire visual pathway were segmented, a reference –or template– image was generated. The first step in generating this reference image was averaging the images of all structures of interest. Following this, the individual structures of interest were deformed and registered as closely as possible to this reference image. Next, using the registered structures of interest images, a new average reference image was created to which the individual structures of interest images were again registered. After 6 of these averaging and registration cycles, the final reference image was generated. The final reference image was then used as the template to which the native segmentations of the individual structures of interest in the study were registered and modulated.

5.2.2.4. Diffusion-weighted image processing and analyses

As DW acquisition is usually affected by the occurrence of eddy current, its correction were done for both DW images. The correction procedure was implemented in the FSL. Distortion due to water-fat susceptibility were done using a MATLAB script implemented by J.A. Farrell[24]. The diffusion tensor estimation were done using DTIFIT tool implemented in FSL. This created images of the first, second, and third eigenvalues, as well as their fractional anisotropy (FA) image derivative. The FA is obtained using the formula:

$$FA=\sqrt{\frac{3\left[\left(\lambda_1-D_{av}\right)^2+\left(\lambda_2-D_{av}\right)^2+\left(\lambda_3-D_{av}\right)^2\right]}{2\left(\lambda_1^2+\lambda_2^2+\lambda_3^2\right)}}$$

where , λ_1, λ_2, λ_3 being the 1st, 2nd, and 3rd principal eigenvalues, respectively; and D_{av} being the average of the three eigenvalues above.

We used a portion of SPM8's DARTEL (Diffeomorphic Anatomical Registration through Exponentiated Lie Algebra) suite of tools [22, 23] to create images that were registered to a common reference image specifically representing our sample, instead of registering them to a more general template that comes with SPM8. The study-specific method we used here enabled a more accurate inter-subject registration of brain images with improved localization and sensitivity of the VBM. The first step in generating this reference image was averaging the FA images of all brains. Following this, the individual FA images were deformed and registered as closely as possible to this reference image. Next, using the registered FA images, a new average reference image was created to which the individual FA images were again registered. After 6 of these averaging and registration cycles, the final reference image was generated. The final reference image was then used as the template to which the native FA image of the individual subjects in the study were registered.

5.2.3. Statistical analyses

We performed two type of analyses: (1) region-of-interest or ROI-based analysis; and (2) voxel-wise analyses. In ROI-based analysis, we use masks to extract the ROI volumes or mean FA. The ROI volumes were extracted from modulated normalised brain segments. While in voxel-wise analyses, we compared the brains voxel by voxel along the visual pathway.

As we had mentioned earlier, the six ROIs we compared are *pgcl, lgb, gcr, ocp, icc,* and *occ*. The masks used to extract the volume of the pregeniculate structures and the lateral geniculate bodies were manually made by the investigator, for the boundaries of those structures are feasible to define visually. The mask for the geniculocalcarine radiation for volumetric analyses were derived from Jülich histological atlas [19, 20], whereas the mask for the occipital pole, intracalcarine and supracalcarine regions were derived from Harvard Center for Morphometric Analysis.

The second analysis is VBM, in which we correlated the images voxel by voxel along the visual pathway. The method made it possible for the investigators to spatially detect any deviation in the pathway. Threshold-free cluster enhancement (TFCE) method was applied to minimize the need of large scale smoothing or of predefining the significant cluster size. We performed factorial design analyses, with age as a covariate.

5.3. Results

5.3.1. ROI-based findings

We extracted the values from every ROI, both for volumetric and anisotropy analyses.

5.3.1.1. Volumetric analysis

We extracted the volumes from all ROIs and perform correlation and regression analyses with the MD. There is not any significant correlation between the MD and the ROIs volume along the pathway, except for the pregeniculate structures, where there is a positive correlation ($R=0.65$; $p<0.05$, Bonferroni-corrected) between the volume and the MD value. Linear regression of a model in which the MD being the dependent variable, while all ROIs volume and age were the predictors revealed an $R^2=0.75$ ($F=3.95$; $p=0.029$), and the volume of *pgcl* being the only significant predictor ($T=4.08$; $p=0.0027$). Figure 1 shows the MD values against the volume of the ROIs.

5.3.1.2. Anisotropy analysis

From DW images, we extracted the mean FA values from the pregeniculate structures and the geniculocalcarine radiation. We plotted these values against the MD value. We found no significant correlation between the MD and the FA in *pgcl* and *gcr* ($p>0.05$). Figure 2 presents the results.

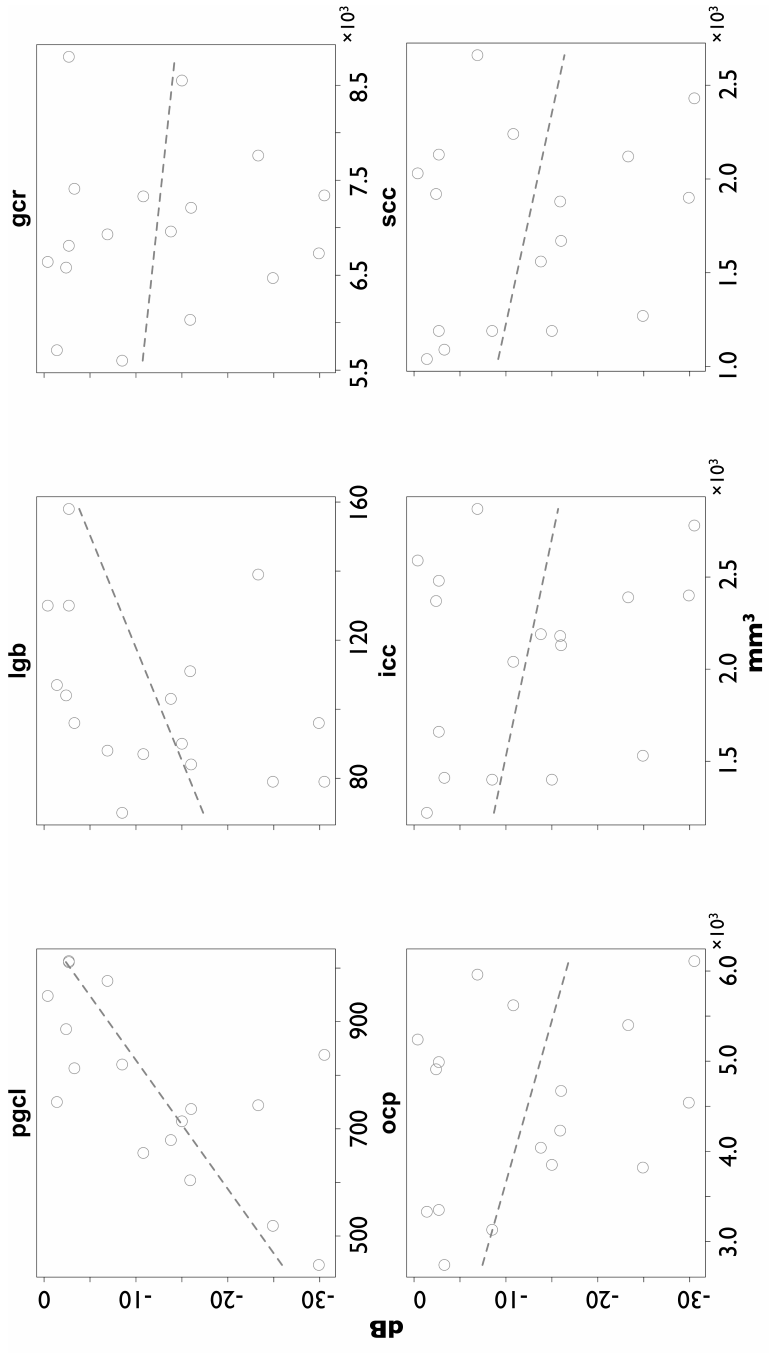

Figure 1. Scatter plot of structure-function relationship in the visual pathway structures. The x-axis is the volume of the visual pathway structures and the y-axis is the visual field mean deviation of sensitivity. There is a significantly positive correlation between the volume of pregeniculate structures and the mean deviation(R=0.65; p=0.005). dB - decibel; pgcl - pregeniculate structures; lgb - lateral geniculate bodies; gcr - geniculocalcarine radiation; ocp - occipital poles; icc - intracalcarine; scc - supracalcarine.

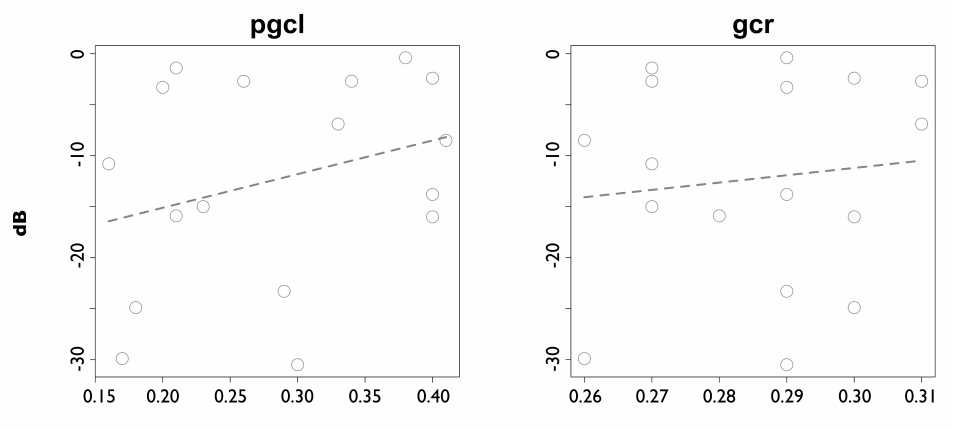

Figure 2. Scatter plot of fiber anisotropy-function correlation in the visual pathway structures. The x-axis is the FA of the visual pathway structures and the y-axis is the visual field mean deviation of sensitivity. There is no significant correlation between the FA and the MD ($p<0.05$). dB - decibel; FA - fractional anisotropy; pgcl - pregeniculate structures; gcr - geniculocalcarine radiation.

5.3.2. Voxel-wise findings

5.3.2.1. Volumetric analysis

Figure 3 shows the visual pathway structures volume correlation with the mean deviation of visual field sensitivity. The optic nerves, chiasm, tracts volume, as well as the volume of the lateral geniculate bodies, are correlated significantly ($p<0.05$, uncorrected) with the MD value. More conservative statistical thresholding left the pregeniculate structures volume still significantly correlated with the MD ($p<0.05$, FWE-corrected). The strength of correlation was presented earlier in the ROI-based analyses.

5.3.2.2. Anisotropy analysis

Figure 4 shows the visual pathway structures FA correlation with the mean deviation of visual field sensitivity. Only geniculocalcarine radiation's FA was correlated significantly ($p<0.05$, uncorrected) with the MD. Pregeniculate structures failed to show any significant correlation with MD value. No structures survived more conservative statistical thresholding (at $p<0.05$; FWE-corrected).

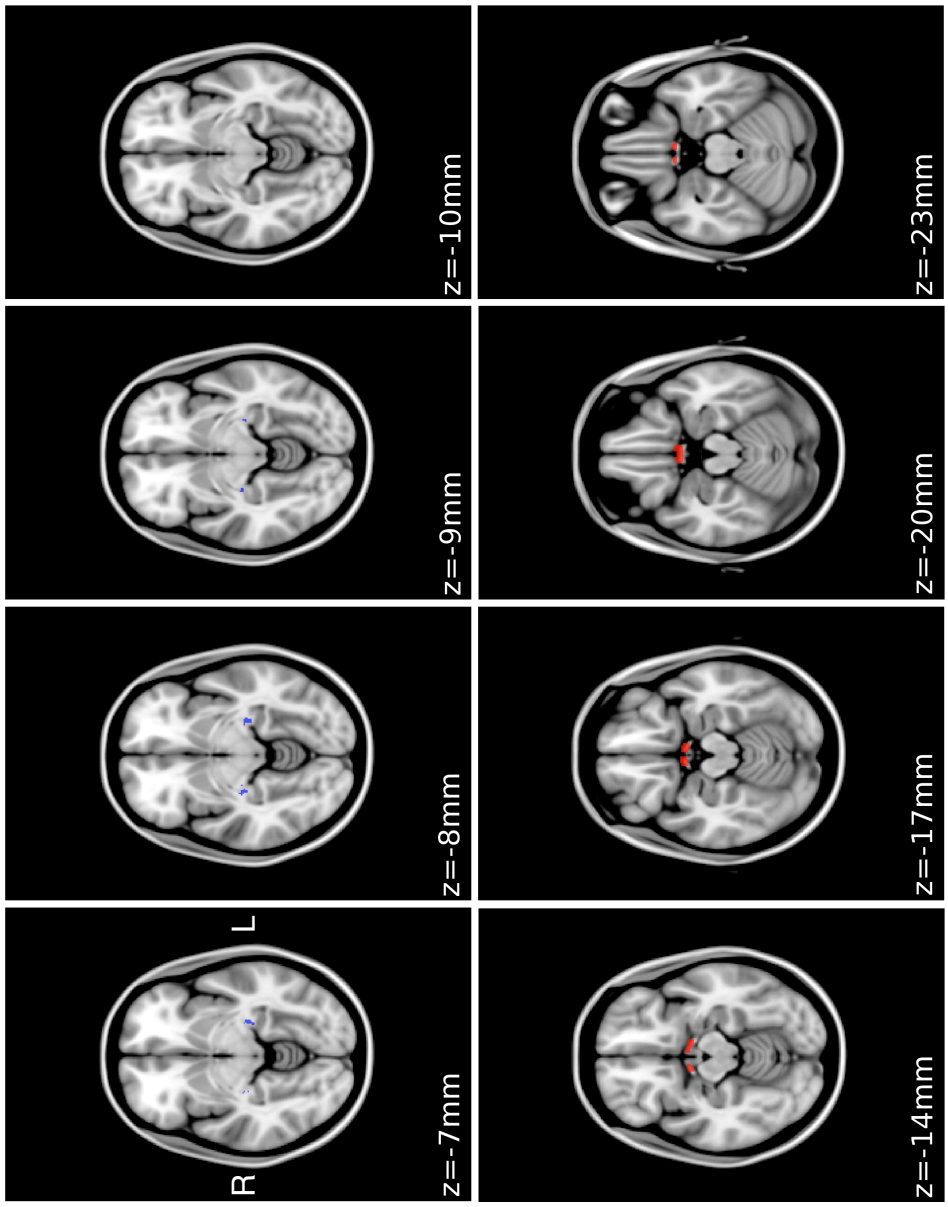

Figure 3. Structure-function correlation in the visual pathway structures. The axial planes were from Talairach plane of z -7 mm down to z -23 mm to visualize the optic nerves, chiasm, tracts, lateral geniculate bodies, and the geniculocalcarine radiation. The red shading shows where in the white matter of the visual pathway, the MD of the visual field is correlated significantly with the volume of the structures. The blue shading shows correlation of the volume of the lateral geniculate bodies to MD. Threshold is at $p<0.05$, uncorrected. MD – mean deviation.

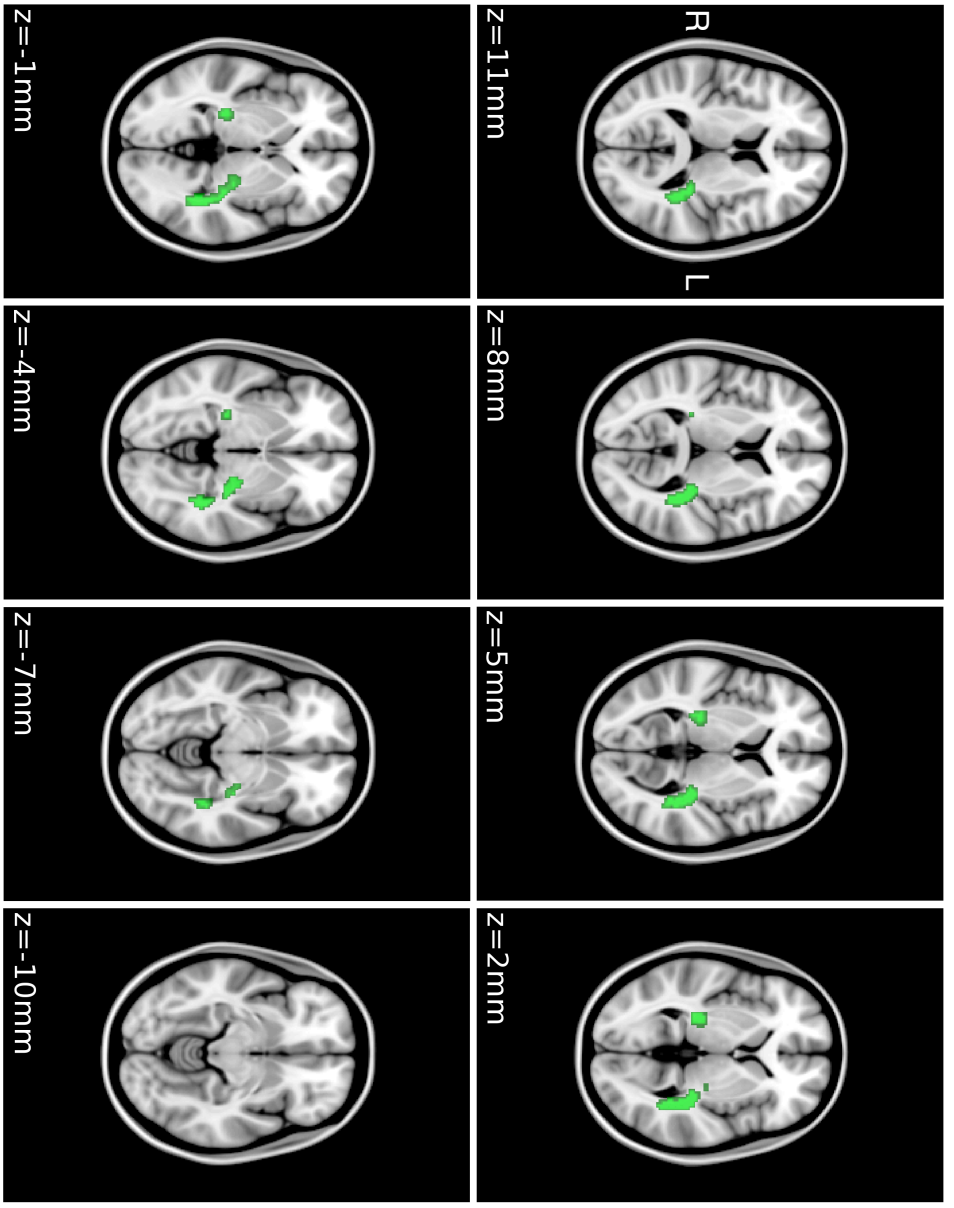

Figure 4. Anisotropy-function correlation in the visual pathway structures. The axial planes were from Talairach plane of z -11 mm down to z -10 mm to visualize the geniculocalcarine radiation. The green shading shows where the MD of the visual field is correlated significantly ($p<0.05$, uncorrected) with the FA value of the structures. The pregeniculate structures' FA showed no significant correlation with the MD, hence the slices are not shown. MD – mean deviation; FA - fractional anisotropy.

5.4. Discussion

In our earlier studies[3, 4], we found that the visual pathway structure in POAG patients are smaller than the healthy controls. The question is, if there is any relationship between the structures and the visual field sensitivity. This report is an effort to try answering this question.

In this study, we modified the standard VBM approach. In standard VBM, image processing is done to the whole brain, thus, any registration and segmentation were based on global brain voxels information. What we did here was, instead of processing the whole brain, we processed the brains according to the structures of interest, i.e. the visual pathway. This was done with the purpose of achieving a better registration of the structure of interest. For example, first we performed a series of registration and segmentation (DARTEL) on the pregeniculate structures. In doing so, we practically disregard the other parts of the brain and only use information from the voxels constituting the structures and their immediate surroundings. Better registration and spatial localisation can then be expected, and voxel-wise statistical inference can be more confidently made.

We discovered that there is a moderate yet very significant correlation between the MD and pregeniculate volume ($p<0.05$, corrected), similar to what Kashiwagi et al[25]. had found up to the optic chiasm. The apparently linear correlation between the MD and the pregeniculate structures might be due to the loss of RGC already in the early stage of the disease[11], and throughout the later stages, with 5 dB loss corresponds to 20-25% of RGC loss[26, 27]. In addition, a loss of 40% of RGC within the central 30° of the retina corresponds to 10 dB decrease in sensitivity[27]. Since the optic nerve, chiasm, and tracts are all basically a continuous structure, the whole pregeniculate structures size should have a linear relationship with the optic nerve fibre count. Even though the volumes of the pregeniculate structures are linearly correlated with visual field sensitivity, this does not necessarily mean that there is also a linear correlation between the volumes of the LGB and beyond with the visual field sensitivity. Perhaps the LGB and the geniculocalcarine radiation structures have some non-linear relationship with the visual field sensitivity. Or perhaps their structure-function correlation measurable only in more severe stage of the disease. We can only speculate at this stage.

From anisotropy analyses, we found that the geniculocalcarine radiation's FA (and not the pregeniculate's FA) was correlated with the MD. Since the MD values can be related to the condition of the RGC and RNFL[28, 29], and since the pregeniculate structures are the continuation of RNFL, the structure-function correlation at the structures might be expected. Yet, FA analyses failed to show it. One of possible sources of the discrepancy is the difference of resolution acquisition. As had been described in the methods section, the T1W acquisition is of 1mm × 1mm × 1mm voxel size, whereas the on of the DW is 1.875mm × 1.875mm × 2mm. The difference may affect the sensitivity of the statistical testing simply because of smaller number of data points in the DWI. Another possible source of discrepancy is the fact that the two acquisition, T1W and DW, gave us different images. The pregeniculate structures seen on a T1W image, visualised the structure with both the bundle of axons and the encapsulating dura. The DW image on the other hand, showed the degree of signal changes due to water molecule displacement along the bundle of axons. Smaller size of the pregeniculate structures might be due to generalised reduction in all components of the structures: the axons, the myelin, and the interstitial space. Due to this generalised shrinkage, the concentration (and the

anisotropy) of the water inside the structure might be preserved, leading to relatively similar FA values between the subjects of different severity. Histological approach may be necessary to test whether the second possibility is true.

In summary, we found that there was a very significant and moderately strong relationship between the volume of the pregeniculate portion of the visual pathway and the visual field sensitivity. The LGB and their geniculocalcarine projections showed at least a correlation trend with the visual field sensitivity. Based on what we have discovered so far from this study and from our earlier reports[3, 4], we argue that glaucoma management really need an integrated approach from neurology and ophthalmology standpoints. The retrobulbar pathway involvement in this POAG implicate the necessity of more attention toward keeping the well-being of the neurons along the entire visual pathway. This is particularly important when in the long term, the declining visual function may be easier to fix (although perhaps only partially) if the neuronal components are still preserved. Neuroprotective approach should perhaps really be considered in the management of patients with glaucoma, or neuro-retinal diseases in general.

Acknowledgments

The authors would like to thank Stichting Nederlands Oogheelkundig Onderzoek (SNOO), Ubbo Emmius foundation of the RUG, and Uitzicht for their fundings in the study.

Bibliography

1. Quigley HA, Broman AT. The number of people with glaucoma worldwide in 2010 and 2020. Br J Ophthalmol 2006;90(3):262-7.
2. Quigley HA. Number of people with glaucoma worldwide. Br J Ophthalmol 1996;80(5): 389-93.
3. Hernowo AT, Boucard CC, Jansonius NM, et al. Automated Morphometry of The Visual Pathway in Primary Open-Angle Glaucoma. Invest Ophthalmol Vis Sci 2011.
4. Boucard CC, Hernowo AT, Maguire RP, et al. Changes in cortical grey matter density associated with long-standing retinal visual field defects. Brain 2009;132(Pt 7): 1898-906.
5. Gupta N, Greenberg G, de Tilly LN, et al. Atrophy of the lateral geniculate nucleus in human glaucoma detected by magnetic resonance imaging. Br J Ophthalmol 2009;93 (1):56-60.
6. Garaci FG, Cozzolino V, Nucci C, et al. Advances in neuroimaging of the visual pathways and their use in glaucoma. Prog Brain Res 2008;173:165-77.
7. Iba-Zizen MT, Istoc A, Cabanis EA. [The results of MRI exploration of glaucoma patients: what are the benefits?]. J Fr Ophtalmol 2008;31(6 Pt 2):2S24-8.
8. Boucard CC, Hoogduin JM, van der Grond J, Cornelissen FW. Occipital proton magnetic resonance spectroscopy (1H-MRS) reveals normal metabolite concentrations in retinal visual field defects. PLoS One 2007;2(2):e222.
9. Duncan RO, Sample PA, Weinreb RN, et al. Retinotopic organization of primary visual cortex in glaucoma: Comparing fMRI measurements of cortical function with visual field loss. Prog Retin Eye Res 2007;26(1):38-56.
10. Gupta N, Ang LC, Noel de Tilly L, et al. Human glaucoma and neural degeneration in intracranial optic nerve, lateral geniculate nucleus, and visual cortex. Br J Ophthalmol 2006;90(6):674-8.
11. Stamper RL. The effect of glaucoma on central visual function. Trans Am Ophthalmol Soc 1984;82:792-826.
12. Imamura K, Onoe H, Shimazawa M, et al. Molecular imaging reveals unique degenerative changes in experimental glaucoma. Neuroreport 2009;20(2):139-44.
13. Yucel YH, Zhang Q, Weinreb RN, et al. Effects of retinal ganglion cell loss on magno-, parvo-, koniocellular pathways in the lateral geniculate nucleus and visual cortex in glaucoma. Prog Retin Eye Res 2003;22(4):465-81.

14. Dandona L, Hendrickson A, Quigley HA. Selective effects of experimental glaucoma on axonal transport by retinal ganglion cells to the dorsal lateral geniculate nucleus. Invest Ophthalmol Vis Sci 1991;32(5):1593-9.
15. Shou T, Liu J, Wang W, et al. Differential dendritic shrinkage of alpha and beta retinal ganglion cells in cats with chronic glaucoma. Invest Ophthalmol Vis Sci 2003;44(7): 3005-10.
16. Garaci FG, Bolacchi F, Cerulli A, et al. Optic nerve and optic radiation neurodegeneration in patients with glaucoma: in vivo analysis with 3-T diffusion-tensor MR imaging. Radiology 2009;252(2):496-501.
17. Heeg GP, Blanksma LJ, Hardus PL, Jansonius NM. The Groningen Longitudinal Glaucoma Study. I. Baseline sensitivity and specificity of the frequency doubling perimeter and the GDx nerve fibre analyser. Acta Ophthalmol Scand 2005;83(1):46-52.
18. Katz J, Sommer A, Gaasterland DE, Anderson DR. Comparison of analytic algorithms for detecting glaucomatous visual field loss. Arch Ophthalmol 1991;109(12):1684-9.
19. Burgel U, Amunts K, Hoemke L, et al. White matter fiber tracts of the human brain: three-dimensional mapping at microscopic resolution, topography and intersubject variability. Neuroimage 2006;29(4):1092-105.
20. Burgel U, Schormann T, Schleicher A, Zilles K. Mapping of histologically identified long fiber tracts in human cerebral hemispheres to the MRI volume of a reference brain: position and spatial variability of the optic radiation. Neuroimage 1999;10(5):489-99.
21. Ashburner J, Friston KJ. Voxel-based morphometry--the methods. Neuroimage 2000;11(6 Pt 1):805-21.
22. Klein A, Andersson J, Ardekani BA, et al. Evaluation of 14 nonlinear deformation algorithms applied to human brain MRI registration. Neuroimage 2009;46(3):786-802.
23. Ashburner J. A fast diffeomorphic image registration algorithm. Neuroimage 2007;38(1): 95-113.
24. Farrell JA, Landman BA, Jones CK, et al. Effects of signal-to-noise ratio on the accuracy and reproducibility of diffusion tensor imaging-derived fractional anisotropy, mean diffusivity, and principal eigenvector measurements at 1.5 T. J Magn Reson Imaging 2007;26(3):756-67.
25. Kashiwagi K, Okubo T, Tsukahara S. Association of magnetic resonance imaging of anterior optic pathway with glaucomatous visual field damage and optic disc cupping. J Glaucoma 2004;13(3):189-95.
26. Kerrigan-Baumrind LA, Quigley HA, Pease ME, et al. Number of ganglion cells in glaucoma eyes compared with threshold visual field tests in the same persons. Invest Ophthalmol Vis Sci 2000;41(3):741-8.
27. Quigley HA, Dunkelberger GR, Green WR. Retinal ganglion cell atrophy correlated with automated perimetry in human eyes with glaucoma. Am J Ophthalmol 1989;107(5): 453-64.
28. Harwerth RS, Vilupuru AS, Rangaswamy NV, Smith EL, 3rd. The relationship between nerve fiber layer and perimetry measurements. Invest Ophthalmol Vis Sci 2007;48(2): 763-73.
29. Harwerth RS, Quigley HA. Visual field defects and retinal ganglion cell losses in patients with glaucoma. Arch Ophthalmol 2006;124(6):853-9.

Chapter 6

General discussion

Chapter contents

The research reported in this thesis has resulted in several findings as well as modifications of methodologies. These have implications for our understanding of the diseases studied and the future approach to dealing with the diseases. The following sections summarise and integrate these findings and methods to reach a final conclusion.*

6.1. Brief summary of the experimental studies

The findings and methods from each experimental chapter are briefly summarised below.

6.1.1. Grey matter density in visual field defects (Chapter 2)

The voxel-based morphometry (VBM) approach, as implemented in SPM5 (Statistical Parametric Mapping version 2005), was used to compare a group of subjects with age-related macular degeneration (AMD) and a group of subjects with primary open-angle glaucoma (POAG) to a group of age-matched controls. Regardless of the disease, all patients had homonymous visual field defect. The defects in the visual fields were mainly central (foveal or macular) in AMD and peripheral in POAG. We found low cortical grey matter density in the occipital lobe in both patient groups. In the AMD group, low grey matter density was found in the posterior half (or approximately at the occipital pole) of the calcarine cortex, whereas in the POAG group, this low density was found in the anterior half. The localisation was roughly retinotopic. This might indicate the presence of structure-function relationship at the level of the primary visual cortex.

6.1.2. Visual pathway morphometry in macular degeneration (Chapter 3)

The loss of cortical grey matter density in AMD and POAG prompted the exploration of both cortical and precortical portions of the visual pathway. We studied two types of macular degeneration: the age-related type (AMD) and the juvenile-type (JMD). Participating in this study were 113 subjects from York (United Kingdom), Regensburg (Germany) and Groningen (the Netherlands). We modified the registration process in VBM to allow structures-of-interest (SOI)-based morphometry. Applying both DARTEL (Diffeomorphic Anatomical Registration through Exponentiate Lie Algebra) as implemented in SPM8 (SPM version 2008) and our own modification of this software, we were able to improve the selective registration of the structures

* The first section of this chapter is about the experimental studies, which were collaborative efforts, therefore the first person plural forms are used. The second and third sections were the opinion of the thesis' author, therefore the first person singular forms are used.

constituting the visual pathway, instead of relying on the registration of the whole brain. Comparing the patient groups against age-matched controls, we discovered that volumetric reductions were present over the full length of the visual pathway, from the optic nerve to the visual cortex. The differences were most pronounced in JMD. We postulate that the relatively longer disease period in JMD may cause this. While previous studies have reported how visual cortex functions are reduced in macular degeneration, to our knowledge ours was the first study to show that the visual pathway anatomy is adversely involved in the disease.

6.1.3. Visual pathway morphometry in glaucoma (Chapter 4)

The research reported in this chapter explored the precortical portion of the visual pathway structure involvement in glaucoma, which was similar to the previous chapter on macular degeneration. We modified the segmentation in SPM8, enabling us to better extract the lateral geniculate bodies (LGB), by changing the tissue probability maps. After applying DARTEL as discussed in the previous chapter, we found that POAG subjects had low volumetric values in the optic nerves, chiasm, tracts, the LGB and at the geniculocalcarine radiation. This neuroimaging study was corroborated by post-mortem findings as well as DTI (diffusion tensor imaging)-based findings from other groups. In addition, this result confirmed the finding of density changes in the visual cortex in glaucoma as reported in Chapter 2.

6.1.4. Visual pathway and glaucoma severity (Chapter 5)

In the previous chapter, we showed that when the visual cortex density was low, the volume of the precortical portion of the visual pathway was also low. This led us to explore how the severity of the visual field defect may correlate with the anatomy of the pathway. In this chapter, we presented findings using volumetric and anisotropy analyses in glaucoma patients. The voxel-wise statistics were based on the same registration approach described in Chapter 3. In the early portion of the pathway (the pregeniculate structures), the volume of the structures was associated with the mean sensitivity of the visual field. Moreover, at the postgeniculate level, we found low integrity (indicated by fractional anisotropy or FA) of the geniculocalcarine radiation. In accordance with the results in Chapter 4, we postulate that a visual field defect in glaucoma patients has a negative effect on the entire visual pathway, instead of being restricted to retinal ganglion cell loss alone.

6.2. General discussion of the findings

The retrobulbar and intracranial part of the human visual pathway consists primarily of third and fourth order neurons. At the same time, the second order neuron (the bipolar cell) is located inside the retina of the eye. My studies focussed on macular degeneration and glaucoma. These diseases affect the photoreceptors and the retinal ganglion cells (RGCs), respectively. Accordingly, clinical management of the diseases has focussed on the eye. My main research question was whether these ocular pathologies, with their associated visual field defects, affect the integrity of the visual pathways leading to the visual cortex. The findings presented in this thesis may challenge the current retina-oriented clinical management of macular degeneration

and glaucoma.

As mentioned in the preceding chapters, reports have been published on how the primary visual cortex functions differently – less effectively – in cases of macular degeneration and glaucoma. As long as the visual cortex is viewed as only functionally representing the stimuli that the retina is able to process, such functional differences are expected and are not surprising. Consequently, the decreased function is not necessarily caused by degenerative changes in the cortex itself; after all, the primary visual cortex is a processor of visual stimuli. However, our studies indicate otherwise. The visual pathway of individuals with macular degeneration or glaucoma were morphometrically smaller, and were not structurally similar to those in healthy brains.

First, I found that the pregeniculate structures – the optic nerve, chiasm and tract – were significantly smaller in subjects with glaucoma or macular degeneration. It is relatively easy to see why this would be the case with glaucoma, but not with macular degeneration. RGC loss and the retinal nerve fibre layer (RNFL) thinning in glaucoma mean that the number and/or size of the axons have decreased. This feasibly explains the smaller size of the pregeniculate structures in subjects with glaucoma. However, in macular degeneration, the disease involves primarily the outer layer of the retina, where the choriocapillary tissue is damaged and the photoreceptors are disrupted. Direct involvement of the RGC in macular degeneration is currently unknown. Even so, the pregeniculate structures were markedly smaller than in the controls. Does this indicate RGC involvement in macular degeneration? I cannot say for certain from my studies, except that the pregeniculate structures are compromised in macular degeneration.

Second, involvement of the LGB, the geniculocalcarine radiation (GCR) and the primary visual cortex is apparent in both conditions, and most pronounced in glaucoma and JMD. These features were smaller, and the decline in size correlated with the severity of the visual field defect in glaucoma. The marked involvement of these structures in glaucoma and macular degeneration indicates that any degenerative changes occurring within the pathway is probably trans-synaptic in nature. If it is assumed that the pathology begins in the retina in both glaucoma and macular degeneration, even the previously discussed involvement of the pregeniculate structures indicates that whatever happened in the outer layer of the retina could influence the axons of the RGC. On the other hand, if the pathology begins in the primary visual cortex, it must have managed to find its way to adversely affect the LGB neurons and their axons (GCR), as well as the pregeniculate structures. Even though my studies are incapable of determining causality (because they had a cross-sectional design), the findings led me to consider the probability of trans-synaptic degeneration, either anterogradely or retrogradely.

During the studies, I also learned that the standard methods of image processing have advantages as well as limitations. I was therefore compelled to develop improvements to the preprocessing steps. The first development involved segmentation. Standard segmentation in SPM effectively separates the cortex from the rest of the brain. However, the lateral geniculate bodies are still inseparable from the white matter. By modifying tissue probability maps, or by applying a six-class segmentation, I was able to automatically extract a previously less separable structures, the LGB in this case.

The second development involved registration. The standard registration available in the softwares I used in my studies allows for adequate inter-brain registration. However, certain brain structures, in particular the pregeniculate structures and the geniculate bodies, were registered more effectively when the registration was applied locally, i.e. involving only the desired structure and not the whole brain. Since the validity of voxel-style statistics results is affected by the quality of registration, performing local registration to improve quality became a necessity, especially for the geniculate bodies and the pregeniculate structures.

Finally, an investigator can never be 100% certain that what he or she has discovered is what really takes place in nature. To the best of my knowledge at the time this thesis was written, the image processing methodology and the statistical methods were reliable for inferring the conclusions that were drawn. Ideas on how to improve methodologies generally do not come in a batch, but one at a time, within a time period that may be short or long – depending on one's perspective. Because the confidence in one's findings is based on the validity and reliability of the methods used, improving the methodology means improving the confidence in future findings. On the other hand, the improvements may cast doubt on previous findings. When this is the case, healthy scepticism and meticulous procedures are the main things I can rely on in my effort to understand what is really going on in the visual pathway.

6.3. Future directions in research

The series of studies presented in this thesis suggest that retinal and optic nerve diseases should not be considered entirely ocular in nature. The apparent involvement of the retrobulbar pathway could perhaps encourage ophthalmologists to consider "treating the brain" and not just the eye. Clinically, collaboration between (neuro-) ophthalmologists, glaucoma specialists, and neurologists should be encouraged to develop neuro-protective approaches to the diseases. Meanwhile in the laboratory, collaboration between neuroscientists and pharmacologists will be essential to develop novel treatments that may protect the neurons from the effects of the disease.

The current development of neuro-imaging techniques, coupled with retinal imaging, can be expected to pave the way for more sensitive diagnostic imaging methods. Many advances have taken place in functional diagnostic techniques for vision examination, including psychophysics, electroretinography and functional magnetic resonance imaging. Moreover, retinal and brain morphometry are not yet being intensively used in vision impairment. When combined, functional and structural analyses of the complete pathway from the eye to the visual cortex may ultimately provide us with much better comprehension of the dynamics of the visual pathway. This improved comprehension is expected to be important in the effective and timely management of retinal and optic nerve diseases.

Summary

Vision is a crucial sensory function for humans. People benefit from a visual field that is almost 180° wide from both top to bottom and from side to side, which allows them to be constantly aware of their surrounding. The most central part of this visual field is used for precision visual tasks, for example reading, observing the details of an object or recognising colours. We can refer to this part of the field as central vision. The peripheral field is useful when there is little light and it allows us to detect movement at the periphery of our vision. I will refer to this as peripheral vision.

Like any other bodily functions, the visual field can be affected by disease. Central vision may be lost in macular degeneration, where the light-receiving cells in the central part of the retina are disrupted (the retina is a layer at the back of the eyeball that receives and processes the light entering the eye). Peripheral vision may be lost due to glaucoma, where the retinal nerve cells distributed all over the retina begin to die. Using MRI (magnetic resonance imaging), we studied the brain anatomy of subjects with these eye diseases. After several image processing steps, we compared the volume of parts of the brains of various patient and control groups. Specifically, we investigated the visual pathway, which is the part of the brain through which the visual information is transmitted from the eye to the part of the brain relevant to vision (the visual cortex).

Two general types of macular degeneration can be distinguished, based on the onset of the disease: the juvenile type (starts in childhood or teenage) and the age-related type (starts in the fifth decade of life or later). We examined the brains of patients with macular degeneration and compared them to the brains of healthy individuals. We found that the visual pathway volume of patients with macular degeneration is lower than in healthy individuals (Chapters 2 and 3). This lower volume occurred along the entire pathway, from behind the eyeball to the brain, and this was most pronounced in the juvenile type of the disease. This might be caused by the fact that the disease starts early in life, and consequently the disease period is longer.

We also studied glaucoma, a disease that starts with loss of peripheral vision. Described in more detail in Chapters 2, 4, and 5, we found that patients with glaucoma also have a lower visual pathway volume than healthy individuals. In addition, the volume and the integrity of the pathway is negatively correlated with the severity of the disease. The worse the visual field sensitivity, the smaller the volume of the visual pathway.

The results in this thesis indicate that glaucoma and macular degeneration are not strictly eye diseases, but also involve the brain. We argue that if the visual pathway and the brain have been adversely affected by an eye disease, vision restoration or rehabilitation effort may have less likelihood of success. We recommend to direct more attention towards the brain in the management of eye diseases such as macular degeneration and glaucoma. In our view, this should be done in the hope of preventing widespread changes in the brain. Future studies should aim to find ways to protect the nerve cells in the brain from such change and damage.

Samenvatting

Het gezichtsvermogen is een cruciale sensorische functie voor de mens. Mensen hebben een gezichtsveld dat van boven naar beneden en van links naar rechts bijna een gebied van 180 graden omvat. Hierdoor zijn zij zich constant bewust van hun omgeving. Het centrale deel van het gezichtsveld, de fovea of macula, wordt gebruikt voor nauwkeurige visuele taken zoals lezen, het waarnemen van details van een object of het herkennen van kleuren. De rest van het gezichtsveld, ook wel het perifere gezichtsveld genoemd, geeft ons overzicht en stelt ons in staat om beweging waar te nemen. Het stelt ons ook in staat om nog wat zien wanneer er weinig licht is.

Het netvlies is een laag met zenuwcellen aan de achterkant van het oog. Het netvlies vangt het licht op dat binnenvalt in het oog en zet dit om in een neuraal signaal. Net als andere lichaamsfuncties kan het netvlies, en daarmee het gezichtsveld, worden aangetast door ziektes. Het centrale gezichtsveld kan aangetast worden door maculadegeneratie, waarbij de zenuwcellen in het centrale deel van het netvlies beschadigd worden. Bij de oogziekte glaucoom wordt vooral het perifere deel van het netvlies aangetast. Met behulp van MRI (magnetic resonance imaging) hebben we beelden gemaakt van de hersenen van patiënten met deze oogziekten. Na een uitgebreide bewerking van deze beelden konden we de inhoud van delen van de hersenen van verschillende patiënten- en controlegroepen vergelijken. Hierbij hebben we specifiek gekeken naar de visuele banen. Dat is het deel van de hersenen waar de visuele informatie van het oog wordt doorgegeven naar het deel van de hersenen dat betrokken is bij het zien (de visuele cortex).

De oogziekte maculadegeneratie kan worden onderverdeeld in twee types, gebaseerd op het moment van aanvang van de ziekte. Het juveniele type begint in de kinder- of tienerjaren. Het leeftijdgebonden type begint meestal na het vijftigste levensjaar. We onderzochten de hersenen van patiënten met maculadegeneratie en vergeleken ze met de hersenen van gezonde personen. We vonden dat de visuele banen van patiënten met maculadegeneratie een minder grote inhoud hadden dan die van gezonde personen (hoofdstuk 2 en 3). Deze kleinere inhoud vonden we langs de hele lijn van visuele banen; van achter het oog tot aan de hersenen. De kleinere inhoud was het meest uitgesproken bij de juveniele vorm van maculadegeneratie. Dit kan het gevolg zijn van het feit dat deze ziekte al eerder tijdens het leven begint, waardoor de ziekte bij de proefpersonen al verder gevorderd was.

Ook bij de patiënten met glaucoom vonden we een verminderde inhoud van de visuele banen ten opzichte van gezonde individuen. Daarnaast vonden we dat bij deze patiënten de inhoud van de visuele banen samenhing met de gevoeligheid van het gezichtsveld, hetgeen een maat is voor de ernst van de ziekte. Hoe lager de gevoeligheid van het gezichtsveld, des te kleiner bleek het volume van de visuele banen. Dit is meer in detail beschreven in de hoofdstukken 2, 4, en 5.

De resultaten in dit proefschrift geven aan dat glaucoom en maculadegeneratie niet alleen oogziekten zijn, maar ook invloed kunnen hebben op de hersenen. Mogelijk is het dus zo dat als de visuele banen in de hersenen zijn aangetast door een oogziekte, eventueel herstel van het gezichtsvermogen of revalidatie minder kans op succes hebben. Wij adviseren daarom om bij de behandeling van oogziekten, zoals maculadegeneratie en glaucoom, ook aandacht te besteden aan de hersenen. Daarmee kunnen grootschalige veranderingen in de hersenen worden voorkomen. Toekomstige studies zullen manieren moeten gaan vinden om de zenuwcellen in de hersenen te beschermen tegen veranderingen en beschadigingen.

Ringkasan

Penglihatan adalah fungsi inderawi yang penting bagi manusia. Manusia mendapatkan manfaat dari luasnya lapangan pandang yang hampir 180° dari atas ke bawah dan dari sisi ke sisi, yang memungkinkan manusia menyadari lingkungan sekitarnya secara berkesinambungan. Bagian yang paling tengah dari lapangan pandang dipakai untuk tugas-tugas penglihatan yang membutuhkan ketepatan, misalnya untuk membaca, mengamati rincian benda atau mengenali warna. Lapangan pandang tersebut kita sebut juga lapangan pandang tengah. Lapangan pandang tepi sangat berguna ketika hanya ada sedikit cahaya dan memungkinkan manusia mendeteksi gerakan di pinggiran lapangan pandang. Lapangan pandang ini kita sebut juga lapangan pandang tepi.

Seperti fungsi tubuh lainnya, lapangan pandang bisa dipengaruhi oleh penyakit. Lapangan pandang tengah bisa rusak akibat degenerasi makula, dimana sel-sel peka cahaya di bagian tengah selaput jala terganggu (selaput jala adalah lapisan pada bagian belakang dalam bola mata yang menerima dan memproses cahaya yang memasuki mata). Lapangan pandang tepi bisa rusak akibat glaukoma, dimana sel-sel saraf yang tersebar luas di selaput jala mati satu per satu. Menggunakan pencitraan resonansi magnetik (*MRI - magnetic resonance imaging*), kami mempelajari anatomi otak para pasien dengan penyakit mata. Setelah melalui beberapa langkah pengolahan citra, kami bandingkan citra otak kelompok pasien dengan kelompok kontrol (orang sehat). Dengan memakai teknik pengolahan citra kami menyelidiki ukuran bagian-bagian otak yang melayani fungsi penglihatan (kortels visual).

Secara umum, dapat dibedakan dua jenis degenerasi makula berdasarkan waktu timbulnya penyakit: jenis remaja (mulai anak-anak atau remaja) dan jenis yang terkait penuaan (dimulai pada dekade kelima dari kehidupan atau lambat). Kami memeriksa otak pasien dengan degenerasi makula dan membandingkannya dengan otak orang sehat. Secara lebih spesifik, kami meneliti jaras penglihatan, yaitu bagian yang menjembatani lalu lintas informasi penglihatan dari mata ke otak. Kami menemukan bahwa ukuran jaras penglihatan pasien dengan degenerasi makula lebih kecil dibandingkan ukuran jaras penglihatan orang sehat (Bab 2 dan 3). Kecilnya ukuran jaras ini terdeteksi di sepanjang jaras, mulai dari belakang bola mata hingga ke otak. Temuan ini lebih menonjol pada degenerasi makula jenis remaja. Hal ini bisa jadi karena degenerasi makula jenis remaja muncul lebih awal (usia muda) sehingga masa sakitnya labih panjang.

Kami juga meneliti glaukoma, suatu penyakit yang dimulai dengan hilangnya penglihatan tepi. Dijelaskan secara lebih rinci dalam Bab 2, 4 dan 5, kami menemukan bahwa pasien dengan glaukoma juga memiliki ukuran jaras penglihatan yang lebih kecil daripada orang sehat. Selain itu, jaras dan keutuhan jaras berhubungan dengan keparahan penyakit. Semakin buruk kepekaan lapangan pandang, semakin kecil ukuran jaras penglihatan.

Hasil studi dalam disertasi ini menunjukkan bahwa glaukoma dan degenerasi makula bukan sekedar penyakit mata, namun juga melibatkan otak. Kami berpendapat bahwa jika jaras penglihatan dan otak telah terpengaruh oleh penyakit mata, upaya pemulihan atau rehabilitasi penglihatan akan lebih sulit berhasil. Kami menyarankan untuk menambah perhatian kepada otak dalam pengelolaan penyakit mata, terutama degenerasi makula dan glaukoma. Dengan demikian, kami berharap keterlibatan yang lebih luas di otak bisa diantisipasi. Penelitian di masa depan sebaiknya ditujukan untuk mencarai cara untuk melindungi sel-sel saraf di otak dari

kerusakan.

List of abbreviations

3D	three dimensional
AMD	age-related macular degeneration
ANCOVA	analysis of covariance
AP	antero-posterior, directional parameter in diffusion-weighted acquisition
BCN	The Research School of Behavioural and Cognitive Neurosciences, University of Groningen
BET	Brain Extraction Tool, a part of FSL
CSF/csf	cerebrospinal fluid
DARTEL	Diffeomorphic Anatomical Registration through Exponentiated Lie Algebra
dB	decibel
DTI	diffusion tensor imaging
DWI	diffusion-weighted imaging
gcr	geniculocalcarine radiation
GM/gm	grey matter
icc	intracalcarine cortex
JMD	juvenile-type macular degeneration
MD	mean deviation (of the sensitivity of the visual field)
MDEFT	modified driven equilibrium Fourier transform
NIFTI	Neuroimaging Informatics Technology Initiative
FA	fractional anisotropy
FAST	FMRIB's Automated Segmentation Tool
FMRIB	Functional Magnetic Resonance Imaging of the Brain
FOV	field of view
FSL	FMRIB Software Library, developed by FMRIB Analysis Group, Oxford, United Kingdom
FSPGR	fast-spoiled gradient recalled (echo pulse sequence)
FWE	family-wise error
fwhm	full-width half-maximum
LGB/lgb	lateral geniculate body, synonymous to lateral geniculate nucleus
LGN/lgn	lateral geniculate nucleus, synonymous to lateral geniculate body
LLGN	left lateral geniculate nucleus
logMAR	the logarithm of the minimum angle of resolution
LON	left optic nerve
LOR	left optic radiation
LOT	left optic tract
MRI	magnetic resonance imaging
OC	optic chiasm
ocp	occipital pole
PA	postero-anterior, directional parameter in diffusion-weighted acquisition
pgcl	pre-geniculate
POAG	primary open-angle glaucoma
RPE	retinal pigment epithelium
RNFL	retinal nerve fiber layer
RGC	retinal ganglion cell
RLGN	right lateral geniculate nucleus
ROI	region-of-interest

RON	right optic nerve
ROR	right optic radiation
ROT	right optic tract
scc	supracalcarine cortex
SITA	Swedish Interactive Threshold Algorithm
SPM5	Statistical Parametric Mapping version 2005
SPM8	Statistical Parametric Mapping version 2008
SPM99	Statistical Parametric Mapping version 1999
SUSAN	Smallest Univalue Segment Assimilating Nucleus
T1/T_1	Also known as spin lattice time or relaxation time, a time taken by protons to realign themselves to the external magnetic field
T1W/T_1W	T1-weighted acquisition with most contrasts due to T_1 value
TBSS	tract-based spatial statistics
TFCE	threshold-free cluster enhancement
TFE	turbo field echo
TPM	tissue probability map
VBM	voxel-based morphometry
VOI	volume-of-interest
WM/wm	white matter

Acknowledgement

Alhamdulillahirobbil'alamin. The PhD program that I had been through was truly a once in a lifetime experience. I realize there are many people who deserve to be thanked for what I have been achieving and for what I have become now.

To my supervisors... ***Frans,*** thank you for giving me the opportunity to work in your lab, for training me to be self-reliance, for encouraging my transformation from being virtually computer illiterate to being self-taught in my field of expertise, for setting examples of good practice of science, and for allowing me to develop myself as a scientist. I really appreciate what you did for me. **Nomdo,** thank you for giving really much appreciated clinical perspectives throughout the process of patients selections, examinations, classifications, and the reviewing of my papers. Thank you also for being optimistic every time I consulted to you.

To my promoter, ***prof. Anneke,*** for believing in my ability to physiologically cope with the transition from living in the tropics to living in the subtropics, for eventually granting me the opportunity to join your department, for evaluating my progress and reminding me the milestones I should reach, and for being my promoter, I thank you very much.

I thank all members of the reading committee of my thesis, ***prof. R.J.W. de Keizer, prof. J.B.M. Kuks, and prof. A.B. Morland,*** for their willingness to review and for their critical appraisals to the thesis. I greatly appreciate the continuous support from my mentors: ***dr. Hartono, dr. Angela, prof. Suhardjo, dr. Agus, prof. Wasisdi, dr. Yanti, dr. Retno, dr. Sundari,*** and ***dr. Haryo.***

I would like to thank ***Wim,*** for helping me with my administrative necessities so that I can do my research work peacefully, as well as to ***Fenna*** and ***Ella,*** for having always been kind and helpful in facilitating my way around the department, in communication with the other staff members, and in many other things. My appreciation to ***dr. Steven Koopmans*** for being independent ophthalmologist for my studies, as well as ***Rogier, Angela, Jose, Stella, Joke, Rogier, all residents, TOAs, and administrative staff of the polikliniek,*** without whom the clinical part of my studies would be difficult to implement. Also special thanks to ***Diana, Janine, Hedwig, Evelyn, Tinie,*** for all the assistance you gave and nice conversations we had.

To my "neuro-colleagues", ***Joyce, JB, Richard, Remco, Doety, Funda, Barbara, Leonardo, Alessandro, Luca, Ramona, Ruud, Shippu, Koen, Erik, Marije, Marc,*** I thank you for the nice discussions and easy conversations we had. To my "ophthalmic-colleagues", ***Kim, Christiaan, Michael, Else, Marielle, Margriet, Tim, Francisco, Tim, Shao chong, Lisanne,*** thank you for the fun working atmosphere and warm welcomes every time I walk into your office. Special thanks to ***Doety, Martine,*** and ***Frans*** for checking my *nederlandse samenvatting,* and to ***JB*** for thesis layout inspiration.

Berada di pengasingan (baca: Belanda) membuatku menemukan keluarga baru yang membuatku tetap kerasan menjalani masa-masa studi yang kadang tidak mudah, terima kasih kepada keluarga Jalan Keyakinan (***Mbak Tina, Bang Fanny, Viny, Klara),*** keluarga Werumeus Buning ***(Mbak Lia, Mas Yayok, Keisha, Katya),*** Keluarga WB ***(Mbak Ike, Mbak Puri, Teh Uyung, Mas Itob, Mbak Dini),*** keluarga catering ***(Teh Nisa, Aa Nandang),*** keluarga pojok daerah lampu merah ***(Rossi, Mas***

Andi, Gietty, Hottie, Eka, Aulia). Kepada sahabat-sahabatku di Belanda dan Indonesia, ***Yoyo, Lukman, Mira, Nana, Dita,*** terima kasih atas waktu yang kalian berikan sehingga bisa berbagi cerita suka duka selama studiku dan terima kasih atas kebersamaan kalian. Kepada teman-teman di Belanda, deGromiest, dan PPIG: ***Wahono, Insanu, Mbak Tita, Muhsin, Pandji & Faizah, Mas Wisnu & keluarga, Oom Yon & Tante Indah, Mutia & keluarga, Mas Adhi & keluarga, Iging & Desti, Kenzie, Tara, Sita, Mbak Aini, Iging, Kadek S, Kadek Y, Arramel & Puti, Tante Tini & Oom Bert, Uwak Aisyak & Oom Meno, Oom Basuki & Tante Pantja, Robby, Lia Atwa, Eryth, Iqbal, Astri, Nizar, Tita, Okta, Mas Teguh, Hendi,*** terima kasih atas waktu dan kebersamaan yang menyenangkan.

Kepada senior, sejawat dokter, dan rekan-rekan di Bagian Mata di Jogja, ***dr. Supanji, dr. Tatang, dr. Tepo, dr. Wati, dr. Bayu, dr. Henry, Mas Putro, Mbak Lia, Bu Nuningsih, Mas Apri, rekan-rekan residen,*** dan ***seluruh keluarga bagian mata*** yang tidak dapat saya sebutkan satu per satu, terima kasih banyak atas dukungan yang diberikan kepada saya.

Kepada Ibu dan Bapak, tidak akan pernah cukup terima kasihku, hanya Allah yang bisa membalas seluruh kasih sayang yang Ibu Bapak curahkan kepadaku, dan doa Adit selalu untuk Ibu Bapak. Kupanjatkan juga doaku teruntuk Memi dan Pepi, sebagai terima kasihku untuk segala perhatian dan dukungan yang kalian berikan padaku. To my beloved wife, Maya, you are the best, and I thank you for always motivating me to be better and better in everything I do. I am grateful to Allah that you're by my side.

I fully understand that my memory serves me well only to a certain extent, rendering a limitation to my recollection of the good deeds that many other people have done to and for me. For those who I have failed to mention, I sincerely apologize, and I thank you from the bottom of my heart.